Crustal Deformation and Silicic Magma Genesis

in the

Lunar Procellarum KREEP Terrane

by

Srinidhi Ravi

A Dissertation Presented in Partial Fulfillment
of the Requirements for the Degree
Doctor of Philosophy

Approved May 2023 by the
Graduate Supervisory Committee:

Mark S. Robinson, Chair
Christy B. Till
Thomas R. Watters
Kelin X. Whipple
Joseph G. O'Rourke

ARIZONA STATE UNIVERSITY

August 2023

ABSTRACT

Both volcanic and tectonic landforms are surface expressions of the inner workings of a planet. On Earth, volcanism and crustal deformation are primarily surface expressions of plate tectonics. In contrast, the lunar crust has been deformed by solely endogenic processes following large impact events.

The Procellarum KREEP (potassium (K), rare earth elements (REE), and phosphorus (P)) Terrane (PKT) is a thermally and chemically distinct geologic province on the Moon. Despite the wealth of remote sensing data, the origin and evolution of the PKT is poorly understood. This study focuses on floor-fractured craters and silicic magma genesis within the PKT.

First, I present a detailed study of floor-fractured craters, including morphometric measurements using topographic datasets from the Lunar Reconnaissance Orbiter Camera (LROC), variations in temporal heat flow, lithospheric rheology and the locations of floor-fractured craters relative to impact basins. The overarching conclusion is viscous relaxation and magmatic intrusion are not necessarily mutually exclusive, as has been argued in earlier studies. This work also provides new evidence for the existence of the putative Procellarum basin.

Next, with rhyolite-MELTS modeling, I demonstrate that fractional crystallization of KREEP basalt magmas is a plausible mechanism for generating silicic melts. The results suggest that following crystallization, the composition of the remaining ~30 wt.% liquids are consistent with returned lunar silicic fragments.

Finally, using crater counting methods I tested the stratigraphic relationship between the floor-fractured crater, Hansteen, and the silicic volcanic landform, Mons

Hansteen. Absolute model ages (AMAs) suggest that the basalts on the floor of Hansteen crater formed contemporaneously with Mons Hansteen, implying that bimodal volcanism might have played a role in silicic magma genesis on the Moon.

DEDICATION

To my parents and brother,

> Thank you for being my rock.

-and-

To my late maternal grandfather,

> Thata, I wish you were here. You are terribly missed.

ACKNOWLEDGMENTS

I want to begin by thanking my wonderful parents for all the sacrifices they made so that I could pursue my dreams. It was their unwavering support and faith in me that motivated me to keep going even during the darkest periods of my life, much of which was encountered in these past five years. I am also grateful to my younger brother whose support, wisdom, humor, and mere presence in Arizona made all the difference during the good times and the bad.

I am indebted to my advisor Mark Robinson for giving me my first research opportunity at LROC when I was a junior undergraduate student in Fall 2015. As it would turn out, my undergraduate research position evolved into my graduate research position. Mark, thank you for giving me the freedom to pursue any and every research area that interested me, for your valuable and timely feedback, for encouraging me to participate in LROC team meetings and telecons, and for giving me the opportunity to present my work at national and international conferences. I have truly enjoyed working with the LROC team and getting a taste of what it is to be a scientist.

To Christy Till, thank you for not only advising my second project but also for being my confidante. Thank you for taking time out of your busy schedule on several occasions to make sure I was okay and caring about me beyond academics.

I want to thank Tom Watters for graciously serving on my committee and for his co-authorship on my first manuscript. Tom, I greatly appreciate your valuable input and patience as I was getting oriented with geophysical modeling. I also want to thank my committee members Kelin Whipple and Joe O'Rourke for their support and encouragement.

TABLE OF CONTENTS

LIST OF TABLES

LIST OF FIGURES

CHAPTER 1

INTRODUCTION

Across the Solar System, volcanism is ubiquitous and is one of the dominant processes for forming planetary crusts. Crusts subsequently undergo large-scale deformation due to tectonic processes. As such, both volcanic and tectonic landforms are surface expressions of the inner workings of a planet. On Earth, volcanism and crustal deformation are primarily surface manifestations of plate tectonics (Kearney et al., 2007). In the absence of plate tectonics, the lunar crust has been deformed by endogenic processes following basin-scale impacts ($D \geq 300$ km). Understanding the formation and deformation of the lunar crust provides insights into the thermal and lithospheric evolution of the Moon. This work addresses two high-priority science questions outlined in the National Aeronautics and Space Administration (NASA) Planetary Decadal Survey – 1) How have myriad chemical and physical processes that shaped the Solar System operated, interacted, and evolved over time, and 2) What are the major surface features and modification processes on each of the inner planets? (NRC, 2011).

There is a distinct topographic and geochemical dichotomy between the nearside and farside. The lunar nearside surface is dominated by large impact basins filled with vast expanses of volcanic deposits. In the nearside, large impacts caused the thinning of the primary crust and were subsequently modified by the infilling of basaltic lavas (mare basalts) formed from the partial melting of the mantle. Much of the nearside surface makes up the Procellarum KREEP (potassium (K), rare earth elements (REE), phosphorus (P)) Terrane (PKT) (Jolliff et al., 2000; Wieczorek & Phillips, 2000).

The PKT is a thermally and chemically unique province delineated by thorium (Th) abundance of > 3 ppm, as measured by the Lunar Prospector Gamma Ray Spectrometer (LP-GRS) (Lawrence et al., 1999). The PKT is home to volcanic landforms such as shield volcanoes, silicic volcanic constructs, and tectonic landforms such as wrinkle ridges, graben, and floor-fractured craters. Four out of the six Apollo missions landed within the PKT; as such, heat flow measurements, seismic data, and much of the samples collected are representative of this region. Since the Apollo era, a wide variety of orbital datasets from the Clementine, Lunar Prospector, Kaguya, and the Lunar Reconnaissance Orbiter (LRO) have improved our understanding of the lunar surface (REFs). However, despite the wealth of data, the origin and evolution of the PKT is still poorly understood (REF). This dissertation focuses on floor-fractured craters and silicic volcanic landforms within the PKT to constrain its thermal and lithospheric evolution.

Floor-fractured craters are a class of impact craters that have undergone deformation due to volcano-tectonic processes and are preferentially distributed along the boundary of the PKT (Schultz, 1976; Jozwiak et al., 2012). In chapter 2, morphometric measurements from Lunar Reconnaissance Orbiter Camera (LROC) topographic datasets (Robinson et al., 2010; Scholten et al., 2010) are presented to test the extent of modification floor-fractured craters underwent relative to non-floor-fractured craters. Temporal heat flow and the geothermal gradient are modeled to test if conditions were viable for viscous relaxation of floor-fractured crater topography early in lunar geologic history (i.e., the pre-Nectarian period).

Silicic volcanic landforms on the Moon are rare and are distributed along the PKT boundary. The presence of silicic volcanic landforms on the Moon is enigmatic given that

the key ingredients (i.e., water and plate tectonics) that are typically invoked for producing large-scale silicic melts on Earth are not part of our foundational understanding of lunar formation and evolution. The work presented in chapter 3 tests the two leading hypotheses for the formation of silicic melts on the Moon – crustal melting and fractional crystallization of KREEP basalt magmas (Hagerty et al., 2003; Ryder, 1976). Both hypotheses are tested using the rhyolite-MELTS program to simulate silicic magma genesis in the lunar environment (Gualda et al., 2012). Chapter 3 also explores the Anorthosite-Mangerite-Charnockite-Granite (AMCG) suite as a potential terrestrial analog to lunar silicic volcanic landforms.

Silicic volcanic landforms and floor-fractured craters are located within ~50 km of each other. Chapter 4 is a pilot study that tests the potential stratigraphic relationship between Hansteen crater, a floor-fractured crater and Mons Hansteen, a silicic volcanic landform in southern PKT. Due to the lack of samples from both Mons Hansteen and Hansteen craters, absolute model ages (AMAs) are derived from crater size-frequency distribution (CSFD) measurements. From the derived AMAs, I test whether bimodal volcanism was plausible in the geologic history of the Moon.

Chapter 5 summarizes the findings of the three studies presented in this dissertation and outlines knowledge gaps that need to be addressed in the future.

References

Gualda, G. A. R., Ghiorso, M. S., Lemons, R. v., & Carley, T. L. (2012). Rhyolite-MELTS: A modified calibration of MELTS optimized for silica-rich, fluid-bearing magmatic systems. Journal of Petrology, 53(5), 875–890.

Hagerty, J. J., Lawrence, D. J., Hawke, B. R., Vaniman, D. T., Elphic, R. C., & Feldman, W. C. (2006). Refined thorium abundances for lunar red spots: Implications for evolved,

nonmare volcanism on the Moon. Journal of Geophysical Research E: Planets, 111(6), 1–20.

Jolliff, B. L., Gillis, J. J., Haskin, L. A., Korotev, R. L., and Wieczorek, M. A., 2000. Major Lunar Crustal Terranes: Surface Expression and Crust-Mantle Origin. Journal of Geophysical Research 105, 4197-4216.

Jozwiak, L. M., Head, J. W., and Zuber, M. T., 2012. Lunar Floor-Fractured Craters: Classification, Distribution, Origin, and Implications for Magmatism and Shallow Crustal Structure. Journal of Geophysical Research 117, E11005.

Kearney, P., Klepeis, K.A., and Vine, F.J. (2007). Global Tectonics. Wiley-Blackwell, UK.

Lawrence, D. J., Feldman, W. C., Barraclough, B. L., Binder, A. B., Elphic, R. C., Maurice, S., Miller, M. C., & Prettyman, T. H. (1999). High resolution measurements of absolute thorium abundances on the lunar surface. Geophysical Research Letters, 26(17), 2681–2684.
National Rearch Council, 2011. Vision and Voyages for Planetary Science in the Decade 2013- 2022. Washington, DC: The National Academies Press.

Robinson, M. S., Brylow, S. M., Tschimmel, M., 2010. Lunar Reconnaissance Orbiter Camera (LROC) Instrument Overview, Space Science Reviews 150, 81-124.

Ryder, G. (1976). Lunar sample 15405: Remnant of a KREEP basalt-granite differentiated pluton. *Earth and Planetary Science Letters,* 29(2), 255–268

Scholten, F., Oberst, J., Matz, K.-D., et al., 2012. GLD100: The Near-Global Lunar 100 m Raster DTM from LROC WAC Stereo Image Data. Journal of Geophysical Research 117, E00H17.

Schultz, P.H., 1976. Lunar Floor-Fractured Craters. The Moon 15, 241-273

Wieczorek, M. A., and Phillips, R. J., 2000. The "Procellarum KREEP Terrane": Implications for Mare Volcanism and Lunar Evolution. Journal of Geophysical Research 105, 20417-20430.

CHAPTER 2
ORIGIN OF LUNAR FLOOR-FRACTURED CRATERS: REVISITING THE

VISCOUS RELAXATION HYPOTHESIS

This is a manuscript in preparation with co-authors M. S. Robinson and T. R. Watters

2.1 Abstract

The origin of the Procellarum potassium, rare earth elements, and phosphorus (KREEP) Terrane (PKT) is not well understood. The PKT contains the largest concentration of floor-fractured craters and silicic volcanic landforms on the Moon. The mechanisms contributing to the formation of floor-fractured craters remain enigmatic after decades of study. The current widely accepted floor-fractured crater origin hypothesis is magmatic intrusion; primarily based on heterogeneous gravity anomalies exhibited by these landforms. However, unmodified craters also exhibit similar gravity characteristics, making the magmatic intrusion hypothesis problematic. The other hypothesized formation mechanism is viscous relaxation, where short wavelength topographic features of a crater undergo a reduction in amplitude in response to viscous flow enabled by elevated lithospheric temperatures.

Here we test the viscous relaxation and magmatic intrusion formation hypotheses using morphometric measurements, temporal heat flow models, and the spatial distribution of floor-fractured craters. Floor-fractured craters exhibit significantly lower volumes than unmodified craters of all age ranges, indicating an extensive modification to their topography. Rim-crest relief measurements reveal that ~40% of the floor-fractured craters exhibit lower rims than unmodified craters. Our estimated heat flow values within the PKT during floor-fractured crater formation (i.e., 4 Ga – 3.5 Ga) coupled with their

spatiotemporal association in areas with initial geothermal gradients $> 30°K\ km^{-1}$ and topographically subsided pre-Nectarian basins, is consistent with the viscous relaxation hypothesis. Lastly, we find circumstantial evidence for the existence of the Procellarum basin based on the spatial distribution of floor-fractured craters circumferential to the PKT.

2.2 Introduction
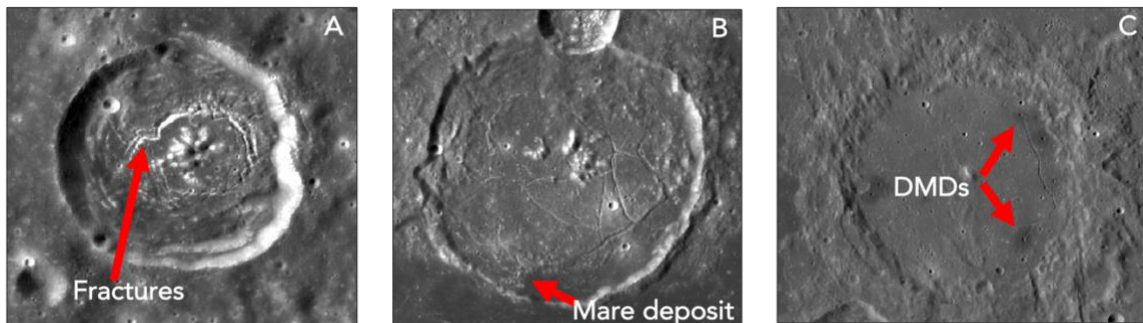
Figure 2.1 Characteristics of lunar floor-fractured craters. (A) Vitello crater (D = 40 km, -30.4°, 322.5°) exhibits radial/concentric fractures, (B) Gassendi crater (D = 100km, -17.4°, 320°) exhibits mare basalt infill, and (C) Alphonsus crater (D = 110km, -13.4°, 357°) exhibits DMDs.

Floor-fractured craters are impact craters that underwent modification by volcano-tectonic processes as evidenced by polygonal, radial, or concentric fractures, normal faults, and graben. They sometimes host volcanic landforms such as mare basalt infill and dark mantle deposits (DMDs) (Fig. 2.1 A-C). Morphometric studies show that floor-fractured craters exhibit low depth/diameter (d/D) ratios compared to morphologically fresh craters (i.e., Copernican and Eratosthenian) of the same size (Schultz, 1976; Jozwiak et al., 2012; Ravi and Robinson, 2019). Floor-fractured craters were formed either by viscous relaxation

or magmatic intrusion (Schultz, 1976; Jozwiak et al., 2012; Hall et al., 1981). In the magmatic intrusion hypothesis, crater floors undergo uplift and fracturing due to an intruding magma body such as a dike or a laccolith. This mechanism contributes to floor uplift and thus shallowing of the craters, as evidenced by low d/D ratios. In the viscous relaxation hypothesis, short wavelength topographic features of the host crater (i.e., crater rims) undergo modification through a reduction in amplitude long wavelength crater floors are uplifted due to lateral viscous flow of crustal materials in response to elevated temperatures.

Floor-fractured craters occur preferentially along mare basin margins with >60% concentrated along the western boundary of the Procellarum KREEP (potassium (K), rare earth elements (REE), and phosphorus (P)) Terrane (PKT; Fig. 2.2). However, the age of the host crater, the timing of fracture formation, and the formation mechanism of floor-fractured craters are not well constrained.

Here we test the leading hypotheses for the formation of floor-fractured craters using morphometric measurements (crater volumes and rim-crest height measurements) and the geospatial association of floor-fractured craters with mare basins using image and topography datasets from the Lunar Reconnaissance Orbiter Camera (LROC; Scholten et al., 2012; Robinson et al., 2010). Determining the mechanism(s) that resulted in these landforms and documenting their spatial distribution is essential to constraining spatio-temporal variations in the heat flow within and the thickness of the lunar lithosphere.

2.3 Geologic Background

2.3.1 Procellarum KREEP Terrane

There are three major geological provinces on the Moon – the PKT (Fig. 2.2), the Feldspathic Highlands Terrane (FHT), and the South Pole Aitken Terrane (SPAT) (Jolliff et al., 2000). Observations from the Lunar Prospector Gamma Ray Spectrometer (LP-GRS) shows that the PKT is a thermally and geochemically unique province delimited by Th abundance (Wieczorek and Phillips, 2000; Jolliff et al., 2000). The highly incompatible KREEP material in urKREEP formed the last remains of the lunar magma ocean between the anorthositic crust and the denser, mafic-ultramafic mantle (Wieczorek and Phillips, 2000; Jolliff et al., 2000; Warren, 1985; Wood et al., 1970).

There are two widely debated hypotheses for the presence of the PKT. On the one hand, the presence of the PKT and the asymmetry in the crustal thickness between the near and farside are attributed to the formation of a "Gargantuan basin" early in lunar history at ~4.1-4.2 Ga, as evidenced by whole-rock isochrons from returned Apollo samples (Cadogan, 1974). Additionally, the thinner nearside crust (relative to the farside) is attributed to ejecta from the "Gargantuan basin." Whitaker (1981) postulated the presence of the "Gargantuan basin," henceforth, the Procellarum basin, bounded by Mare Frigoris to the north, Mare Vaporum to the east, Mare Cognitum to the south, and western Oceanus Procellarum. The highly subdued relief (i.e., lack of multiple ring systems common in large impact basins) of the putative Procellarum basin is attributed to its formation in early lunar history, at a time when the relatively thin lithosphere coupled with relatively higher geothermal gradients led to viscous relaxation (Whitaker, 1981). Additionally, formation

8

of the Procellarum basin would have excavated and distributed KREEP-rich materials (Whitaker, 1981; Wilhelms, 1983; Wilhelms, 1987; McEwen, 1994).

Alternatively, the Imbrium impact event was responsible for excavating KREEP-rich materials as evidenced by high-Th concentrations in the central nearside (e.g., Schultz and Spudis, 1985; Spudis and Schultz, 1985). In this hypothesis, the presence of the PKT is attributed solely to the Imbrium impact event (e.g., Schultz and Spudis, 1985; Spudis and Schultz, 1985), and the boundary for the proposed Procellarum basin (Whitaker, 1981) represents the outer ring of the Imbrium basin (Schultz and Spudis, 1985; Spudis and Schultz, 1985; Spudis, 1993).
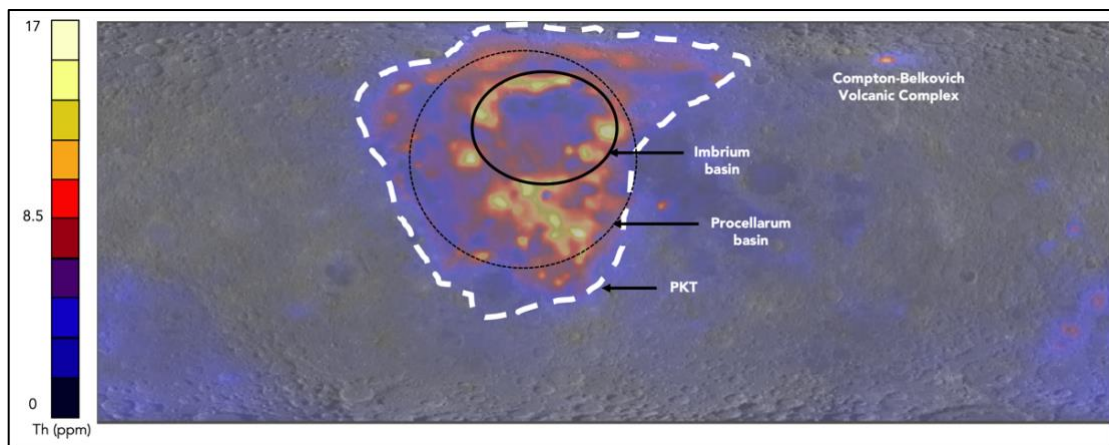
Figure 2.2 Lunar Prospector Gamma Ray Spectrometer (LP-GRS) thorium abundance map (Lawrence et al., 1998) overlain on the Lunar Reconnaissance Orbiter Camera (LROC) Wide Angle Camera (WAC) monochrome mosaic (Robinson et al., 2010). Lat: $\pm$ 65°; Lon: $\pm$ 180°. The PKT is defined by this compositional anomaly and is shown in white (Jolliff et al., 2000; Wieczorek and Phillips, 2000), the Imbrium basin (Spudis, 1993) is shown in a solid black line, and the proposed Procellarum basin (Whitaker, 1981) in shown in a dotted black line.

2.3.2 Formation hypotheses for Floor-fractured craters

2.3.2.1 Magmatic intrusion
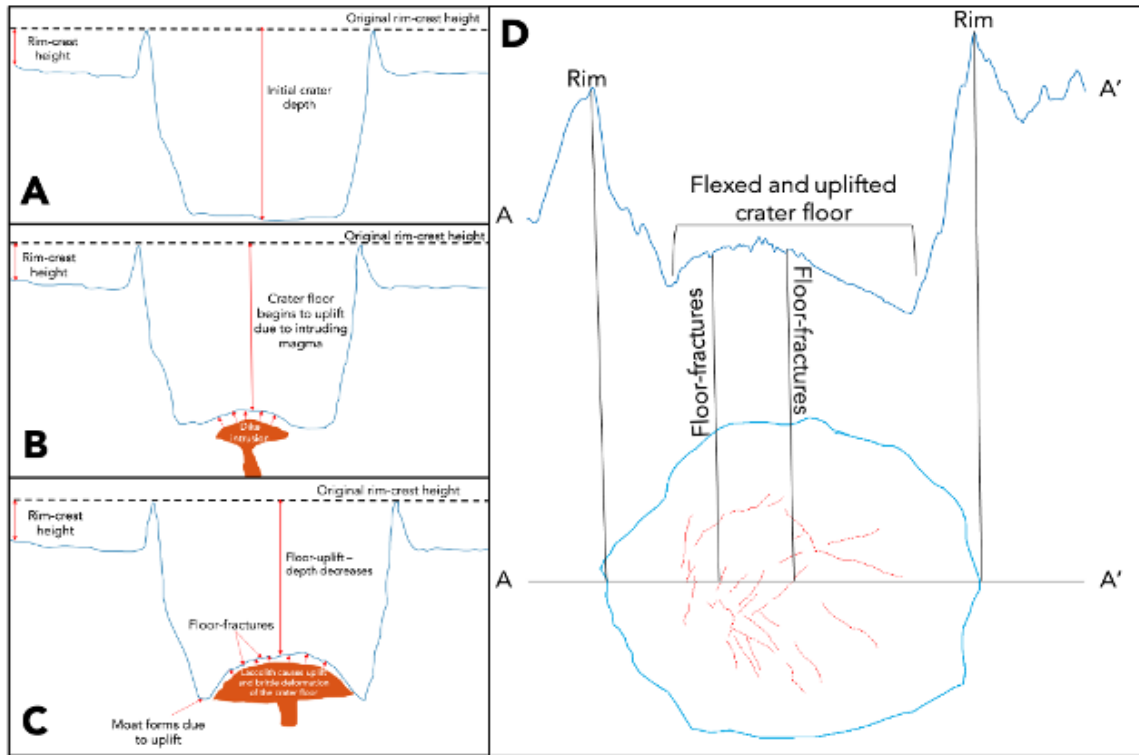
Figure 2.3 Diagram illustrating the magmatic intrusion hypothesis. (A) Pre-existing impact crater topography; (B) the crater floor experiences flexure in response to intruding magma at the base of the crater floor; (C) the intruding laccolith causes uplift and brittle deformation of the crater floor, resulting in fractures; (D) topographic profile of Mersenius crater (floor-fractured crater) and corresponding plan view.

In the magmatic intrusion model, the floors of pre-existing craters are uplifted and deformed by the intrusion of dikes and sills (Schultz, 1976; Jozwiak et al., 2012). Since most floor-fractured craters formed along the margins of impact basins, it was postulated that the magmatic intrusions that gave rise to the maria likely also deformed overlying impact craters (Schultz, 1976; Jozwiak et al., 2012). The intruding laccolith causes the

crater floor uplift, which results in isotropic extensional stresses, thereby forming polygonal normal faults and graben (Fig. 2.3). The magmatic intrusion mechanism only affects long-wavelength topographic features such as the crater floor, while short wavelength topographic features such as the rim-crest height remain unchanged (Schultz, 1976; Jozwiak et al., 2012; Fig. 2.3). However, the shallowing of crater floors could also be the effect of viscous relaxation (Schultz, 1976; Hall et al., 1981; Jozwiak et al., 2012). Jozwiak et al. (2017) interpreted heterogeneous gravity anomalies associated with floor-fractured craters resulted from magmatic intrusions of varying density (Jozwiak et al., 2017). However, we observe that the floors of morphologically fresh craters also exhibit similar heterogeneous gravity anomalies, inconsistent with the magmatic intrusion hypothesis.

2.3.2.2 Viscous relaxation
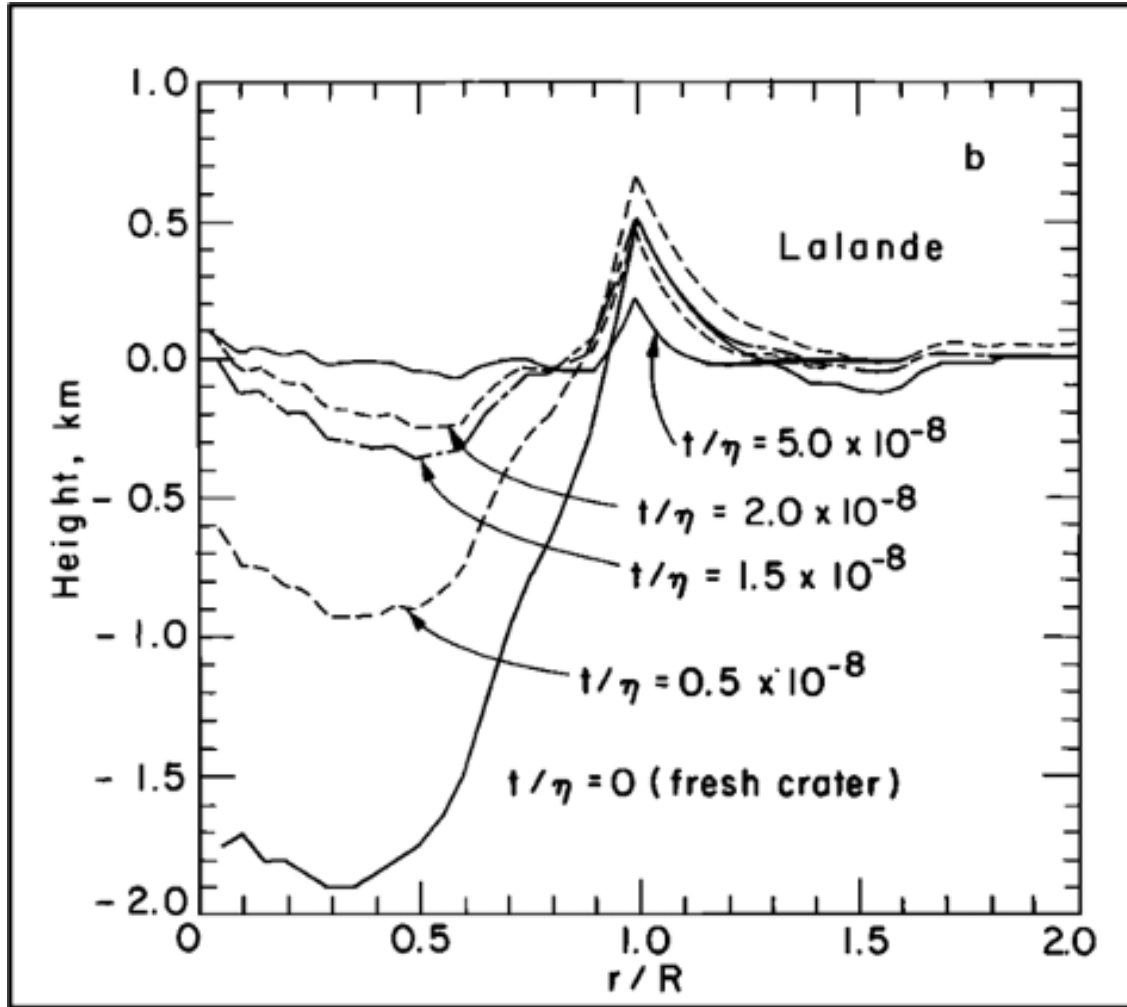
Figure 2.4 Diagram illustrating the modification of Lalande crater due to viscous relaxation (Hall et al., 1981). In this half-space model, both long and short wavelength features experience modification as exhibited by the shallowing of crater floor and the subsidence of the rim-crest.

In the viscous relaxation model, the pre-existing crater (i.e., the crater prior to fracture formation) undergoes modification and deformation due to thermal anomalies (Schultz, 1976; Hall et al., 1981; Jozwiak et al., 2012). Viscous relaxation contributed to the

shallowing of long-wavelength topographic features (i.e., crater floors) via uplift and the subsidence of short wavelength topographic features (i.e., rim-crest relief) of the impact craters that formed during basin relaxation (Fig. 2.4). While the duration of basin-scale viscous relaxation is not well constrained, it is likely that Copernican and Eratosthenian aged craters are largely unaffected by this mechanism. However, rim-crest relief measurements of floor-fractured craters (n = 10) appear unchanged compared to Copernican and Eratosthenian age craters, leading Jozwiak et al. (2012) to discount viscous relaxation as a formation mechanism (Fig. 2.9). Dombard and Gillis (2001) tested the viscous relaxation hypothesis by approximating the rheology of the lunar lithosphere using the strain rate ($\dot{\epsilon}$) of Columbia dry diabase and present-day heat flow measurements and concluded that the lunar lithosphere was too rigid for viscous relaxation to have contributed to the formation of floor-fractured craters (Dombard and Gillis, 2001).

2.3.3 Spatial distribution of floor-fractured craters with respect to impact basins

Floor-fractured craters are generally distributed along the mare-highlands boundary, with >50% ($n = 100$) preferentially clustered along the boundary of the PKT, 4% ($n = 5$) within Imbrian basins, 15% ($n = 30$) within Nectarian basins, and 32% ($n = 65$) within pre-Nectarian basins (Schultz, 1976; Jozwiak et al., 2012; this study; Fig. 2.5).

Lunar impact basins (D $\geq$ 300km) exhibit a concentric peak ring, which formed between 4.3 Ga and ~3.5 Ga. The South Pole Aitken (SPA basin) is the oldest, and the Orientale basin the youngest (Hartmann and Wood, 1971; Wilhelms, 1987; Spudis, 1993). The basins are divided into three groups based on morphologic characteristics and gravity signatures – group 1 basins exhibit well-preserved topography, strong gravity signatures, and little to no mare infill; group 2 basins exhibit large volumes of mare basalt deposits,

and their topography and gravity are primarily influenced by mare deposits; and group 3 basins exhibit low amplitude relief and weak gravity signatures (Table 1; Mohit and Phillips, 2006). All group 3 basins are pre-Nectarian in age, suggesting that they likely underwent viscous relaxation, given that the early lunar lithosphere was probably thinner and weaker, consistent with the highly subdued relief of these basins (Table 1; Mohit and Phillips, 2006). While previous studies report the association of floor-fractured craters with mare basins, their potential association with pre-Nectarian, group 3 basins have not yet been observed.
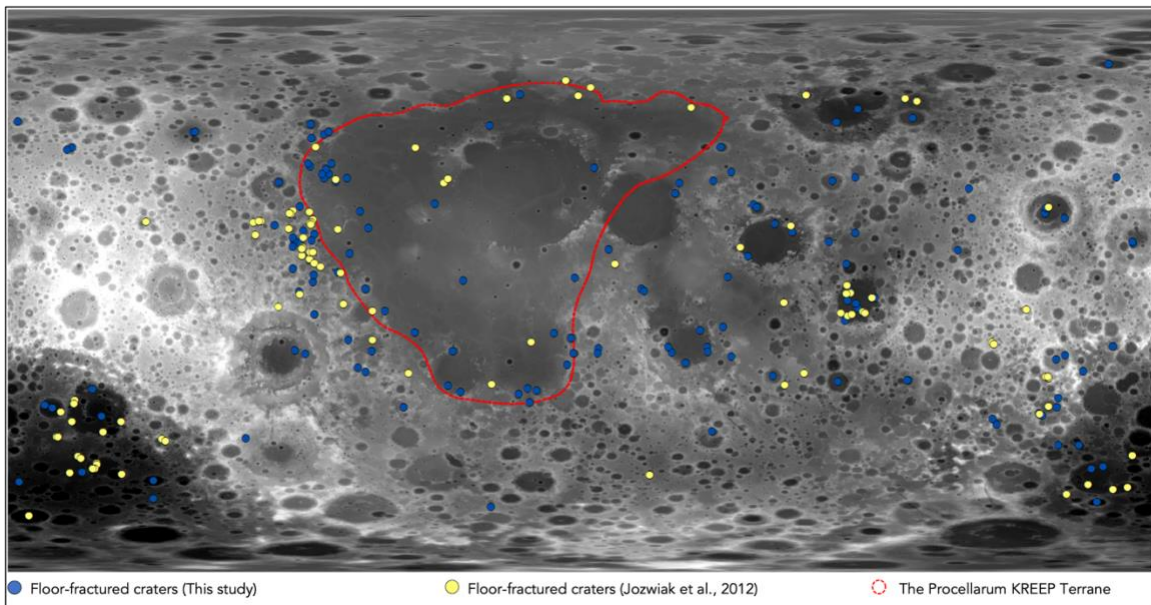
Figure 2.5 Global spatial distribution of floor-fractured craters. The PKT is shown in red (Wieczorek and Phillips, 2000). Base map: LROC WAC GLD100 DTM (Scholten et al., 2012), map is centered on 0°N,0°E; Lat: $\pm$ 90°; Lon:$\pm$180°.

Table 2.1 Lunar basins classified based on their topographic characteristics and gravity signatures (from Mohit and Phillips, 2006). [a]P: pre-Nectarian; N: Nectarian; I: Imbrian; numbers increase with age.

Basin	Diameter (km)	Age[a]	Group	Region
South Pole-Aitken	2500	P-14	1	SPA
Orientale	930	I-1	1	Limb
Mendel-Rydberg	630	N-6	1	Limb
Humboldtianum	600	N-4	1	Limb
Freundlich-Sharanov	600	P-8	1	Far
Hertzsprung	570	N-4	1	Far
Coulomb-Sarton	530	P-11	1	Far
Korolev	440	N-6	1	Far
Moscoviense	440	N-6	1	Far
Imbrium	1160	I-3	2	PKT
Crisium	1060	N-4	2	Near
Nectaris	860	N-6	2	Near
Smythii	840	P-11	2	Limb

Humorum	820	N-4	2	PKT
Serenitatis	740	N-4	2	Near
Grimaldi	430	P-7	2	PKT-adj
Fecunditatis	990	P-13	3	Near
Australe	880	P-13	3	Limb
Tranquillitatis	800	P-13	3	Near
Mutus-Vlacq	700	P-13	3	Near
NW Procellarum	700	P	3	PKT
Tsiolkovskiy- Stark	700	P-14	3	Far
Nubium	690	P-13	3	PKT
Lomonosov- Fleming	620	P-13	3	Far
Balmer	500	P(>=11)	3	Near
Keeler- Heaviside	500	P-12	3	Far

2.4 Methods

2.4.1 Volumetric analysis

Crater volume as a function of diameter is an indicator of the extent of crater modification due to uplift and intrusion (Fig. 2.6). We estimate the volumes of floor-fractured craters ($n = 200$; Jozwiak et al., 2012; this study) and compare them to volumes

of unmodified craters of Copernican and Eratosthenian ($n = 170$; Ravi et al., 2017), Imbrian ($n = 14$; Wilhelms, 1987), and Nectarian ($n = 30$; Wilhelms, 1987) age. The volumes are calculated using the LROC WAC GLD100 Digital Terrain Model (DTM) at the 100 meter/pixel scale (Scholten et al., 2012). We exclude non-floor-fractured craters with mare basalt infill as they would skew our results. The volume of the crater V is given by:

$$V = \sum_{i=1}^{n} (E_R - E_i) \times P^2$$

where E_R is the average rim elevation, E_i is the elevation at each point inside the crater, and P is the pixel scale.
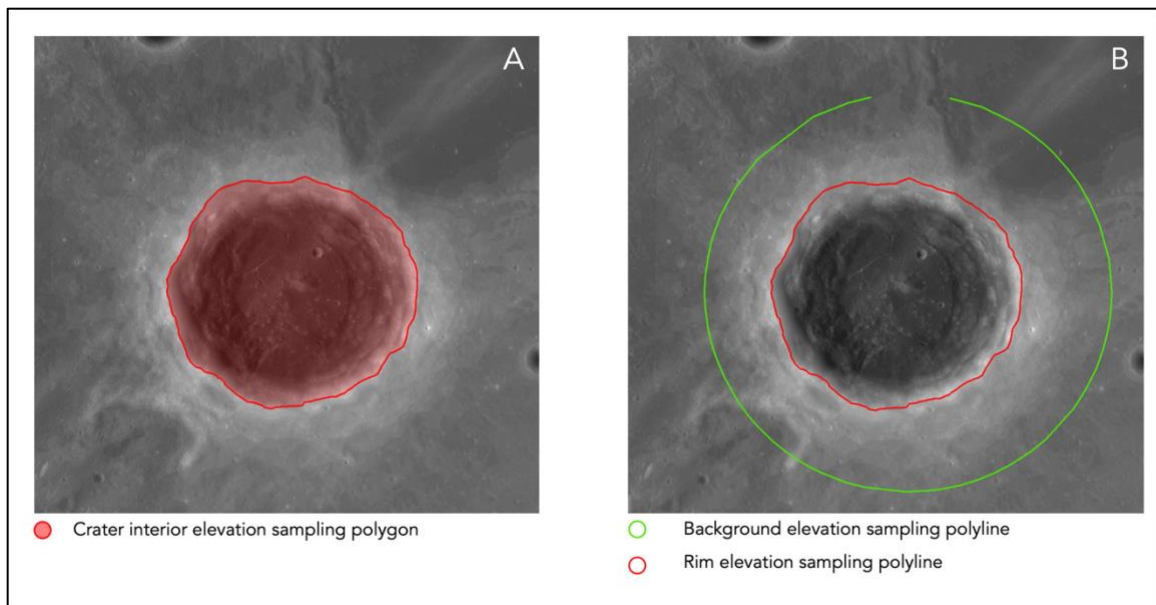
Figure 2.6 Visual representation of the methods used to compute (A) crater volume and (B) crater rim-crest heights. The floor-fractured crater shown here is Cardanus (D = 50 km). Base maps: LROC WAC GLD100 DTM (Scholten et al., 2012) overlain on LROC WAC monochrome mosaic (Robinson et al., 2009).

2.4.2 Rim-crest height measurements

We measure and compute the exterior rim-crest heights of floor-fractured craters (n = 200; Jozwiak et al., 2012; Ravi and Robinson, 2019) using the LROC WAC GLD100 DTM 100 meter/pixel scale (Scholten et al., 2012). We then compare the rim crest heights to non-floor-fractured craters of Imbrian (n = 14; Wilhelms, 1987), Nectarian (n = 30; Wilhelms, 1987), and pre-Nectarian (n = 51; Losiak et al., 2014) ages to test the viscous relaxation hypothesis (Fig. 2.6). The relief H of the rim-crest of a crater is given by:

$$H = E_R - E_B$$

where E_B is the average elevation of the surrounding area beyond the ejecta blanket (i.e., 1.5 radii from the center of the crater; Fig. 2.6).

2.4.3 Heat flow model

The present-day heat flow at the Apollo 15 and Apollo 17 sites were measured as 21mWm^{-2} and 15 mWm^{-2} respectively (Langseth et al., 1976). The thickness of the Earth's elastic lithosphere is given by the depth to the 250°C to 450°C isotherm (Chen & Molnar, 1983; Wiens & Stein, 1983; see fig. 6 in Watters, 2022), which is likely appropriate for the lunar highlands. This corresponds to a present-day lunar lithospheric thickness of 30 km to 50 km (Watters, 2022). The evolution of the lunar lithospheric thickness over time is not well constrained. Watters (2022) estimated the thickness of the lunar lithosphere beneath the PKT to be 10-18km if the heat flux was comparable to that of old terrestrial oceanic lithosphere, and ~5–9 km if heat flux was comparable to young oceanic lithosphere during early wrinkle ridge formation (~4Ga).

We estimate heat flow measurements beneath the PKT at 4Ga using Fourier's law (Turcotte and Schubert, 1982).

Fourier's law is given by:

$$q = \frac{k \, \Delta T}{l}$$

where, q is the heat flux through a slab of thickness l, k is the thermal conductivity of the slab material assumed to be 2 W m^{-1} K^{-1}, which is a reasonable estimate for the fractured anorthositic highlands crust (Wieczorek & Phillips, 2000; Watters, 2022), and ΔT is the temperature difference between the surface and base of the elastic lithosphere (Turcotte and Schubert, 1982). The global average surface temperature is estimated to be 262 K (Hurley et al., 2015). We find that a 10% uncertainty in the global average surface temperatures does not have any significant effect on the heat flow calculations. The heat flow measurements are calculated assuming an initial lithospheric thickness of 5 km to 9 km and 10 km to 18 km (Watters, 2022). The thickness of the oceanic lithosphere increases linearly with the $\sqrt{t}$, however this relation does not hold for t $\geq$ 70 Ma (Calmant et al., 1990). Therefore, we assume a simple linear increase in the thickness of the lithosphere over a timeframe extending billions of years.

2.5   Results

2.5.1 Volumetric analysis

The volumes of floor-fractured craters are 45%, 90%, and 35% that of unmodified craters of Copernican and Eratosthenian (combined), Imbrian, and Nectarian age craters normalized to their diameters, respectively (this study; Fig. 2.7). Both magmatic intrusion and viscous relaxation can contribute to the shallowing of crater floors and as such overall volume of floor-fractured craters. Hence, this does not constrain the mechanism, prompting

19

the need to measure short-wavelength topographic features such as exterior rim-crest relief measurements.
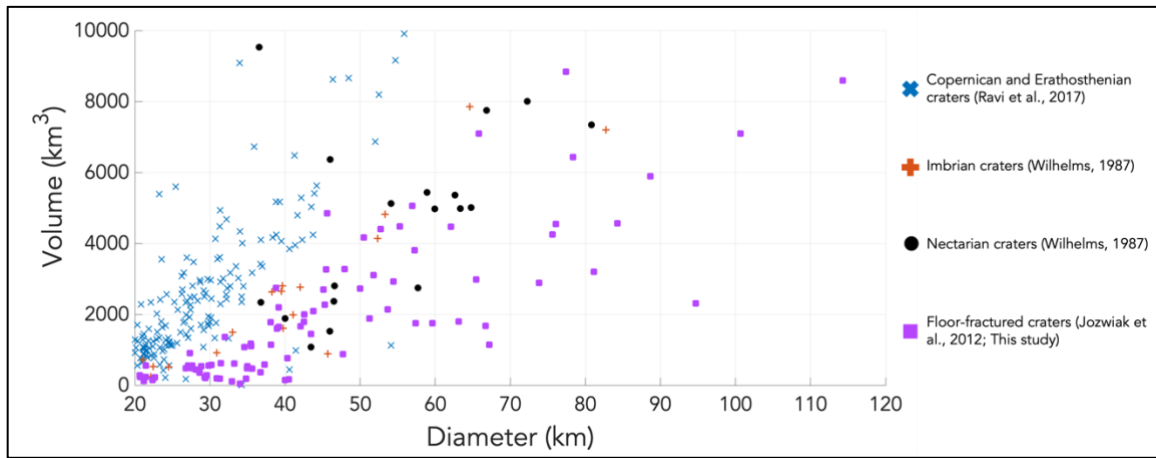
Figure 2.7 Volume vs. diameter for floor-fractured craters compared to unmodified Nectarian, Imbrian, and Copernican and Eratosthenian relative ages.

2.5.2 Rim-crest height measurements

Jozwiak et al. (2012) noted that both floor-fractured craters and non-floor-fractured craters of Copernican and Eratosthenian age exhibit similar rim-crest relief with respect to diameter, leading them to discount the viscous relaxation hypothesis. However, we noted that ~40% of floor-fractured craters exhibit rim-crest heights lower than non-floor-fractured craters of Imbrian, Nectarian, and pre-Nectarian ages with respect to diameter (Fig. 2.8), consistent with the viscous relaxation hypothesis. Furthermore, we compared our rim-crest relief measurements of floor-fractured craters to that of Jozwiak et al. (2012), and non-floor-fractured craters of Copernican and Eratosthenian craters from Pike (1976) (Fig. 2.9). We find that 96% of floor-fractured craters have lower rim-crest heights compared to unmodified Copernican and Eratosthenian craters from Pike (1976) (Fig. 2.9). Jozwiak et al. (2012) only reported rim-crest relief measurements for 11 floor-fractured

20

craters and five fresh (i.e., Copernican and Eratosthenian age) craters, leading them to reject the viscous relaxation hypothesis as a plausible formation mechanism for floor-fractured craters (Fig. 2.9). The discrepancies between the rim-crest height measurements of Jozwiak et al. (2012), Pike (1976), and this study remain unexplained, as the results of Jozwiak et al. (2012) are not reproducible.
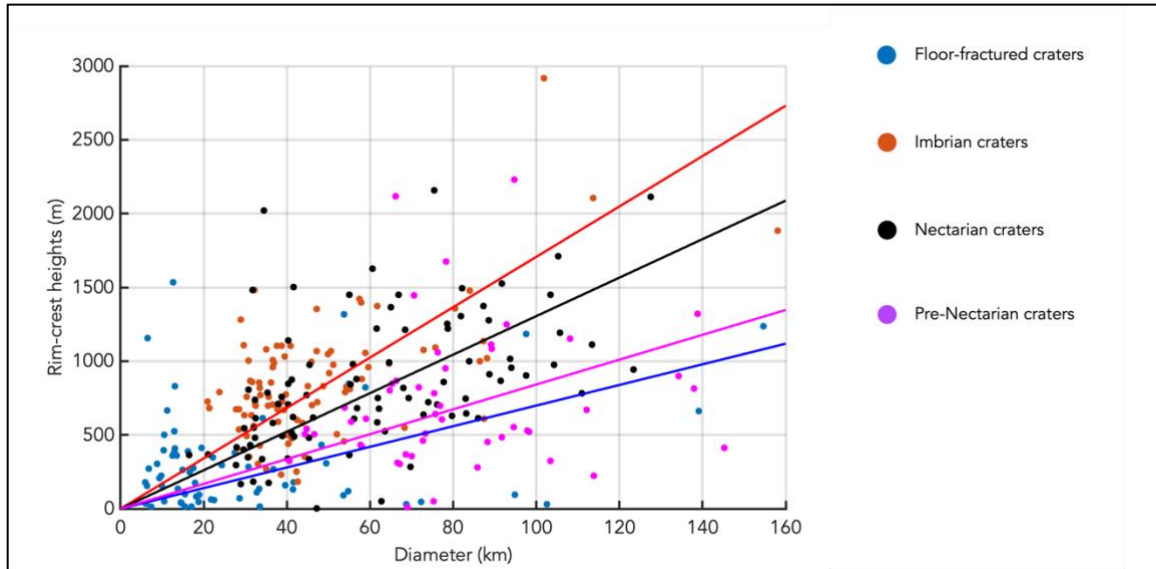
Figure 2.8 Rim-crest height measurements for floor-fractured craters (Jozwiak et al., 2012; this study) compared to unmodified craters of pre-Nectarian (Wilhelms, 1987), Nectarian (Wilhelms, 1987), and Imbrian (Wilhelms, 1987) relative ages. The data are fitted to a linear regression.
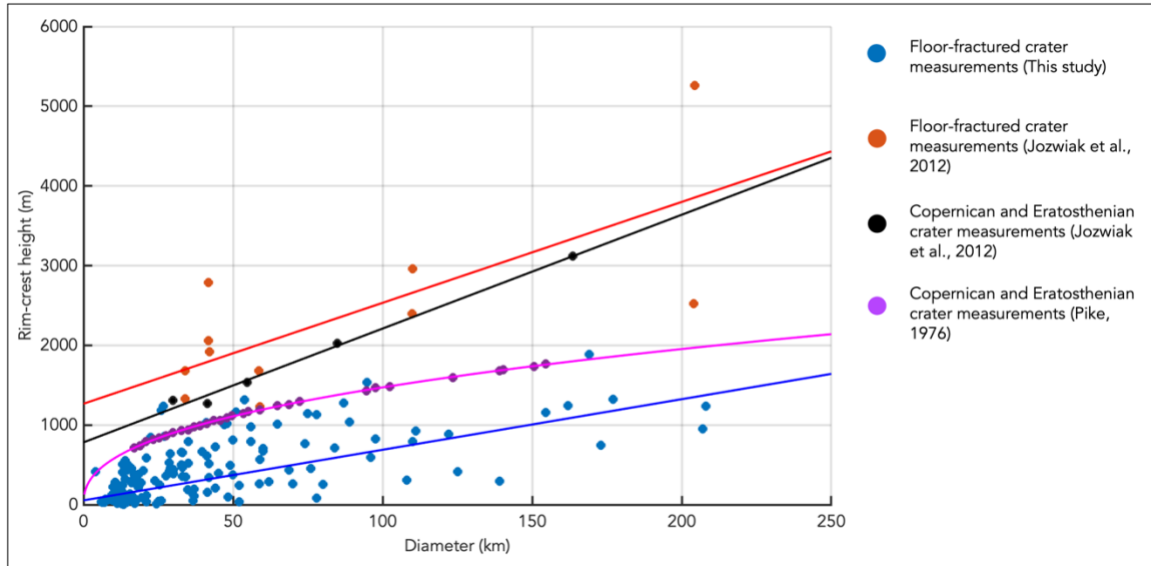
Figure 2.9 Rim-crest height measurements for floor-fractured craters (Jozwiak et al., 2012; this study) compared to fresh craters (Pike,1976; Jozwiak et al., 2012). Data from this study and Jozwiak et al. (2012) are fitted to a linear regression. Data from Pike (1976) are fitted to a power law regression.

2.5.3 Heat flow model

Based on the shock physics code iSALE and thermal models, Ding and Zhu (2022) showed that a thermal gradient of >30 K km^{-1} is required for viscous relaxation of lunar topography. The threshold of 30 K km^{-1} was calculated based on the assumption of Th abundance of 4ppm for the bulk lunar crust or 10ppm for a 10km thick KREEP layer beneath the crust. We calculated the heat flow beneath the PKT as 104 mWm^{-2} to 64 mWm^{-2} (assuming initial elastic lithospheric thickness T_e = 5 km to 9 km) and 52mWm^{-2} to 41mWm^{-2} (assuming initial T_e = 10 km to 18 km) between 4 Ga and 3.5 Ga (Fig. 2.10), which are timescales corresponding to the formation of floor-fractured craters (Schultz, 1976; Jozwiak et al., 2012). We calculated the corresponding thermal gradients as 52° K

km^{-1} to 32° K km^{-1} (assuming initial T_e = 5 km to 9 km) during the formation of floor-fractured craters (Fig. 2.11), consistent with the conditions favorable for viscous relaxation (Ding and Zhu, 2022).

Kamata et al. (2013) computed heat flow and corresponding thermal gradients of lunar impact basins at the time of their formation (Fig. 2.12). We observe that floor-fractured craters are preferentially distributed within basins with initial thermal gradients > 30° K km^{-1}, consistent with viscous relaxation (Fig. 2.12).
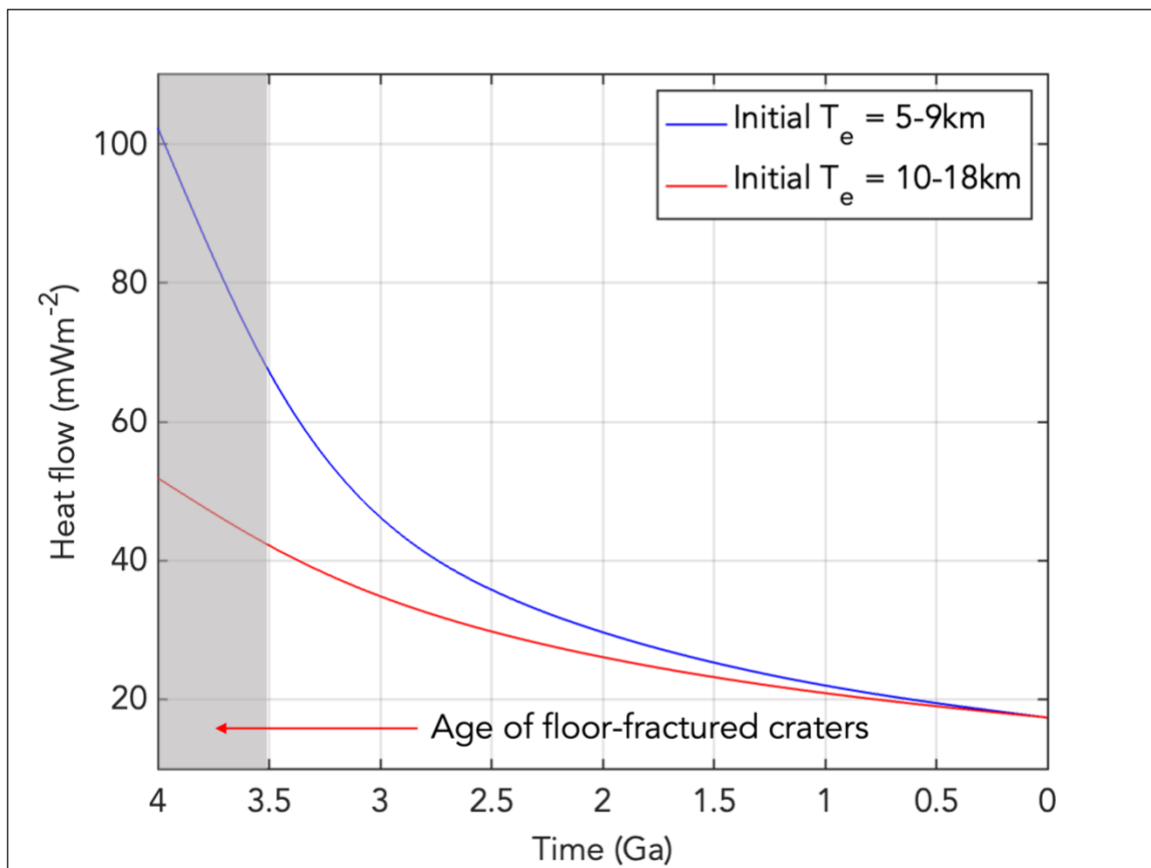
Figure 2.10 Temporal heat flow variations beneath the PKT. The blue line represents an initial lithospheric thickness of 5 km to 9 km, and the red line represents an initial lithospheric thickness of 10 km to18 km given by the 250°C and 450°C isotherms

respectively. Shading indicates the range in age estimated for the formation of floor-fractured craters.
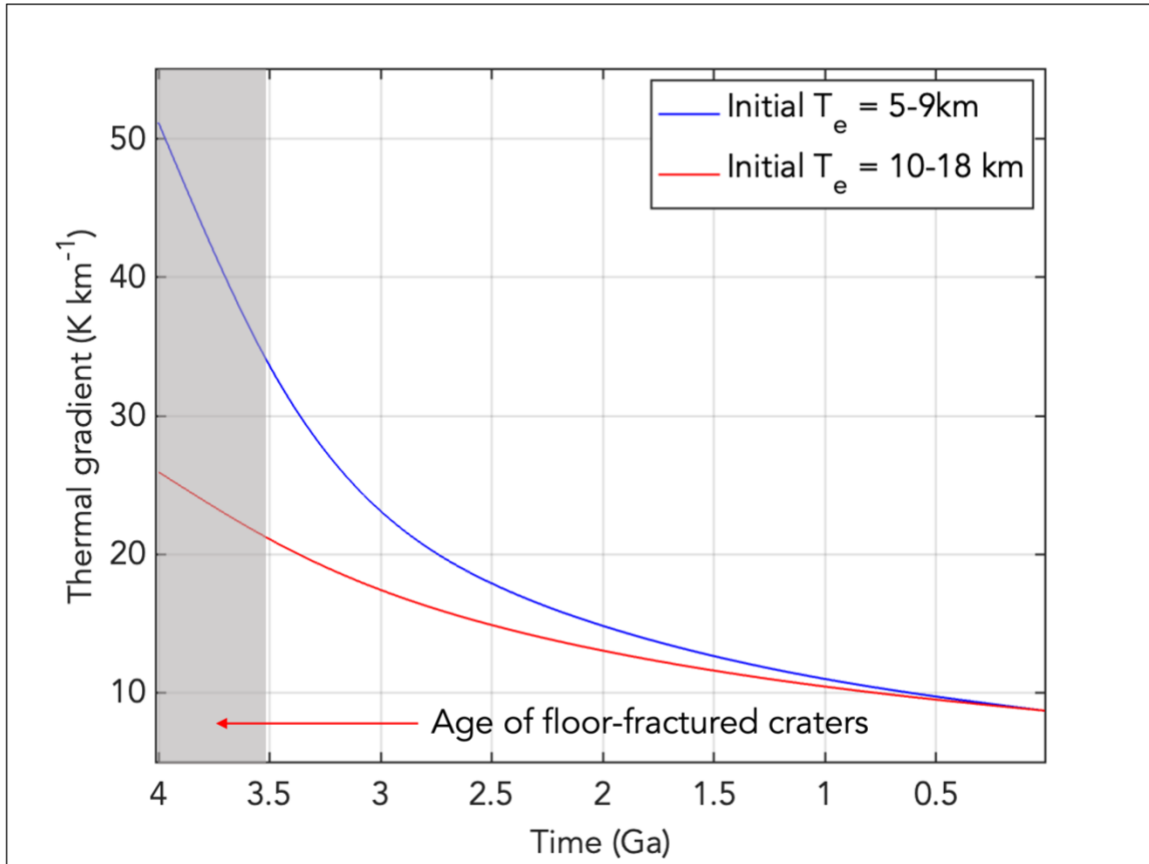
Figure 2.11 Temporal variations in the thermal gradient beneath the PKT derived from heat flow models. Shading indicates the range in age estimated for the formation of floor-fractured craters.
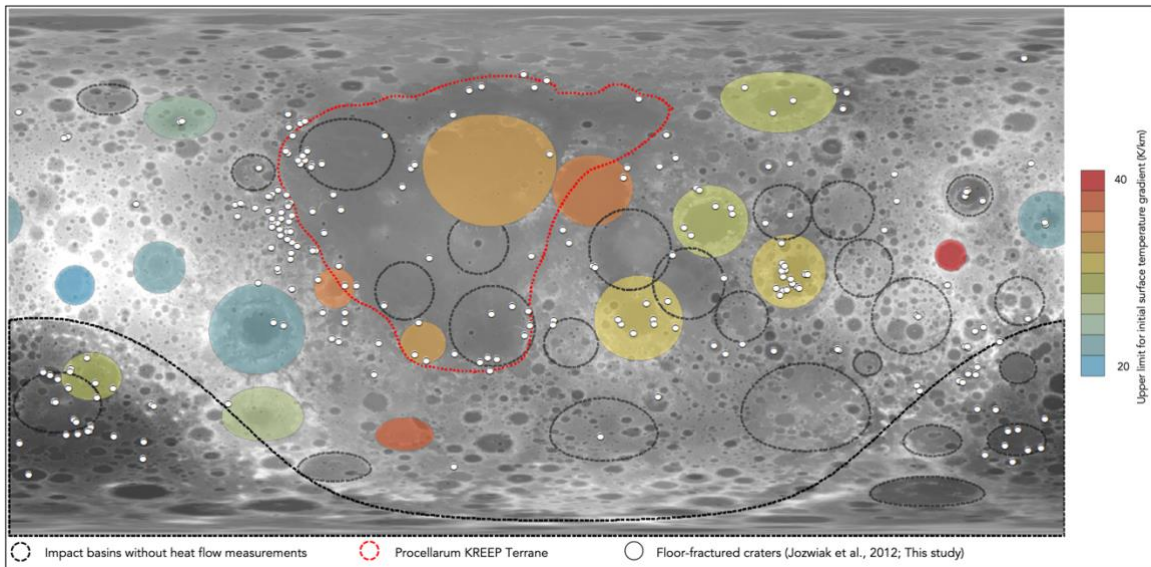
Figure 2.12 Spatial distribution of floor-fractured craters, the PKT, and impact basins with modeled initial thermal gradients (i.e., thermal gradients due to basin impacts) (Kamata et al., 2013). Base map: LROC WAC GLD100 DTM (Scholten et al., 2012), map is centered on 0°N,0°E; Lat: ± 90°; Lon: ±180°.

2.5.4 Spatial distribution of floor-fractured craters with respect to impact basins
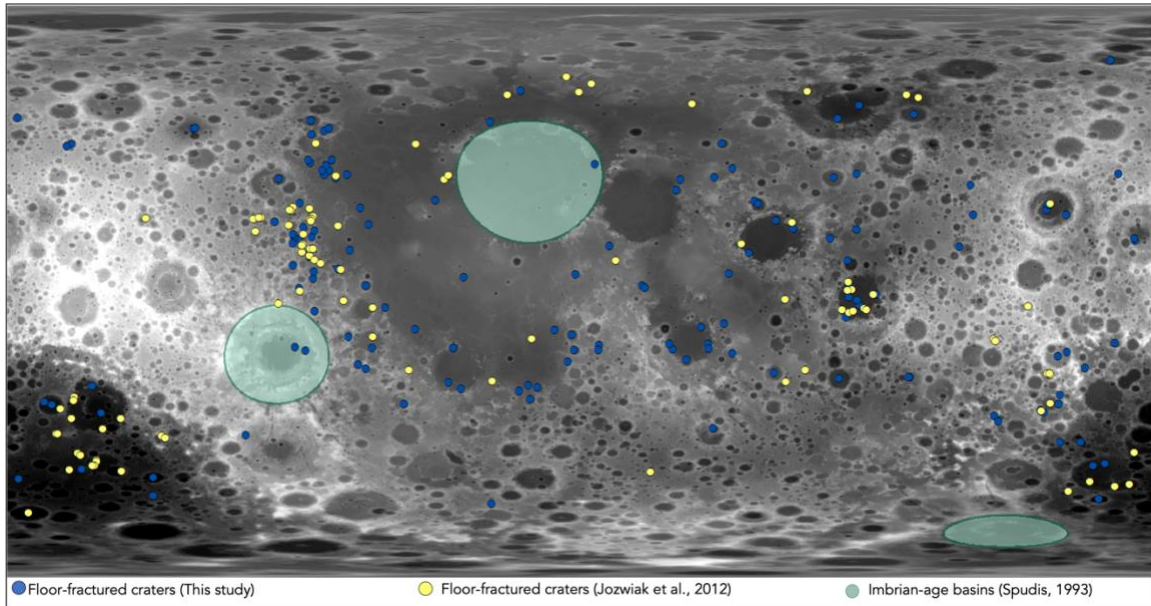
Figure 2.14 Global spatial distribution of floor-fractured craters with respect to Imbrian-age basins. Base map: LROC WAC GLD100 DTM (Scholten et al., 2012). Base map: LROC WAC GLD100 (Scholten et al., 2012), map centered on 0°N, 0°E; Lat: $\pm$ 90°; Lon: $\pm$ 180°.
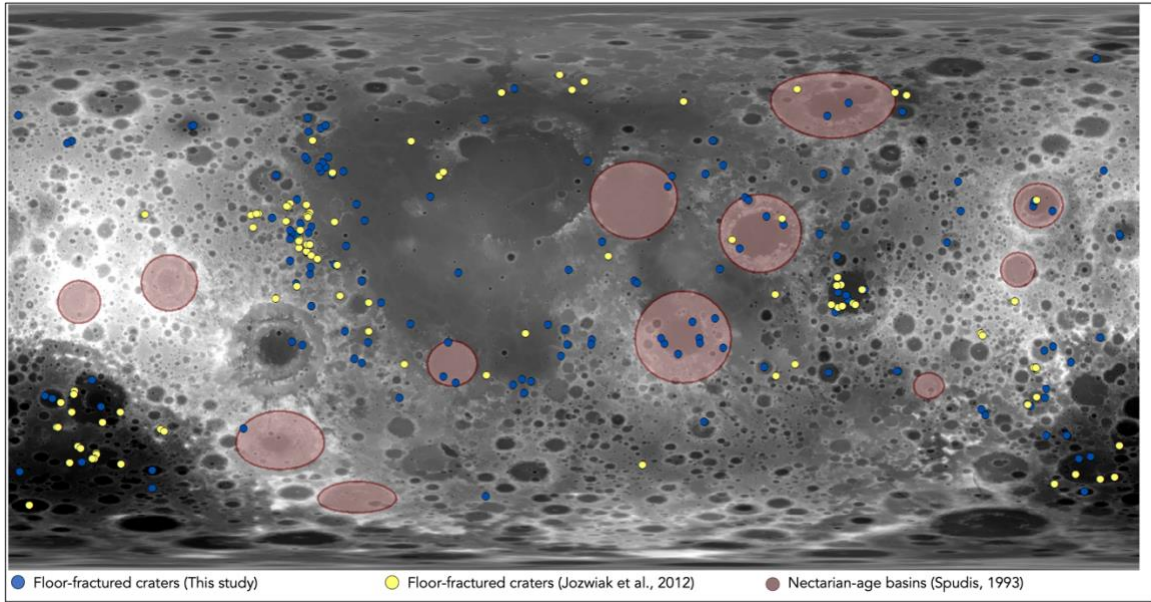
Figure 2.15 Global spatial distribution of floor-fractured craters with respect to Nectarian-age basins. Base map: LROC WAC GLD100 (Scholten et al., 2012), map centered on 0°N, 0°E; Lat: ± 90°; Lon: ± 180°.
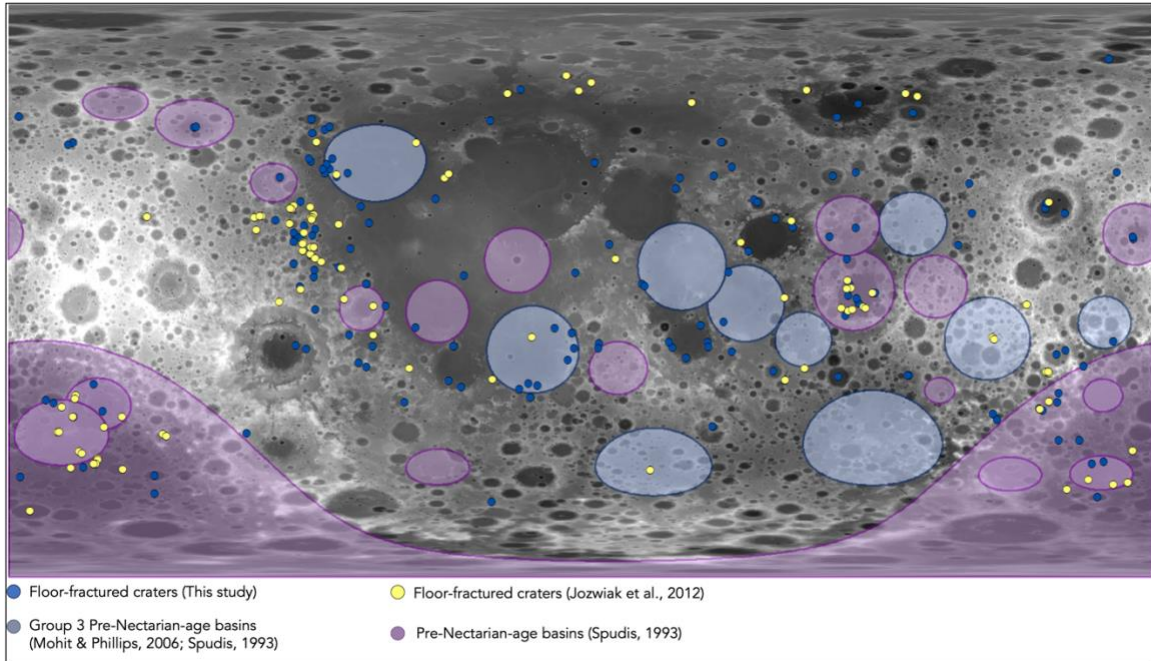
Figure 2.16 Global spatial distribution of floor-fractured craters with respect to pre-Nectarian-age basins. Base map: LROC WAC GLD100 (Scholten et al., 2012), map centered on 0°E; Lat: ± 90°; Lon: ± 180°.
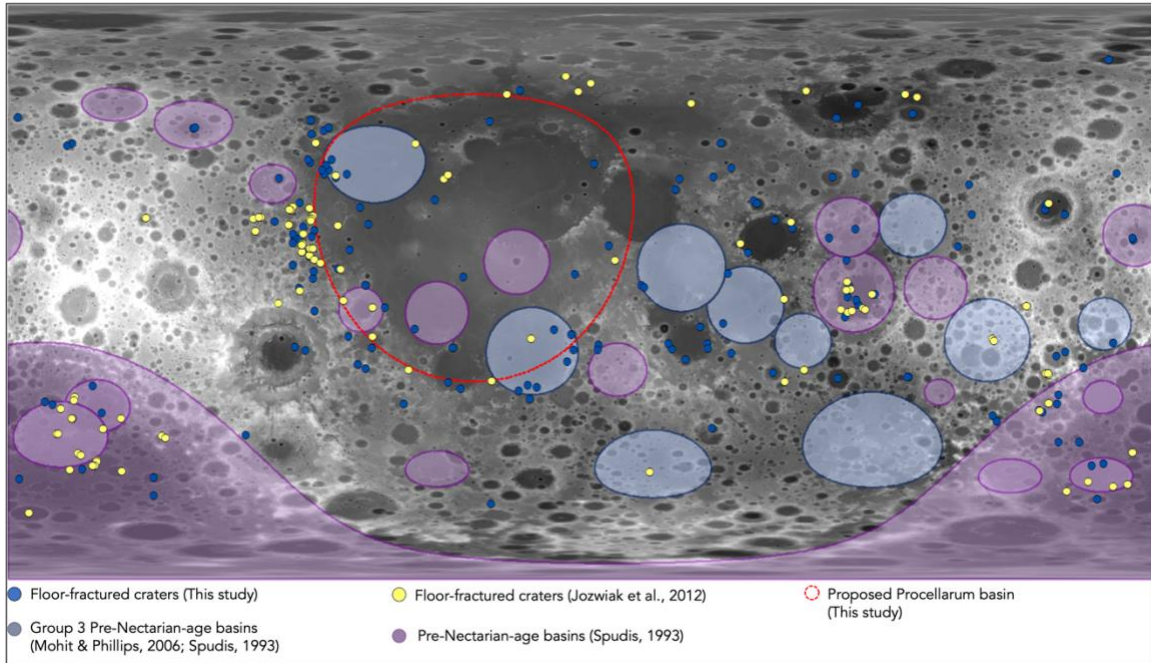
Figure 2.17 Relationship between the spatial distribution of floor-fractured craters and the proposed boundary for the Procellarum basin. Base map: LROC WAC GLD100 (Scholten et al., 2012), map centered on 0°N, 0°E; Lat: $\pm$ 90°; Lon: $\pm$ 180°.
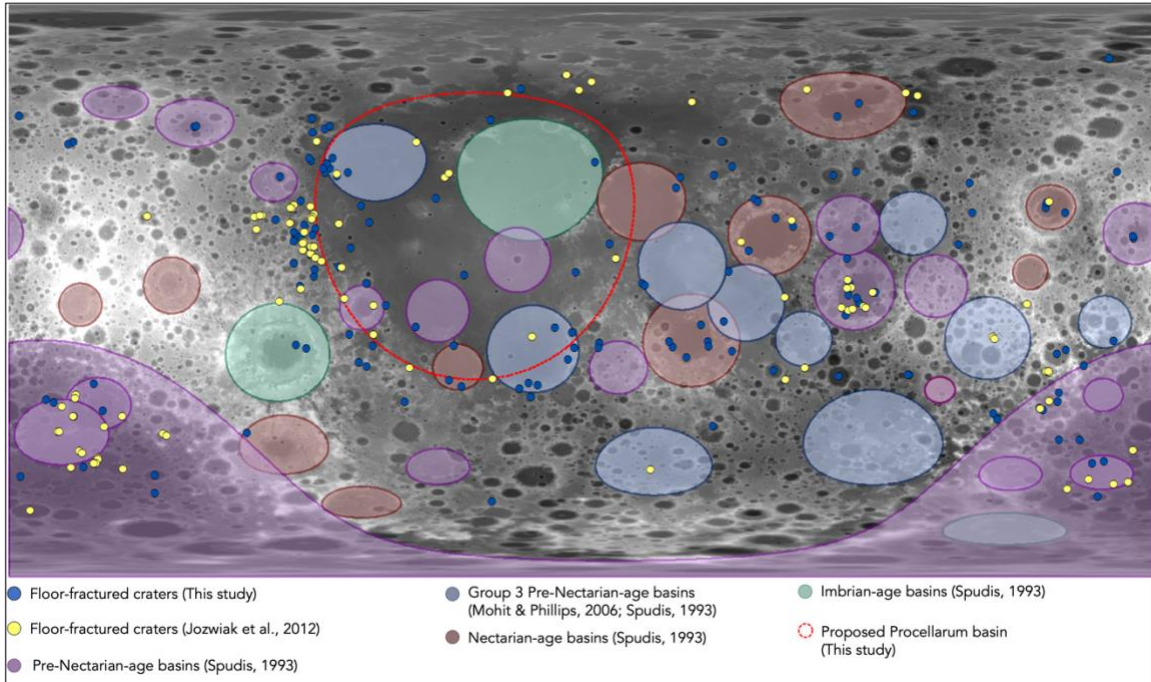
Figure 2.18 Global spatial distribution of floor-fractured craters with respect to basins of all relative ages. Base map: LROC WAC GLD100 (Scholten et al., 2012), map centered on 0°N, 0°E; Lat: $\pm$ 90°; Lon: $\pm$ 180°.

2.6 Discussion

Here we examine the magmatic intrusion and viscous relaxation formation mechanisms for floor-fractured craters using morphometric measurements, temporal heat flow models and the spatial distribution of floor-fractured craters. The volumes of floor-fractured craters are less than those of unmodified craters of all relative ages, which is indicative of the extensive modification to the topography but does not constrain which mechanism is responsible (i.e., magmatic intrusion vs. viscous relaxation; Fig. 2.7). 40% of the floor-fractured craters exhibit lower rim-crest relief compared to morphologically fresh craters of all relative ages, consistent with the viscous relaxation hypothesis (Fig. 2.8). Thermal

anomalies associated with basin-forming events could have contributed to the reduction in relief of short-wavelength topographic features such as crater rims. However, modeling has shown that viscous relaxation can cause an uplift of the crater rim in the unlikely case that long wavelength topography relaxes more rapidly than short wavelength features (Hall et al., 1981).

Floor-fractured craters formed between 4 Ga and 3.5 Ga (Schultz, 1976; Jozwiak et al., 2012) and we find they are preferentially (~76%) distributed circumferentially to the thermally anomalous PKT (Figs. 2.5, 2.13-2.17). Our temporal heat flow models beneath the PKT are 104 mWm^{-2} to 64 mWm^{-2} and the corresponding thermal gradient beneath the PKT as 52 K km^{-1} to 32 K km^{-1} (Fig. 2.11) (assuming initial T_e = 5 km to 9 km) and 52 mWm^{-2} – 41 mWm^{-2} (assuming initial T_e = 10 km to 18 km) between 4 Ga and 3.5 Ga: conditions favorable to viscous relaxation (Ding and Zhu, 2022; Fig. 10). Since floor-fractured craters are spatio-temporally associated with regions of high heat flow (Fig. 12), viscous relaxation is a viable formation mechanism for floor-fractured craters contrary to recent studies (Jozwiak et al., 2012; Dombard and Gillis, 2001). However, the caveat is that the thermal gradient threshold of 30 K km^{-1} is dependent on the assumption that the Th abundance is $\geq$ 4 ppm for the bulk lunar crust or $\geq$ 10 ppm for a 10 km KREEP layer underlying the nearside crust (Ding & Zhu, 2022), which are reasonable estimates (see fig. 2; Wieczorek & Phillips, 2000). However, the thickness of the KREEP layer is not known and since the Th abundance estimates depend on the assumed thickness of the KREEP layer (i.e., 10 km), the thermal gradient threshold of 30° K km^{-1} for viscous relaxation relies on these assumptions.

Floor-fractured craters (> 85%) are preferentially spatially distributed within pre-Nectarian and Nectarian age basins, particularly, those basins that have undergone significant topographic subsidence (i.e., group 3 pre-Nectarian age basins; Fig. 15) compared to Imbrian and Nectarian basins (Figs. 2.13-2.14). In the case of Nectaris, Crisium, Humboldtianum, Moscoviense, and Smythii basins, floor-fractured craters are preferentially located within the first peak ring. Since the mantle (and corresponding thermal gradient) is uplifted in the center of the basin (i.e., within the first peak ring) (e.g., Muller & Sjogren, 1968; Neumann et al., 1996; Wieczorek & Phillips, 1999; Melosh, 2013) conditions were favorable for viscous relaxation of floor-fractured craters during the pre-Nectarian and Nectarian periods. The lack of association of floor-fractured craters within relatively younger basins (i.e., Imbrian age basins) alludes to the state of the lithosphere at the time.

The origin of the PKT has been attributed to the hypothetical Procellarum basin impact (Cadogan, 1974; Cadogan, 1975; Whitaker, 1981; Wilhelms, 1983; Wilhelms, 1987; Figs. 2.16, 2.17). Several lines of evidence have been proposed for the existence of the Procellarum basin including but not limited to: (1) The Procellarum basin is thought to have excavated the primary crust in the lunar nearside, contributing to the thinning of the nearside crust and thickening of the farside crust; (2) the presence KREEP materials along the circumference of the PKT has been proposed to have excavated by the Procellarum basin (Cadogan, 1974; Cadogan, 1975; Whitaker, 1981; Wilhelms, 1983; Wilhelms, 1987) ; (3) the presence of arcuate graben circumferential to the PKT has been attributed to the subsidence of a relatively weaker and thinner lithosphere post-Procellarum basin impact (Wilhelms, 1983); (4) low-Ca pryoxenes are spatially associated with impact basins such

32

as Imbrium, SPA, and Orientale based on Kaguya/SELENE spectral data (Nakamura et al., 2012). The presence of low-Ca pyroxenes along the circumference of the PKT has been attributed to the Procellarum basin impact (Nakamura et al., 2012). The spatial distribution of floor-fractured craters circumferential to the PKT is consistent with the existence of the Procellarum basin, an area where the crust was thinned, and the crust-mantle interface was uplifted (Cadogan, 1974; Cadogan, 1975; Whitaker, 1981; Wilhelms, 1983; Wilhelms, 1987; Figs. 2.16, 2.17). The results of this study show that the existence of the Procellarum basin is a possibility based on the abundance of floor-fractured craters circumferential to the PKT and the lack thereof around Imbrium and Serenitatis basins. The lithospheric strength within the PKT may have increased over time to support the Apennine mountains, which were likely uplifted during the Imbrium impact event (Cadogan, 1974; Cadogan, 1975; Whitaker, 1981; Wilhelms, 1983; Wilhelms, 1987). Since the Imbrium and Serenitatis basins are superposed within the Procellarum basin, the increase in lithospheric strength over time likely restricted the formation of floor-fractured craters within these basins.

2.7 Conclusions

Based on our robust morphometric analysis of floor-fractured craters, their spatial distribution with respect to impact basins, and temporal heat flow models beneath the PKT, we conclude that viscous relaxation as a formation mechanism for floor-fractured crater is plausible, contrary to previous studies (Schultz, 1976; Dombard & Gillis, 2001; Jozwiak et al., 2012; Jozwiak et al., 2015; Jozwiak et al., 2017). Some key take-aways from this study are:

1. Volumetric measurements show that floor-fractured craters underwent extensive modification to their topography compared to non-floor-fractured craters, but such measurements do not constrain the mechanism (Fig. 2.7)

2. Subsidence in external rim-crest heights is indicative of viscous relaxation (Fig. 2.4; Hall et al., 1981). We find that 40% of floor-fractured craters exhibit lower rims than non-floor-fractured craters, thereby indicating that viscous relaxation cannot be ruled out as a plausible formation mechanism of floor-fractured craters (Fig. 2.8)

3. Floor-fractured craters formed between the pre-Nectarian and Nectarian periods. Temporal heat flow models beneath the PKT and corresponding thermal gradients show conditions favorable for viscous relaxation (Figs. 2.10-2.12)

4. The preferential spatial distribution of floor-fractured craters within pre-Nectarian and Nectarian periods coupled with our temporal heat flow models is suggestive of a weaker and thinner early lunar lithosphere, conducive to viscous relaxation (Figs. 2.12, 2.14-2.16)

5. Given the preferential spatial distribution of floor-fractured craters within pre-Nectarian basins (Figs. 2.15-2.16) and the relatively high heat flow associated with the early lunar lithosphere (Figs. 2.10, 2.12), the floor-fractured craters distributed circumferentially to the PKT can be interpreted as the boundary of the proposed Procellarum basin (Cadogan, 1974; Cadogan, 1975; Whitaker, 1981; Wilhelms, 1983; Wilhelms, 1987).

In other words, the results of our study suggest not only is viscous relaxation as a likely formation mechanism for floor-fractured craters, but it also provides new

evidence for the existence of the Procellarum basin and by extension, the origin of the

PKT.

2.8 Acknowledgements

References

Cadogan, P. H. (1974), Oldest and Largest Lunar basin? *Nature, 250*, 315-316. doi: 10.1038/250315a0

Cadogan, P. H. (1975), The Gargantuan Basin: Some Implications. *Lunar and Planetary Institute.*

Calmant, S., Francheteau, J., and Cazenave, A. (1990). Elastic layer thickening with age of the Oceanic Lithosphere: A tool for the prediction of age of volcanoes or oceanic crust. *Geophysical Journal International, 100,* 59-67. doi: 10.1111/j.1365-246X.1990.tb04567.x

Chen, W., and Molnar, P. (1983), Focal depths of intracontinental and intraplate earthquakes and their implications for the thermal and mechanical properties of the lithosphere. *Journal of Geophysical Research, 88*, 4183–4214. doi: 10.1029/JB088IB05P04183

Ding, M. Zhu, M. H. (2022), Effects of regional thermal state on the crustal annulus relaxation of lunar large impact basins. *Journal of Geophysical Research Planets, 127* (3), e2021JE007132. doi: 10.1029/2021JE007132

Dombard, A.J., and Gillis, J.J. (2001), Testing the Viability of Topographic Relaxation as a Mechanism for the Formation of Lunar Floor-fractured craters. *Journal of Geophysical Research: Planets 106*, 27901-27909. doi: 10.1029/2000JE001388

Hall, J. L., Solomon, S. C., and Head, J. W. (1981), Lunar Floor-fractured craters: Evidence for Viscous Relaxation of Crater Topography. *Journal of Geophysical Research, 86*, 9537-9552. doi: 10.1029/JB086iB10p09537

Jolliff, B. L., Gillis, J. J., Haskin, L. A., Korotev, R. L., and Wieczorek, M. A. (2000). Major Lunar Crustal Terranes: Surface Expression and Crust-Mantle Origin. *Journal of Geophysical Research 105*, 4197-4216. doi: 10.1029/1999JE001103

Jozwiak, L. M., Head, J. W., and Zuber, M. T. (2012), Lunar Floor-fractured craters: Classification, Distribution, Origin, and Implications for Magmatism and Shallow Crustal Structure. *Journal of Geophysical Research, 117*, E11005. doi: 10.1029/2012JE004134

Jozwiak, L. M., Head, J. W., Neumann, G. A., and Wilson, L. (2017), Observational Constraints on the Identification of Shallow Lunar Magmatism: Insights from Floor-fractured craters. *Icarus 283*, 224-231. doi: 10.1016/j.icarus.2016.04.020

Kamata, S., Sugita, S., Abe, Y. et al. (2013), Viscoelastic deformation of lunar impact basins: Implications for heterogeneity in the deep crustal paleo-thermal state and radioactive element concentration. *Journal of Geophysical Research Planets, 118* (3), 398-415. doi: 10.1002/JGRE.20056

Langseth, M. G., Keihm, S. J., and Peters, K. (1976), Revised lunar heat-flow values. *Lunar and Planetary Science Conference Proceedings, 7*, 3143–3171.

Melosh, H.J., Freed, A.M., Johnson, B.C., Blair, D.M., Andrews-Hanna, J.C., Neumann, G.A., Phillips, R.J., Smith, D.E., Solomon, S.C., Wieczorek, M.A., and Zuber, M.T. (2013). The Origin of Lunar Mascon Basins. *Science 340* (6140), 1552-1555. doi: 10.1126/science.1235768

Mohit, P. S., and Phillips, R. J. (2006). Viscoelastic Evolution of Multi-Ring Basins. *Journal of Geophysical Research 111*, E12001. doi: 10.1029/2005JE002654

McEwen, A., Davis, P., and Howington-Kraus, A. (1994). Evidence for a Pre-Nectarian Impact Basin in Northwestern Procellarum. *Lunar and Planetary Science Conference XXV*.

Muller, P.M., and Sjogren, W.L. (1968). Mascons: Lunar Mass Concentrations. *Science 161* (3482), 680-684. doi: 10.1126/SCIENCE.161.3842.680

Nakamura, R., Yamamoto, S., Matsunaga, T., Ishihara, Y., Morota, T., Hiroi, T., Takeda, H., Ogawa, Y., Yokota, Y., Hirata, N., Ohtake, M., and Saiki, K. (2012), Compositional evidence for an impact origin of the Moon's Procellarum region. *Nature Geoscience 5*, 775-778. doi: 10.1038/ngeo1614

Neumann G. A., Zuber M. T., Smith D. E., Lemoine F. G. (1996), Global structure and signature of major basins. *Journal of Geophysical Research 101*, 16,841. doi: 10.1029/96JE01246

Ravi, S., Mahanti, P. M., Meyer, H. M., and Robinson, M. S. (2017), Impact Craters: Size-Dependent Degradation Rates, Abstract P41D-2864, presented at 2017 AGU Fall Meeting, New Orleans, LA, 11-15 Dec.

Ravi, S., and Robinson, M.S. (2019), So Creepy: Creep in the Procellarum KREEP Terrane, Abstract P53C-3460, presented at 2019 AGU Fall Meeting, San Francisco, CA

Ravi, S., Robinson, M.S., and Watters, T.R. (2022), *Origin of Lunar Floor-Fractured Craters: Revisiting the Viscous Relaxation Hypothesis* (Data set). Zenodo. doi: 10.5281/zenodo.7483821

Robinson, M. S., Brylow, S. M., Tschimmel, M., Humm, D., Lawrence, S.J., Thomas, P.C., Denevi, B.W., Bowman-Cisneros, E., Zerr, J., Ravine, M.A., Caplinger, M.A., Ghaemi, F.T., Schaffner, J.A., Malin, M.C., Mahanti, P., Bartels, A., Anderson, J., Tran, T.N., Eliason, E.M., McEwen, A.S., Turtle, E., Jolliff, B.L., Hiesinger, H. (2010), Lunar Reconnaissance Orbiter Camera (LROC) Instrument Overview, *Space Science Reviews, 150*, 81-124. doi: 10.1007/S11214-010-9634-2

Scholten, F., Oberst, J., Matz, K.-D., Roatsch, T., Wählisch, M., Speyerer, E.J., and Robinson, M.S. (2012), GLD100: The Near-Global Lunar 100 m Raster DTM from LROC WAC Stereo Image Data. *Journal of Geophysical Research, 117*, E00H17. doi: 10.1029/2011JE003926

Schultz, P.H. (1976), Lunar Floor-fractured craters. *The Moon, 15*, 241-273. doi: 10.1007/BF00562240

Schultz, P. H. and Spudis, P. D. (1985), Procellarum Basin: A Major Impact or the Effect of Imbrium? *Lunar and Planetary Science Conference XVI*

Spudis, P. D., and Schultz, P. H. (1985), Geochemical Problems with Procellarum Basin. *Lunar and Planetary Science Conference XVI*

Spudis, P. H. (1993), The Geology of Multi-Ring Impact Basins. Cambridge Univ. Press, New York.

Watters, T.R. (2022), Lunar Wrinkle Ridges and the Evolution of the Nearside Lithosphere. *Journal of Geophysical Research Planets, 127*, e2021JE007058. doi: 10.1029/2021JE007058
Whitaker, E. A. (1966). The surface of the Moon. In *The nature of the lunar surface: Proceedings of the 1965 IAU-NASA Symposium*, ed. W. N. Hess, D. H. Menzel and J. A. O'Keefe. Baltimore, MD: Johns Hopkins Press, pp. 79-98.

Whitaker, E.A. (1981). The lunar Procellarum basin. *Multi-Ring Basins, Proceedings of the Lunar and Planetary Science Conference,* 12 A, 105-111.

Wieczorek, M. A., and Phillips, R. J. (1999), Lunar Multiring Basins and the Cratering Process. *Icarus 139* (2), 246-259. doi: 10.1006/ICAR.1999.6102

Wieczorek, M. A., and Phillips, R. J. (2000), The "Procellarum KREEP Terrane": Implications for Mare Volcanism and Lunar Evolution. *Journal of Geophysical Research, 105*, 20417-20430. doi: 10.1029/1999JE001092

Wiens, D. A., and Stein, S. (1983), Age dependence of oceanic intraplate seismicity and implications for lithospheric evolution. *Journal of Geophysical Research, 88*, 6455–6468. doi: 10.1029/JB088IB08P06455

Wilhelms, D.E. (1987), The Geologic History of the Moon. *USGS Professional Paper 1348*. doi: 10.3133/PP1348

Wilhelms, D. E. (1983), Effects of the Procellarum Basin on Lunar Geology, Petrology, and Tectonism. *Lunar and Planetary Science Conference XIV*.

CHAPTER 3

LUNAR SILICIC MAGMA GENESIS: INSIGHTS FROM PETROLOGIC MODELING

This is a manuscript in preparation with co-authors C. B. Till and M. S. Robinson

3.1 Abstract

The origins of lunar silicic magmas are not well understood. Lunar silicic volcanic landforms are rare and are predominantly distributed along the boundary of the thermally and geochemically anomalous geologic province, the Procellarum KREEP Terrane. While a few grains of silicic materials have been returned, none of the Apollo missions visited a silicic landform. Despite the wealth of remotely-sensed lunar datasets, their low spectral resolution has limited our ability to constrain the bulk composition of lunar silicic volcanic landforms and determine their formation mechanism and, by extension, their pressure-temperature-composition (P-T-x) evolution.

Here we test two proposed formation mechanisms for lunar silicic magma genesis – 1) crustal melting and 2) fractional crystallization of KREEP-rich basaltic magmas using rhyolite-MELTS models. Rhyolite-MELTS models of crustal melting show that only 10%-20% partial melting of two likely starting compositions produces melts with > 60 wt% SiO_2 and < 3 wt% total alkalis, compared to > 5 wt% for returned lunar granitic fragments. Alternatively, rhyolite-MELTS models of fractional crystallization of KREEP basalt residual liquids can produce silicic melt compositions with >68 wt% SiO_2 and >7 wt% total alkalis, consistent with returned Apollo silicic fragments. Furthermore, thorium (Th) partitioning calculations for fractional crystallization of KREEP basalt show the resulting silicic melts contain >60 ppm Th, consistent with returned samples. We further argue that fractional crystallization of KREEP basalt liquids at shallow depths along a relatively high

geotherm at low fO$_2$ and nominally anhydrous conditions is the most likely formation mechanism for lunar silicic magmas based on analogous terrestrial Anorthosite-Mangerite-Charnockite-Granite (AMCG) suites.

3.2 Introduction

Lunar silicic volcanic landforms are rare and are predominantly distributed along the boundary of the thermally and geochemically distinct province, the Procellarum KREEP Terrane (potassium (K), rare earth elements (REE), and phosphorus (P)) Terrane (PKT) (Fig. 1). The presence of silicic volcanic landforms on the Moon are enigmatic given that the key ingredients (i.e., water and plate tectonics) that are typically invoked for producing large-scale silicic melts on Earth are not part of our foundational understanding of lunar formation and evolution. While the Apollo missions returned a few grains of silicic materials, none of the Apollo or Luna missions visited a silicic landform. Our knowledge of these terrains is thus limited to remote sensing observations, motivating the need for petrologic modeling.

3.2.1 Lunar Differentiation and the Procellarum KREEP Terrane

The lunar crust is hypothesized to have evolved from the differentiation and crystallization of a global lunar magma ocean (LMO), thereby giving rise to the less dense anorthositic primary crust and the denser mafic-ultramafic cumulates (e.g., troctolites, norites, gabbros, and dunites) that make up the lunar mantle (Kaula, 1979; Warren, 1985, 1986; Wood et al., 1970). Post-differentiation impact-basin-forming events contributed to the local removal of the anorthositic crust. Impact-generated decompression melting of the ultramafic cumulates is thought to have produced basaltic melts which filled these basins, thereby giving rise to the maria – the secondary crust (Elkins-Tanton et al., 2004, 2011;

Zhong et al., 2000). The highly incompatible KREEP materials are proposed to have originated as the last dregs of the magma ocean, located between the anorthositic crust and the lunar mantle (Warren, 1985; Wieczorek & Phillips, 2000; Wood et al., 1970) (Fig. 3.1).
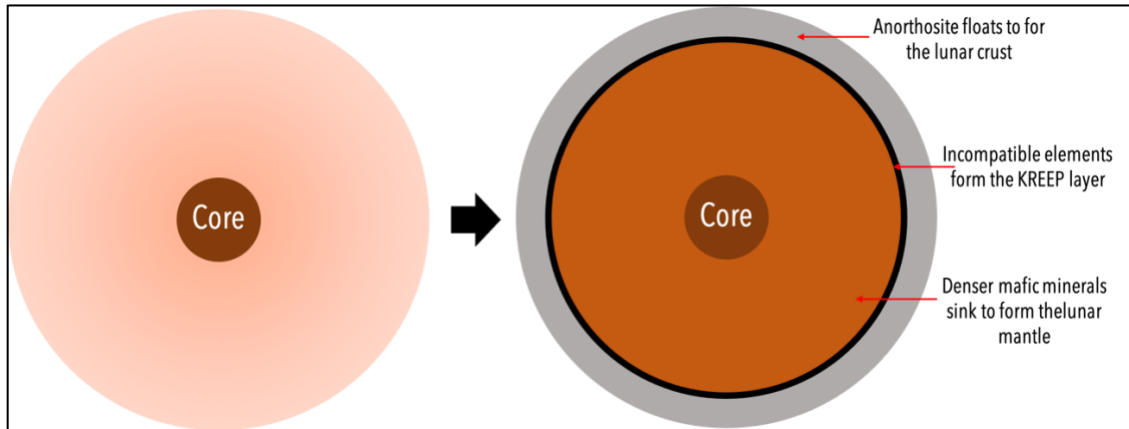
Figure 3.1 Graphic showing the LMO (layer thicknesses not to scale).

There are three distinct geological provinces on the Moon – the Procellarum KREEP Terrane (PKT), the Feldspathic Highlands Terrane (FHT) and the South Pole Aitken Terrane (SPAT). While the PKT constitutes only ~10% of the lunar crust by volume, it contains ~40% of the lunar crustal Th, thereby making it a thermally and geochemically distinct province (Jolliff et al., 2000; Wieczorek & Phillips, 2000). The PKT is home to some of the most enigmatic lunar features such as silicic volcanic landforms, which are predominantly located along the PKT-FHT boundary, except for the Compton-Belkovich Volcanic Complex (CBVC) (Fig. 3.2).
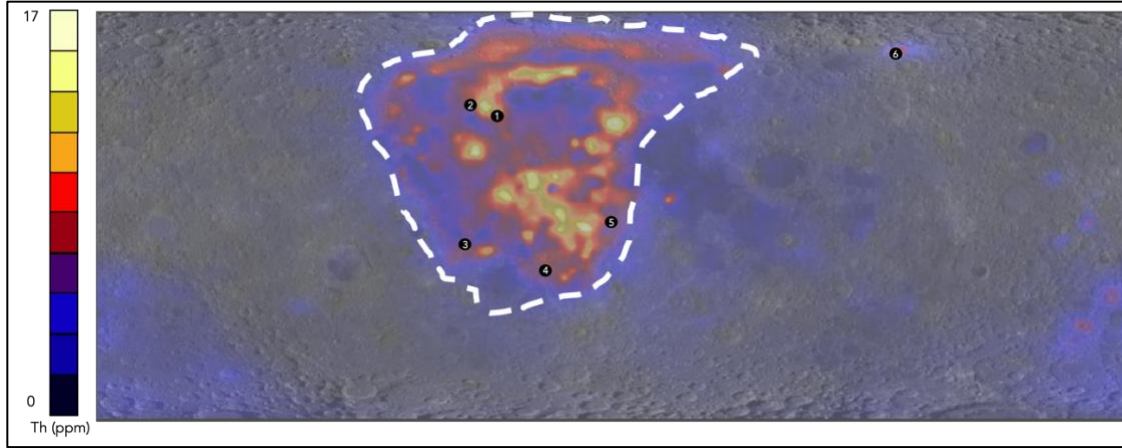
Figure 3.2 Global spatial distribution of lunar silicic volcanic landforms. (1) Gruithuisen domes; (2) Mairan domes; (3) Hansteen Alpha; (4) Wolf crater; (5) Lassell Massif; (6) Compton Belkovich Volcanic Complex. **Map:** Lunar Prospector Gamma Ray Spectrometer (LP-GRS) thorium abundance map (Lawrence et al., 1999) overlain on the Lunar Reconnaissance Orbiter Camera (LROC) Wide Angle Camera (WAC) monochrome mosaic (Robinson et al., 2010). **Lat:** $\pm$ 65; **Lon:** $\pm$ 180. The PKT is defined by this compositional anomaly and is shown in white (Jolliff et al., 2000; Wieczorek & Phillips, 2000)

Post-Apollo era studies based on Lunar Orbiter images identified anomalous features (Fig. 3.2) that are thought to be of silicic compositions based on their high albedo and strong absorption in the UV, leading them to be called "red spots" (Malin, 1974). Morphometric studies of these landforms estimate yield strengths (τ) and plastic viscosity (η) on the order of 10^5 Pa and 10^9 Pa·s respectively, which are characteristic of silicic lavas (Wilson & Head, 2003). The Lunar Prospector Gamma Ray Spectrometer (LP-GRS) detected thorium abundances associated with the "red spots" (Hagerty et al., 2006; Lawrence et al., 1999, 2000, 2005), which are comparable to evolved lithologies such as

42

such as quartz monzogranites (QMGs) in the lunar sample suite ([Th] > 50ppm). Around

six samples of lunar granites (fragments in a lunar breccia) have been identified in the lunar

sample suite and are composed of 60-74 wt% SiO_2, > 6 wt% total alkali ($Na_2O + K_2O$) and

17.2-66 ppmTh (Hagerty et al., 2006).

The most recent remotely-sensed dataset pertaining to silicic landforms is from the

Lunar Reconnaissance Orbiter (LRO) Diviner instrument, a multispectral radiometer,

which has three narrow spectral bandpass filters centered at ~8μm. These channels are used

to characterize the Christiansen Frequency (CF), which is used to detect bulk SiO_2. The

Diviner radiometer detected concave up spectra for Hansteen α, the Gruithuisen domes,

Lassell Massif, and Aristarchus crater (Fig. 3.2), indicative of evolved, silicic compositions

(Boyce et al., 2018; Glotch et al., 2010, 2011, 2017; Greenhagen et al., 2017). Based on

morphological characteristics (i.e., steep slopes of 22°-27°), Hansteen α and the

Gruithuisen domes are interpreted to be extrusive volcanic landforms likely composed of

rhyolite, whereas Aristarchus crater and Lassell Massif are thought to expose excavated

silicic lithologies from depth (Glotch et al., 2010).

3.2.2 Lunar Silicic Magma Genesis Hypotheses

There are three proposed processes for the formation of silicic melts on the Moon –

(1) fractional crystallization of KREEP basalt residual melts from the LMO (Ryder, 1976);

(2) Silicate Liquid Immiscibility (SLI) which occurs when a basaltic magma undergoes >

90% fractional crystallization (e.g., Blanchard et al., 1977; Hess et al., 1975); and (3) partial

melting of the pre-existing lunar crust (composed of anorthosite or ferroan anorthosite) by

basaltic underplating (Hagerty et al., 2003).

Prior work has tested all three possible formation mechanisms, although none have successfully reproduced all the inferred characteristics of lunar silicic landforms. Ryder (1976) petrographically and geochemically examined Apollo sample 15405, which contained coarse grained granite and KREEP basalt clasts, and noted there is granitic residual glass within the KREEP basalt clast. The discovery by Ryder (1976) that the composition of the residual glass was different from that of the granitic clast, was thus interpreted as evidence of slow fractional crystallization of shallow KREEP basalt magma chambers (Ryder 1976).

Hess et al. (1975) conducted fractional crystallization experiments on high-Ti basalt (Apollo 75055, 70017), low-Ti basalt (Apollo 12038), and KREEP basalt (Apollo 14310) compositions at 0.8 log units below the iron-wüstite (Fe-FeO) oxygen fugacity (fO_2) buffer. The experiments reached the liquid immiscibility field at 90% - 95% fractional crystallization and at a temperature range of 975 °C to 1050 °C, thereby producing two coexisting, yet immiscible, melts – one of which is enriched in SiO_2 (felsic component) and the other that is enriched in FeO (mafic component). The composition of the felsic residual liquid was comparable to returned Apollo granitic sample 12013 (Hess et al., 1975). SLI as a formation mechanism for silicic lithologies on the Moon was also proposed by Blanchard et al. (1977) based on geochemical analyses of a felsite clast within Apollo 17 breccia 73125 that exhibits a K/La ratio of 1690 compared to a typical lunar ratio of 70, requiring K to be preferentially concentrated in this silicic liquid relative to other rhyolites (Blanchard et al., 1977).

Gullikson et al. (2016) tested the basaltic underplating hypothesis using experimental petrology. In the basaltic underplating plating model, the injection of KREEP basalt

magmas are thought to partially melt the pre-existing primary crust composed of anorthosites. The partial melt, which is rich is silica and therefore buoyant, erupts at the surface to form silicic domes observed on the lunar surface (Hagerty et al., 2003). In the experiments by Gullikson et al. (2016), pulverized basalt was doped with thorium with similar compositions as Apollo 15 KREEP basalt was melted above the liquidus and was slowly cooled (30°C/h). The basaltic liquid split into two immiscible melts (SLI), however, the thorium partitioned into the mafic component rather than the silicic component, inconsistent with lunar remote sensing observations. The results of the study are thus inconclusive based on the fact that it proposed to test the basaltic underplating hypothesis, yet the experiments were designed to mimic fractional crystallization of basalts and even then, do not support the SLI hypothesis.

To better resolve the outstanding question as to the origin of lunar silicic landforms, here we conduct rhyolite-MELTS models to test two formation hypotheses – basaltic underplating and fractional crystallization of the residual melts of KREEP basalts (Blanchard et al., 1977; Hess et al., 1975; Hildreth, 1981). We compare the modeled compositions of the resulting products to that of returned samples to place constraints on the igneous processes that produced the lunar silicic landforms, as well as the pressure-temperature-composition conditions of those processes, to provide new constraints into the thermal history and differentiation of the Moon.

3.3 Methods

3.3.1 Thermal Calculations

We conduct a series of thermal calculations to the test the plausibility of a KREEP-rich basaltic magma partially melting the pre-existing anorthositic crust (Sparks & Marshall, 1986; Till et al., 2019) using the equation:

$$\text{Initial heat of basalt} = \text{T}_{\text{basalt}} \cdot \text{C}_{\text{p}}$$

where T_{basalt} is the temperature of the basaltic magma (assumed to be the liquidus temperature) and C_{p} is the heat capacity of basalt $= 1100$ J kg^{-1}K^{-1} (Till et al., 2019). We also use the equation:

$$\text{Amount of heat required to drive crustal melting}$$

$$= \text{C}_{\text{p}}(\text{T}_{\text{melt}} - \text{T}_{\text{basalt}}) + \text{H}_{\text{f}} \cdot \text{f}_{\text{melt}} + \text{C}_{\text{p}}(\text{T}_{\text{solidus}} - \text{T}_{\text{crust}})$$

where T_{melt} is the temperature of the partial melt, $\text{T}_{\text{solidus}}$ is the solidus temperature of the crust, which is assumed to be 1273 K (Toksöz et al., 1974), H_{f} is the heat of fusion $= 3 \times 10^{5}$ J kg^{-1} (Till et al., 2019), f_{melt} is the melt fraction, and T_{crust} is the temperature of the crust $= 873$ K (Toksöz et al., 1974).

We then run thermal calculations to determine the amount of heat necessary from underplating KREEP basalt to drive melting of an anorthosite crust at melt fractions from 10% - 100%

3.3.2 Rhyolite-MELTS Modeling

Rhyolite-MELTS is a thermodynamic model for phase equilibria in magmatic systems calibrated on a variety of petrologic experiments on volcanic systems on Earth (Gualda et al., 2012). We employ this program to test both the basaltic underplating and fractional crystallization hypotheses. Using rhyolite-MELTS, we modele the pressure and

temperature regimes under which silicic melts might have been produced in lunar conditions from the bulk compositions of returned lunar anorthosite samples and KREEP basalts (Table 1). Since silicic melts on the Moon are proposed to form at a depth of 1km (Jolliff et al., 1999), we calculated the pressure of the magmatic system from:

$$P = \rho g z$$

where P is pressure (Pa), ρ is density (kg m^{-3}), g is the gravitational acceleration (1.62 m s^{-2}), and z is depth (m) and accordingly ran the models at a constant pressure of 41 bars. Since the redox state of the Moon is reducing, we ran the models with 2 log units below Iron-Wüstite (IW) oxygen fugacity (fO$_2$) buffer (Wadhwa, 2008).

Basaltic Underplating Model

We use a range of lunar anorthosite compositions as the proxy for the lunar crust in our models (Table 1). Since the lunar silicic landforms are enriched in thorium, it is hypothesized that the underplating materials could be KREEP basalts, and as such we also use the compositions of KREEP basalts returned by the Apollo 14 and 15 missions in our model (Table 1).

Fractional Crystallization Model

We simulate isobaric fractional crystallization of KREEP basalts returned by the Apollo missions (Table 1), starting at the calculated liquidus temperature for each starting composition and then stepping down temperature at 50°C intervals until 100% fractional crystallization was reached.

Table 3.1: Bulk compositions of lunar samples relevant for this study returned by the Apollo missions. **Source:** Lunar Sample Compendium.

	SiO$_2$ (wt%)	TiO$_2$ (wt%)	Al$_2$O$_3$ (wt%)	FeO (wt%)	MnO (wt%)	MgO (wt%)	CaO (wt%)	Na$_2$O (wt%)	K$_2$O (wt%)	P$_2$O$_5$ (wt%)
Cataclastic anorthosite (60015)	43.97	0.02	35.83	0.36	-	0.25	18.95	0.34	0.01	-
Ferroan anorthosite (60025)	44.54	0.36	27.65	5.14	-	6.35	15.46	0.34	0.08	-
Granoblastic anorthosite	44.6	0.06	32.9	1.2	0.01	1.68	17.8	0.63	0.04	0.03
Ferroan anorthosite (60629)	44.6	0.01	35.1	0.36	0.05	0.26	19.2	0.41	0.02	0.03
Troctolitic anorthosite	41.94	0.02	28.23	7.4	0.09	6.34	15.74	0.2	0.01	-
Anorthosite (65326)	44.5	-	35.6	0.23	-	0.07	19.1	0.45	0.06	0.03
Ferroan anorthosite (67635)	44.93	0.01	34.77	0.26	0.006	0.16	8.9	0.62	0.02	-
Anorthosite (67636)	44.5	0.036	32.88	1.9	0.006	1.76	17.6	0.52	0.017	-
Noritic anorthosite (67955)	45.01	0.27	27.68	3.84	0.05	7.69	15.54	0.4	0.05	0.03
Noritic anorthosite (67746)	46.7	0.21	24.77	5.46	0.07	9.77	11.24	0.42	0.05	0.01
KREEP basalt (14073)	48.3	1.5	20.74	7.78	0.11	8	11.61	0.76	0.52	0.38
KREEP basalt (14276)	47.6	1.2	21.34	7.94	0.12	7.1	13.18	0.72	0.48	0.4
KREEP basalt (15382)	52.4	1.78	17.8	8.6	0.1	7.1	9.9	0.96	0.57	0.55
KREEP basalt (15386)	50.83	2.23	14.77	10.55	0.16	8.17	9.71	0.73	0.67	0.7

3.3.3 Thorium Partitioning

Since Apollo silicic fragments exhibit Th concentrations of up to ~65 ppm (Korotev et al., 2011; Seddio et al., 2013, 2014), we calculate the Th concentrations in the residual melt for each starting composition (Table 2) as fractional crystallization progresses.

Table 3.2 Modal mineralogy (in %) and the densities of minerals in Apollo KREEP basalts (KB).

	KB 14073[a]	KB 14276[a]	KB 15382[b]	KB 15386[b]	ρ (g cm^{-3})
Plag	50	65	43	43	2.7[c]
Cpx	25	-	-	-	3.37[c]
Opx	20	33	41	43	3.43[c]
Ilm	2	2	6	3	4.8[d]
Cristobalite	-	-	-	8	2.65[c]

Notes: Plag = plagioclase; Cpx = clinopyroxene; Opx = orthopyroxene; Ilm = ilmenite. Data compiled by [a]Gancarz et al., 1971; [b]Taylor et al., 1991; [c]Moore & Ponce, 2001; [d]de Vries et al., 2010.

From the modal % of each mineral for each starting composition (Table 2) and the density of each mineral (Table 3), we calculate the corresponding weight proportions and weight % of each mineral in the sample from:

$$\text{Weight proportion of each mineral}, W_\phi = \text{mode}_\phi \times \rho_\phi$$

where, ρ is the density of the mineral (g cm^{-3}; Table 3) and ϕ is the mineral in question

$$\text{Weight fraction}, X_\phi = \frac{W_\phi}{\text{Total weight proportion}}$$

Table 3.3 Weight fractions (X_ϕ) and distribution coefficient for Th ($D_{Th}{}^{\phi}$) of each mineral phase of Apollo KREEP basalts (KB).

	KB 14073	KB 14276	KB 15382	KB 15386	$D_{Th}{}^{\phi}$
Plag	0.45	0.59	0.41	0.39	0.05[a]
Cpx	0.28	-	-	-	0.0006[b]
Opx	0.23	0.38	0.49	0.49	0.014[c]
Ilm	0.03	0.03	0.1	0.05	0.0006[c]
Cristobalite	-	-	-	8	0.006[d]

<u>Notes:</u> Plag = plagioclase; Cpx = clinopyroxene; Opx = orthopyroxene; Ilm = ilmenite; Opqs = opaques. Data compiled by [a]Mckenzie & O'nions, 1991; [b]Hauri et al., 1994; [c]Klemme et al., 2006; [d]Nash & Crecraft, 1985.

We also calculate the bulk distribution coefficient (D_i; Table 4) for each of the starting compositions from:

$$D_i = \sum_{\phi} X_\phi \, D_i^{\phi}$$

where X_ϕ is the weight fraction of mineral phase ϕ and D_i^{ϕ} is the distribution coefficient of trace element i in mineral phase ϕ (Table 3).

Table 3.4 Th concentrations and bulk distribution coefficients (D_{Th}) of Apollo KREEP basalts (KB)

Sample	C_{Th}^O (ppm)	D_{Th}
KB 14073	11.8[a]	0.0267
KB 14276	8[b]	0.0298
KB 15382	10.5[c]	0.0207
KB 15386	13.7[d]	0.0201

Notes: [a]Tera & Wasserburg, 1972; [b]Brunfelt et al., 1972; [c]O'Kelly et al., 1976; [d]Hubbard et al., 1973

As a magma undergoes fractional crystallization, the concentration of Th changes in the residual melt. We calculate the Th concentration in the residual melt as the magma undergoes fractional crystallization from the Rayleigh equation:

$$C_{Th}^L = C_{Th}^O F^{(D_{Th}-1)}$$

where, C_{Th}^L is the concentration of Th in the residual melt, C_{Th}^O is the concentration of Th in the magma before any crystallization has begun (Table 4), D_{Th} is the bulk distribution coefficient of Th in the magma (Table 4), and F is the melt fraction.

3.4 Results

3.4.1 Basaltic Underplating

Thermal Calculations

Our calculations show that the heat input from underplated KREEP basalts into the lunar crust would range between $1.6 \times 10^5 - 1.7 \times 10^6$ J kg^{-1}, depending on the liquidus

temperature of the basaltic magma. As the thermal energy required to partially melt lunar anorthosites ranges from $4.5 \times 10^5 - 1.2 \times 10^6$ J kg^{-1} depending on the temperature of the partial melt, the higher end of the range of heat input from the underplated basaltic magma would be sufficient to partially melt the anorthositic crust between 0-100% (Fig. 3.3).
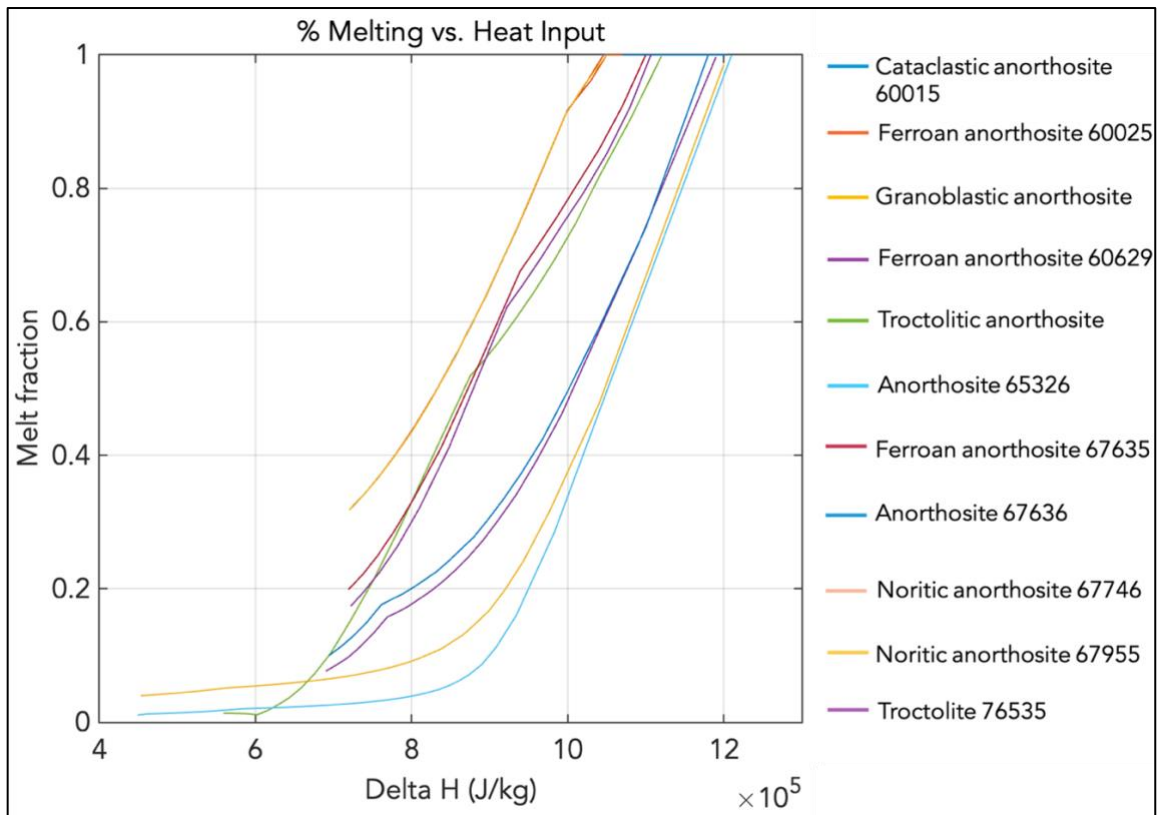
Figure 3.3 Thermal energy required to drive crustal melting on the Moon. The heat input from basaltic magmas is an order of magnitude greater than the required amount of heat to partial melt the anorthositic primary crust of varying compositions.

Rhyolite-MELTS Modeling

Based on our rhyolite-MELTS modeling, very minimal partial melting (10-20%) of two starting compositions of lunar crustal lithologies (i.e., anorthosite 65326 and noritic anorthosite 67955), produce >60 wt% SiO$_2$ (andesitic-dacitic) melts at a pressure of 41 bar

52

and temperature of 900°C (Fig. 3.4). However, the alkali compositions ($Na_2O + K_2O$ wt%) of these resulting melts does not match that of returned lunar silicic fragments (Fig. 3.6). Partial melting of all other starting compositions produces melts that are more mafic than returned lunar silicic fragments as shown in Fig. 3.6).
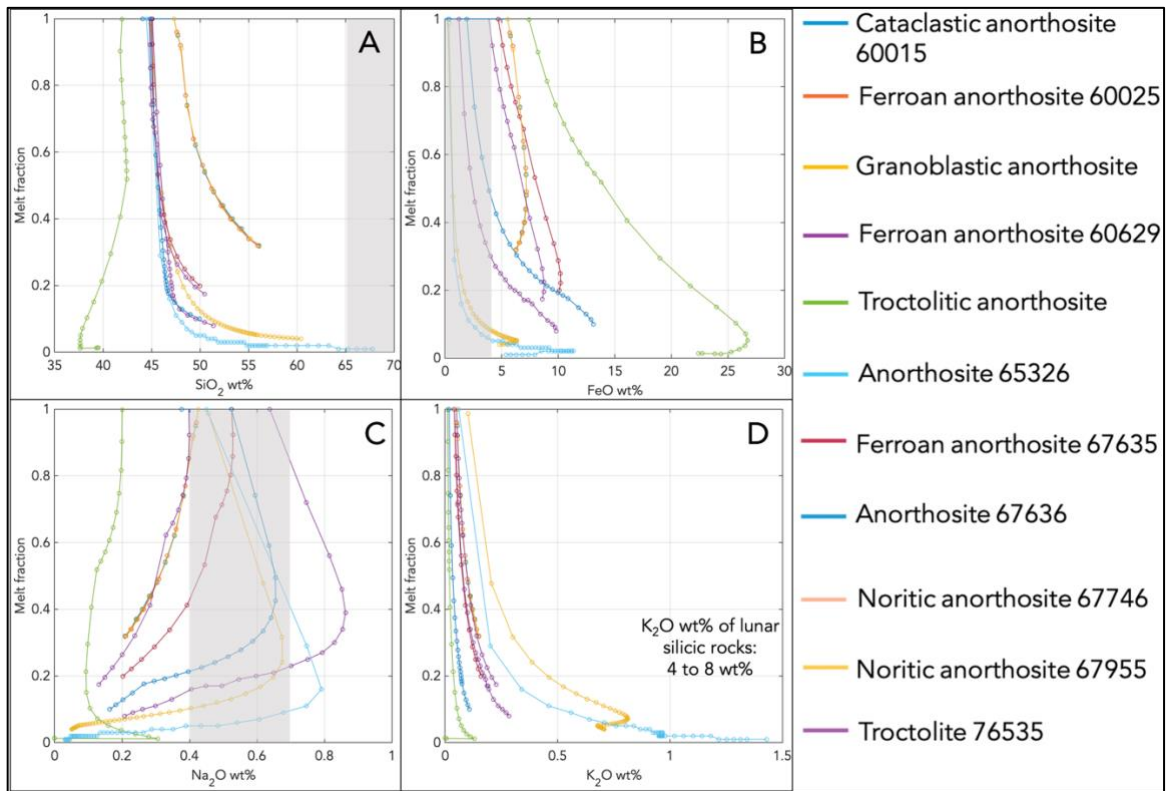
Figure 3.4 Partial melting of various lunar anorthosite compositions using rhyolite-MELTS. Gray regions represent target compositions based on returned lunar silicic fragments.

3.4.2 Fractional Crystallization of KREEP Basalts

Rhyolite-MELTS modeling

Based on our rhyolite-MELTS model, >70% fractional crystallization of KREEP basalts produces silicic melts with $SiO_2 > 65$ wt% and total alkali ($Na_2O + K_2O$) > 6 wt%, which is consistent with returned Apollo samples (Figs. 3.5-3.6). In contrast, the basaltic underplating model only produces <5% partial melt with $K_2O < 1.5$ wt% (Fig. 3.4D), inconsistent with lunar silicic fragments which exhibit K_2O between 4 wt% and 8 wt%.
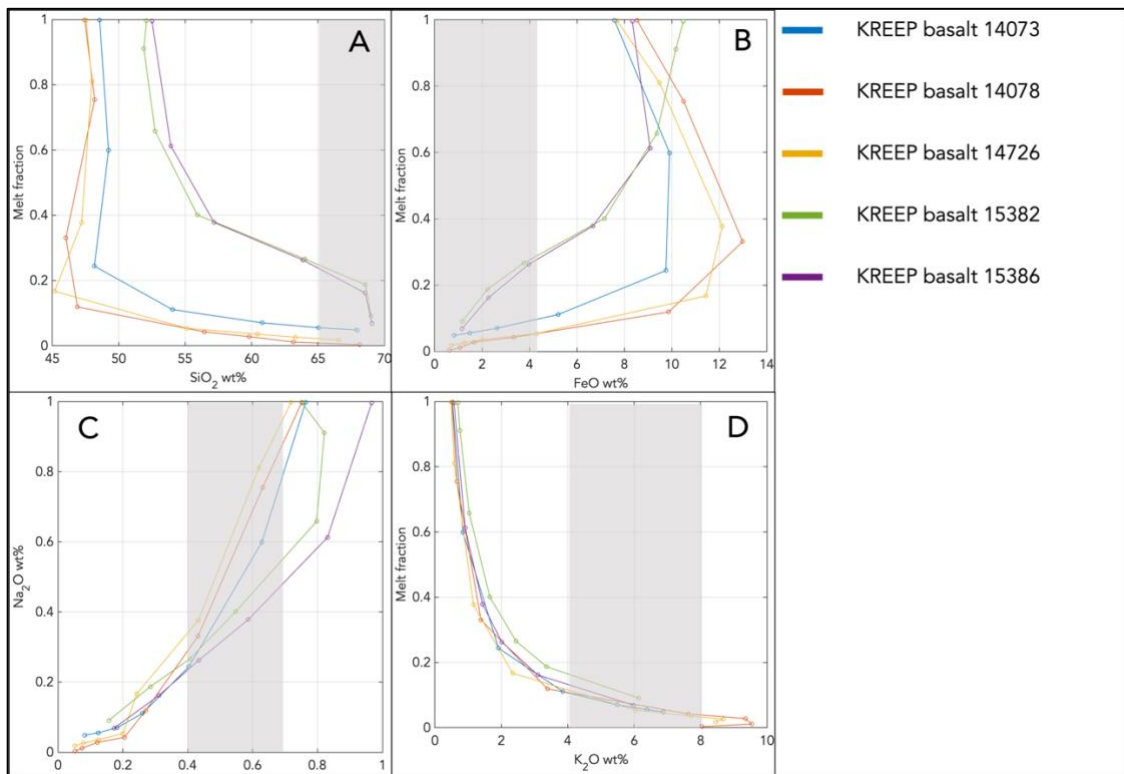
Figure 3.5 Evolution of melt composition through fractional crystallization of lunar KREEP basalts in rhyolite-MELTS model. Gray regions represent target compositions based on returned lunar silicic fragments.
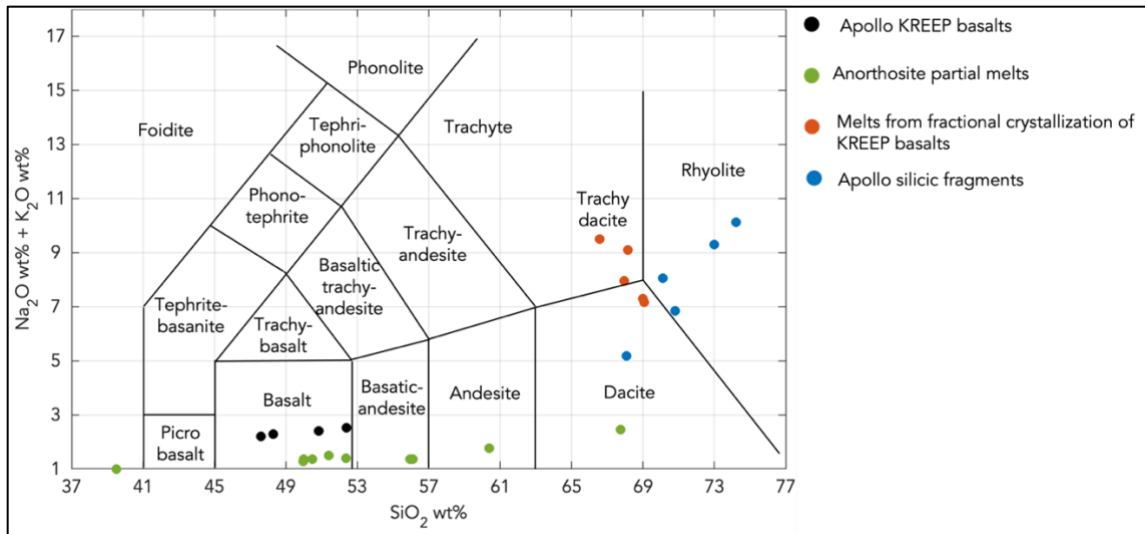
Figure 3.6 Total Alkali-Silica (TAS) diagram representing the KREEP basalts (in black), anorthosite partial melts from rhyolite-MELTS models (in green), melts from the fractional crystallization of KREEP basalts in rhyolite-MELTS (in red), and Apollo silicic fragments.

Thorium partitioning

We calculate the concentration of Th in the residual melt as fractional crystallization progresses for four KREEP basalt starting compositions (Tables 2-4). Since Th is an incompatible element ($D_{Th} < 1$; Table 4), its concentration increases in the residual melt during fractional crystallization (Fig. 3.7 A-D). Using the starting compositions KREEP basalts 14073 and 14276, we find Th concentrations of > 150 ppm in fractionated liquids with SiO_2 > 65 wt% (Fig. 3.7 A-B). For the residual melts (i.e., < 30%) of KREEP basalts 15382 and 15386, we find Th concentrations of > 60 ppm for SiO_2 > 65 wt% (Fig. 3.7 C-D), which is consistent with both remote observations and returned silicic samples (Hagerty et al., 2006; Korotev et al., 2011; Seddio et al., 2013, 2014).
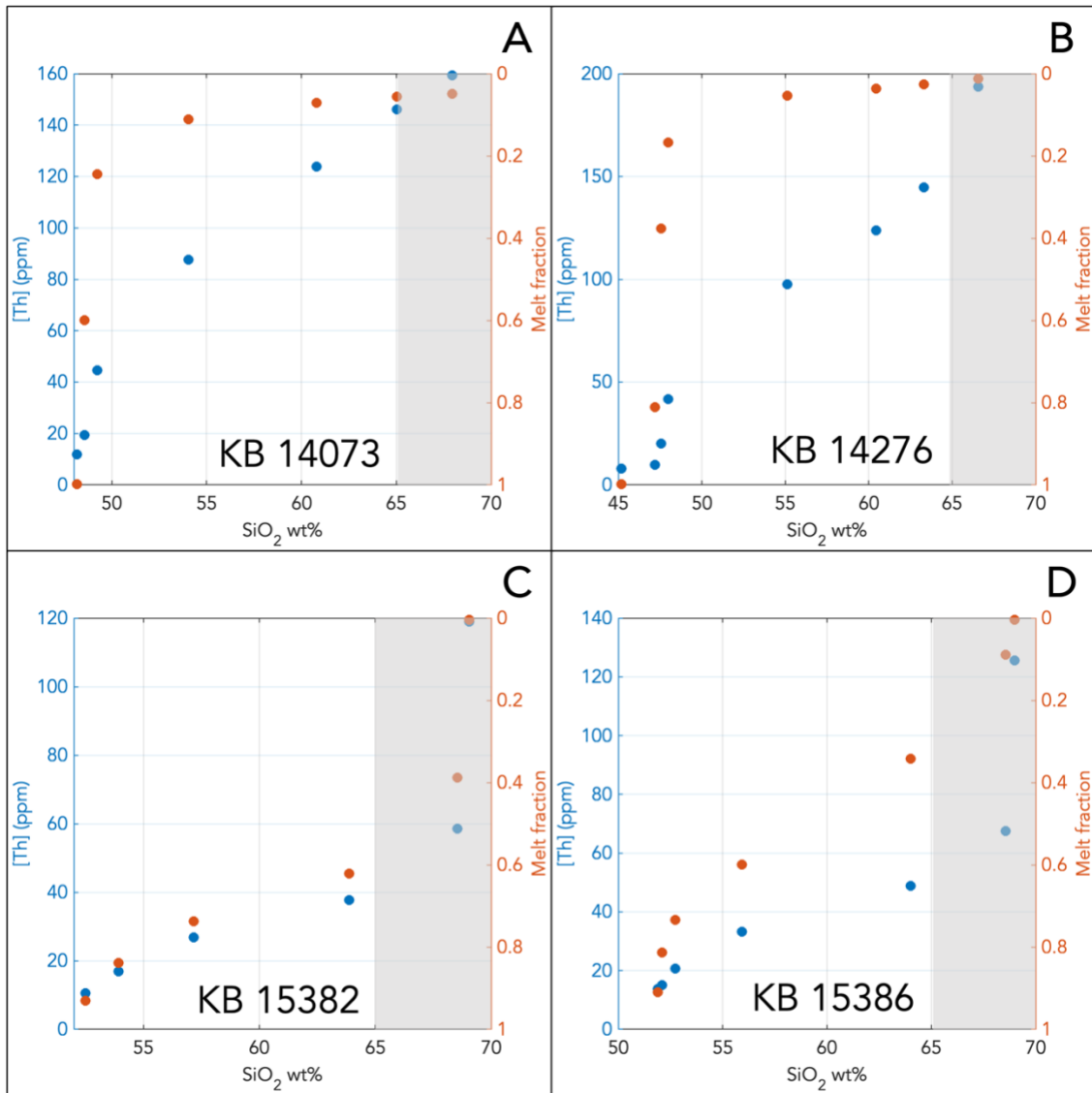
Figure 3.7 Results of Th partitioning model for KREEP basalt starting compositions (A) 14073; (B) 14276; (C) 15382; (D) 15386. The evolution of [Th] as fractional crystallization progresses is shown in blue and melt fraction is shown in red. Gray regions represent target SiO₂ compositions based on returned lunar silicic fragments.

3.5 Discussion

3.5.1 Testing Two Hypotheses for Lunar Silicic Magma Genesis

Results from our thermal models show that a KREEP-rich basaltic magma has approximately an order of magnitude higher heat capacity than is required to partially melt the pre-existing anorthositic crust of a wide range of compositions (Fig. 3.4). While our rhyolite-MELTS model shows that only a 10%-20% partial melting of two of these starting compositions(anorthosite 65326 and noritic anorthosite 67955) can produce melts with > 60 wt% SiO_2 consistent with lunar silicic volcanic lithologies (Korotev et al., 2011; Ryder, 1976; Seddio et al., 2013, 2014; Warren et al., 1983) (Fig. 3.4) their total alkali (Na_2O + K_2O) contents (Fig. 3.6) is significantly lower than returned fragments,. Therefore, partial melting of the primary crust by basaltic underplating does not meet all the criteria for generating silicic melts with all their presently understood characteristics.

Previous studies testing the fractional crystallization hypothesis showed that starting liquids of alkali gabbronorite composition produce silicic melt (67 wt% SiO_2) only after 95% fractional crystallization. In contrast, starting liquids of monzogabbro composition can produce up to 40% melt of intermediate composition (56 wt% SiO_2). However, all these melt compositions do not match the compositions of the Apollo sample suite (Gullikson et al., 2016). Additionally, fractional crystallization experiments conducted by Gullikson et al. (2016) resulted in SLI, producing two co-existing silicate melts, one mafic and one silicic, yet Th was partitioned into the immiscible mafic melt rather than the silicic melt, inconsistent with remote observations and returned samples of lunar silicic magmas. However, the rhyolite-MELTS modeling simulating fractional crystallization of KREEP basalts conducted here produces silicic melts with major element

consistent with returned Apollo silicic fragments (Ryder, 1976; Seddio et al., 2013; Warren et al., 1983, 1987)(Fig. 3.6)

One of the limitations of the rhyolite-MELTS model is that it is not designed to simulate SLI. However, there is little to no evidence of SLI based on returned lunar silicic fragments. While Ryder (1976) argues against SLI as a formation mechanism for lunar silicic melts based on the high amounts of Fe and Mg in lunar granites,. if SLI was responsible for silicic magmas on the Moon, returned fragments would lack mafic minerals, as they would preferentially be found in the mafic residual liquid (Ryder, 1976), which they do not. Futhermore, even if SLI was a plausible mechanism, it would only occur at >90% fractional crystallization in the rhyolite-MELTS models, based on the results of Gullikson et al. (2016). Accordingly, the results of the rhyolite-MELTS model pertaining to 10% to 30% residual liquid (i.e., 70% - 90% fractional crystallization) should still be below the point at which SLI occurs, and as such, the compositions of the residual liquids remain consistent with returned lunar silicic fragments (Figs. 3.5-3.6). In the case of <10% residual melts in our models, the plausibility of their migration through the lunar crust and subsequent eruption without crystallizing seems unlikely. Therefore, we favor 70% - 90% fractional crystallization of KREEP basalt magmas to produce lunar silicic melts.

Thorium behavior in analogous magmatic systems is also consistent with fractional crystallization origin for lunar silicic magmas. The results of our Th partitioning calculations suggest Th concentrations of > 150 ppm in the residual melts after > 70% fractional crystallization of a liquid with the composition of KREEP basalts 14073 and 14276 (Fig. 3.7 A-B), compared with a maximum of 65 ppm Th inferred from remote observations, and measured in returned Apollo fragments (Hagerty et al., 2006; Korotev et

al., 2011; Seddio et al., 2013, 2014). The apparent discrepancy between the modeled Th concentration in the silicic melt and other observations could be the result of the low spatial resolution of the LP-GRS (15 km/pixel) (Hagerty et al., 2006; Lawrence et al., 1999, 2000), and the scarcity and the lack of known provenance for returned lunar silicic fragments. Nevertheless, the increase in Th concentration with increasing SiO_2 content (Fig. 3.7 A-D) is consistent with the compositions of returned Apollo silicic fragments (Korotev et al., 2011; Seddio et al., 2013; Warren et al., 1983, 1987). (Fig. 3.7 C-D). Our results demonstrate that KREEP basalts were plausibly the parent magmas for lunar silicic magmas consistent with the work of Ryder (1976), rather than alkali gabbronorite or monzogabbro identified by previous work (Gullikson et al., 2016).

While the results of our model have demonstrated that fractional crystallization of KREEP basalt magmas gives rise to silicic residual liquids with both major and trace element (i.e., Th) compositions comparable to returned lunar fragments, the probability of eruption of <30% residual liquid is still an outstanding question. This is because >70% crystallization of a KREEP basalt magma would likely lead to a locked matrix of crystals, inhibiting the eruption of the residual silicic liquid (Cooper and Kent, 2014). Instead, we propose that silicic magmas were likely extruded effusively to make dome-like structures due to nearby impacts, which would not inhibited by the presence of >70% crystals and is consistent with previous studies (e.g., Ryder, 1976; Glotch, 2010). Alternatively, the locked matrix of crystals could be remobilized by the heat of a subsequent magma intrusion and/or convection within the magmatic reservoir (Cooper and Kent, 2014).

3.5.2 Terrestrial Analogs

Proterozoic Anorthosite Mangerite Charnockite Granite (AMCG) Suite

Settings and compositions similar to those proposed for lunar silicic magma genesis are found on Earth. The Anorthosite Mangerite Charnockite Granite (AMCG) belts are restricted in time to the Proterozoic eon (Barker et al., 1975a; Emslie, 1978a, 1985; F. H. Hubbard & Whitley, 1978; Smith et al., 1999) but are found globally, including but not limited to the Arabian-Nubian shield (Arabian peninsula), the Dharwar craton (India), the Baltic shield (Scandinavia), and the Kaapvaal craton (South Africa) (Ashwal, 1993). The granites associated with the AMCG suite are identified as A-type (or anorogenic) and are thought to have formed due to intraplate volcanism rather than at convergent plate boundaries (e.g., Anderson & Bender, 1989; Ashwal, 1993; Barker et al., 1975; Emslie, 1978, 1991; F. H. Hubbard & Whitley, 1978; Simmons & Hanson, 1978; Smith et al., 1999). A-type granites are formed in low fO$_2$ (i.e., more reducing and anhydrous), high-temperature magmas, and are enriched in REEs, particularly Th, and exhibit high alkali content (Anderson & Bender, 1989; Ashwal, 1993; Barker et al., 1975a; Emslie, 1978a, 1991; Frost & Frost, 1997; Haapala & Rämö, 1999; F. H. Hubbard & Whitley, 1978; Smith et al., 1999) (Fig. 3.8). The similarity in the composition and formation conditions of AMCG A-type granites and our modeled lunar silicic melts make the Proterozoic AMCG suites a potential terrestrial analog for lunar silicic magmas (Fig. 3.8). The spatio-temporal association of Proterozoic A-type granites with anorthosite massifs led early workers to conclude a cogenetic magmatic origin (i.e., same parent magma) for A-type granites and anorthosites (e.g., Ashwal, 1993; Barker et al., 1975b; Emslie, 1978b; Simmons & Hanson, 1978). However, recent studies have shown that while the anorthosites and A-type granites

of the Proterozoic AMCG suite are spatio-temporally related, the A-type granites likely formed from the fractional crystallization of magma of basaltic composition (e.g., Barker et al., 1975a; Frost et al., 2002; Scoates & Chamberlain, 2003; Smith et al., 1999). The Proterozoic basalts (i.e., the likely protoliths for terrestrial A-type granites) are also compositionally similar (silica and alkali) to returned Apollo KREEP basalts (Fig. 3.8). Therefore, we interpret lunar silicic magmas to have erupted through bimodal volcanism, formed from the fractional crystallization of KREEP basaltic plutons at shallow crustal depths, consistent with previous work (Ryder, 1976; Seddio et al., 2013) (Fig. 3.8). The close spatial association of mare basalts and lunar silicic volcanic landforms is also consistent with bimodal volcanism (Fig. 3.2). The silicic melts plausibly exposed on the lunar surface by impact events as proposed by previous work (e.g., Glotch et al., 2010; Jolliff et al., 1999; Seddio et al., 2013).
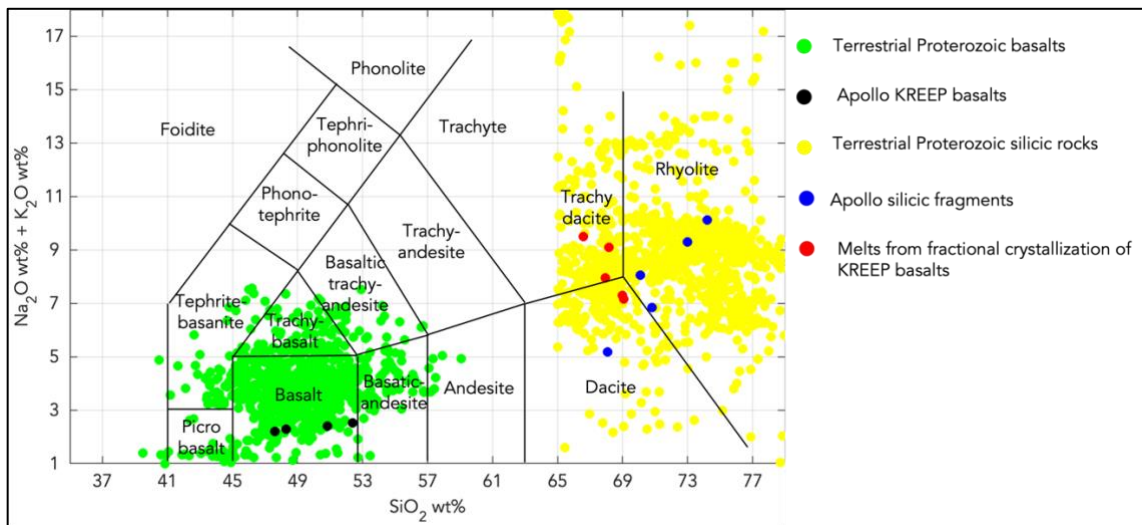
Figure 3.8 TAS diagram representing terrestrial Proterozoic lithologies, returned lunar samples, and results of rhyolite-MELTS modeling fractional crystallization of KREEP basalts.

3.6 Conclusions

Here we demonstrate that fractional crystallization of KREEP basalt magmas is a plausible mechanism for the formation of lunar silicic melts in early lunar geologic history. Specifically, the results of our rhyolite-MELTS modeling suggest that following crystallization, the composition of the remaining ~30 wt.% liquids are consistent with returned lunar silicic fragments (Figs. 6-8). Lastly, we note that fractional crystallization of anhydrous basalts, which produce lunar silicic melts, may be analogous to the terrestrial Proterozoic AMCG suites. Since lunar silicic melts formed in anhydrous (low fO$_2$), high-temperature magmas (900°C-950°C – from rhyolite-MELTS models) at shallow crustal depths, we conclude that the geothermal gradient within the PKT, where the majority of the silicic landforms are located, was relatively high at the time of silicic magma genesis (3.8-3.9 Ga).

References

Anderson, J. L., & Bender, E. E. (1989). Nature and origin of Proterozoic A-type granitic magmatism in the southwestern United States of America. LITHOS. https://doi.org/10.1016/0024-4937(89)90021-2

Ashwal, L. D. (1993). Anorthosites. Springer-Verlag.

Barker, F., Wones, D. R., Sharp, W. N., & Desborough, G. A. (1975a). The Pikes Peak batholith, Colorado front range, and a model for the origin of the gabbro-anorthosite-syenite-potassic granite suite. Precambrian Research. https://doi.org/10.1016/0301-9268(75)90001-7

Barker, F., Wones, D. R., Sharp, W. N., & Desborough, G. A. (1975b). The Pikes Peak batholith, Colorado front range, and a model for the origin of the gabbro-anorthosite-syenite-potassic granite suite. Precambrian Research, 2(2). https://doi.org/10.1016/0301-9268(75)90001-7

Blanchard, D. P., Jacobs, J. W., & Brannon, J. C. (1977). Chemistry of the ANT-suite and felsite clasts from the consortium breccia 73255. Proceedings of the Eigth Lunar and Planetary Science Conference, 2507–2524.

Boyce, J. M., Giguere, T., Mouginis-Mark, P., Glotch, T., & Taylor, G. J. (2018). Geology of Mairan middle dome: Its implication to silicic volcanism on the Moon. Planetary and Space Science, 162(January 2017), 62–72. https://doi.org/10.1016/j.pss.2017.12.009

Brunfelt, A. O., Heier, K. S., Nilssen, B., & Sundvoll, B. (1972). Distribution of elements between different phases of Apollo 14 rocks and soils. Proceedings of the Third Lunar Conference, 2, 1133–1147.

Cooper, K. M., and Kent, A. J. R. (2014). Rapid remobilization of magmatic crystals kept in cold storage. Nature, 506, 480-483.

de Vries, J., van den Berg, A., & van Westrenen, W. (2010). Formation and evolution of a lunar core from ilmenite-rich magma ocean cumulates. Earth and Planetary Science Letters, 292(1–2), 139–147. https://doi.org/10.1016/J.EPSL.2010.01.029

Elkins-Tanton, L. T., Burgess, S., & Yin, Q. Z. (2011). The lunar magma ocean: Reconciling the solidification process with lunar petrology and geochronology. Earth and Planetary Science Letters, 304(3–4), 326–336. https://doi.org/10.1016/j.epsl.2011.02.004

Elkins-Tanton, L. T., Hager, B. H., & Grove, T. L. (2004). Magmatic effects of the lunar late heavy bombardment. Earth and Planetary Science Letters, 222(1), 17–27. https://doi.org/10.1016/j.epsl.2004.02.017

Emslie, R. F. (1978a). Anorthosite massifs, rapakivi granites, and late proterozoic rifting of north America. Precambrian Research. https://doi.org/10.1016/0301-9268(78)90005-0 Emslie, R. F. (1978b). Anorthosite massifs, rapakivi granites, and late proterozoic rifting of north America. Precambrian Research, 7(1), 61–98. https://doi.org/10.1016/0301-9268(78)90005-0

Emslie, R. F. (1985). Proterozoic anorthosite massifs. The Deep Proterozoic Crust in the North Atlantic Provinces, 39–60. https://doi.org/10.1007/978-94-009-5450-2_4

Emslie, R. F. (1991). Granitoids of rapakivi granite-anorthosite and related associations. Precambrian Research. https://doi.org/10.1016/0301-9268(91)90100-O

Frost, C. D., & Frost, B. R. (1997). Reduced rapakivi-type granites: The tholeiite connection. Geology. https://doi.org/10.1130/0091-7613(1997)025<0647:RRTGTT>2.3.CO;2

Frost, C. D., Frost, B. R., Bell, J. M., & Chamberlain, K. R. (2002). The relationship between A-type granites and residual magmas from anorthosite: Evidence from the northern Sherman batholith, Laramie Mountains, Wyoming, USA. Precambrian Research. https://doi.org/10.1016/S0301-9268(02)00117-1

Gancarz, A. J., Albee, A. L., & Chodos, A. A. (1971). Petrologic and mineralogic investigation of some crystalline rocks returned by the Apollo 14 mission. Earth and Planetary Science Letters, 12(1), 1–18. https://doi.org/10.1016/0012-821X(71)90050-1

Gilmore, M. S., & Head, J. W. (2000). Sequential deformation of plains at the margins of Alpha Regio, Venus: Implications for tessera formation. Meteoritics and Planetary Science, 35(4), 667–687. https://doi.org/10.1111/J.1945-5100.2000.TB01451.X

Gilmore, M. S., Mueller, N., & Helbert, J. (2015). VIRTIS emissivity of Alpha Regio, Venus, with implications for tessera composition. Icarus, 254, 350–361. https://doi.org/10.1016/J.ICARUS.2015.04.008

Glotch, T. D., Hagerty, J. J., Lucey, P. G., Hawke, B. R., Giguere, T. A., Arnold, J. A., Williams, J. P., Jolliff, B. L., & Paige, D. A. (2011). The Mairan domes: Silicic volcanic constructs on the Moon. Geophysical Research Letters, 38(21), 1–5. https://doi.org/10.1029/2011GL049548

Glotch, T. D., Lucey, P. G., Bandfield, J. L., Greenhagen, B. T., Thomas, I. R., Elphic, R. C., Bowles, N., Wyatt, M. B., Allen, C. C., Hanna, K. D., & Paige, D. A. (2010). Highly silicic compositions on the moon. Science, 329(5998), 1510–1513. https://doi.org/10.1126/SCIENCE.1192148/SUPPL_FILE/GLOTCH.SOM.PDF

Glotch, T.D.; Elder, C.M.; Hayne, P.O.; Greenhagen, B.T., Dhingra, D.; Kiefer, W. S. (2017). Overview of Silicic Magmatic Activity on the Moon. New Views of the Moon 2. https://doi.org/10.1017/CBO9781107415324.004

Greenhagen, Benjamin T.; Cahill, J.T.S.; Jolliff, B.L.; Lawrence, S.J.; Glotch, T. D. (2017). Investigating Evolved Compositions Around Wolf Crater. LPSC 2017. https://doi.org/10.1017/CBO9781107415324.004

Gualda, G. A. R., Ghiorso, M. S., Lemons, R. v., & Carley, T. L. (2012). Rhyolite-MELTS: A modified calibration of MELTS optimized for silica-rich, fluid-bearing magmatic systems. Journal of Petrology, 53(5), 875–890. https://doi.org/10.1093/petrology/egr080

Gullikson, A. L., Hagerty, J. J., Reid, M. R., Rapp, J. F., & Draper, D. S. (2016). Silicic lunar volcanism : Testing the crustal melting model. 101(June), 2312–2321.

Haapala, I., & Rämö, O. T. (1999). Rapakivi granites and related rocks: An introduction. Precambrian Research. https://doi.org/10.1016/S0301-9268(98)00124-7

Hagerty, J. J., Lawrence, D. J., Hawke, B. R., Vaniman, D. T., Elphic, R. C., & Feldman, W. C. (2006). Refined thorium abundances for lunar red spots: Implications for evolved,

nonmare volcanism on the Moon. Journal of Geophysical Research E: Planets, 111(6), 1–20. https://doi.org/10.1029/2005JE002592

Hauri, E. H., Wagner, T. P., & Grove, T. L. (1994). Experimental and natural partitioning of Th, U, Pb and other trace elements between garnet, clinopyroxene and basaltic melts. Chemical Geology, 117(1–4), 149–166. https://doi.org/10.1016/0009-2541(94)90126-0

Hess, P. C., Rutherford, M. J., Guillemette, R. N., Ryerson, F. J., & Tuchfeld, H. A. (1975). Residual products of fractional crystallization of lunar magmas: an experimental study. Proceedings of the Sixth Lunar Science Conference, 895–909.

Hildreth, W. (1981). Gradients in silicic magma chambers: Implications for lithospheric magmatism. Journal of Geophysical Research: Solid Earth, 86(B11), 10153–10192. https://doi.org/10.1029/JB086IB11P10153

Hubbard, F. H., & Whitley, J. E. (1978). Rapakivi granite, anorthosite and charnockitic plutonism. Nature. https://doi.org/10.1038/271439a0

Hubbard, N. J., Rhodes, J. M., Gast, P. W., Bansal, B. M., Shih, C.-Y., Weismann, H., & Nyquist, L. E. (1973). Lunar rock types: The role of plagioclase in non-mare and highland rock types. Proceedings of the Fourth Lunar Science Conference, 2, 1297–1312.

Jolliff, B. L., Floss. C, Mccallum, I. S., & Schwartz, J. M. (1999). Geochemistry, petrology, and cooling history of 14161,7373: A plutonic lunar sample with textural evidence of granitic-fraction separation by silicate-liquid immiscibility. American Mineralogist. https://www.degruyter.com/document/doi/10.2138/am-1999-5-617/html

Jolliff, B. L., Gillis, J. J., Haskin, L. A., Korotev, R. L., & Wieczorek, M. A. (2000). Major lunar crustal terranes: Surface expressions and crust-mantle origins. Journal of Geophysical Research E: Planets, 105(E2), 4197–4216. https://doi.org/10.1029/1999JE001103

Kaula, W. M. (1979). Thermal evolution of Earth and Moon growing by planetesimal impacts. Journal of Geophysical Research: Solid Earth, 84(B3), 999–1008. https://doi.org/10.1029/JB084IB03P00999

Klemme, S., Günther, D., Hametner, K., Prowatke, S., & Zack, T. (2006). The partitioning of trace elements between ilmenite, ulvospinel, armalcolite and silicate melts with implications for the early differentiation of the moon. Chemical Geology, 234(3–4), 251–263. https://doi.org/10.1016/J.CHEMGEO.2006.05.005

Korotev, R. L., Jolliff, B. L., Zeigler, R. A., Seddio, S. M., & Haskin, L. A. (2011). Apollo 12 revisited. Geochimica et Cosmochimica Acta, 75(6), 1540–1573. https://doi.org/10.1016/J.GCA.2010.12.018

Lawrence, D. J., Feldman, W. C., Barraclough, B. L., Binder, A. B., Elphic, R. C., Maurice, S., Miller, M. C., & Prettyman, T. H. (1999). High resolution measurements of absolute thorium abundances on the lunar surface. Geophysical Research Letters, 26(17), 2681–2684. https://doi.org/10.1029/1999GL008361

Lawrence, D. J., Feldman, W. C., Barraclough, B. L., Binder, A. B., Elphic, R. C., Maurice, S., Miller, M. C., & Prettyman, T. H. (2000). Thorium abundances on the lunar surface. Journal of Geophysical Research: Planets, 105(E8), 20307–20331. https://doi.org/10.1029/1999JE001177

Lawrence, D. J., Hawke, B. R., Hagerty, J. J., Elphic, R. C., Feldman, W. C., Prettyman, T. H., & Vaniman, D. T. (2005). Evidence for a high-Th, evolved lithology on the Moon at Hansteen Alpha. Geophysical Research Letters, 32(7), 1–4. https://doi.org/10.1029/2004GL022022

Malin, M. C. (1974). Lunar Red Spots. Earth, 21, 331–341.

Moore, D. E., & Ponce, D. A. (2001). Petrography and Physical Properties of Selected Rock Types Associated with the Hayward Fault, California. United States Geological Survey Open-File Report 01-263, 1–33. https://www.researchgate.net/publication/242169854

Nash, W. P., & Crecraft, H. R. (1985). Partition coefficients for trace elements in silicic magmas. Geochimica et Cosmochimica Acta, 49(11), 2309–2322. https://doi.org/10.1016/0016-7037(85)90231-5

Nikolayeva, O. v. (1990). Geochemistry of the Venera 8 material demonstrates the presence of continental crust on Venus. Earth, Moon, and Planets 1990 50:1, 50(1), 329–341. https://doi.org/10.1007/BF00142398

O'Kelly, G. D., Eldridge, J. S., Northcutt, K. J., & Schonfeld, E. (1976). Radionuclide Concentrations in KREEP Basalt Samples 15382 and 15386. Lunar and Planetary Science Conference.

Robinson, M. S., Brylow, S. M., Tschimmel, M., Humm, D., Lawrence, S. J., Thomas, P. C., Denevi, B. W., Bowman-Cisneros, E., Zerr, J., Ravine, M. A., Caplinger, M. A., Ghaemi, F. T., Schaffner, J. A., Malin, M. C., Mahanti, P., Bartels, A., Anderson, J., Tran, T. N., Eliason, E. M., … Hiesinger, H. (2010). Lunar Reconnaissance Orbiter Camera (LROC) Instrument Overview. Space Science Reviews 2010 150:1, 150(1), 81–124. https://doi.org/10.1007/S11214-010-9634-2

Ryder, G. (1976). Lunar sample 15405: Remnant of a KREEP basalt-granite differentiated pluton. Earth and Planetary Science Letters, 29(2), 255–268. https://doi.org/10.1016/0012-821X(76)90129-1

Scoates, J. S., & Chamberlain, K. R. (2003). Geochronologic, geochemical and isotopic constraints on the origin of monzonitic and related rocks in the Laramie anorthosite complex, Wyoming, USA. Precambrian Research, 124(2–4), 269–304. https://doi.org/10.1016/S0301-9268(03)00089-5

Seddio, S. M., Jolliff, B. L., Korotev, R. L., & Carpenter, P. K. (2014). Thorite in an Apollo 12 granite fragment and age determination using the electron microprobe. Geochimica et Cosmochimica Acta, 135, 307–320. https://doi.org/10.1016/J.GCA.2014.03.020

Seddio, S. M., Jolliff, B. L., Korotev, R. L., & Zeigler, R. A. (2013). Petrology and geochemistry of lunar granite 12032,366-19 and implications for lunar granite petrogenesis. American Mineralogist, 98(10), 1697–1713. https://doi.org/10.2138/AM.2013.4330

Simmons, E. C., & Hanson, G. N. (1978). Geochemistry and origin of massif-type anorthosites. Contributions to Mineralogy and Petrology. https://doi.org/10.1007/BF00372151

Smith, D. R., Noblett, J., Wobus, R. A., Unruh, D., Douglass, J., Beane, R., Davis, C., Goldman, S., Kay, G., Gustavson, B., Saltoun, B., & Stewart, J. (1999). Petrology and geochemistry of late-stage intrusions of the A-type, mid-Proterozoic Pikes Peak batholith (Central Colorado, USA): Implications for petrogenetic models. Precambrian Research. https://doi.org/10.1016/S0301-9268(99)00049-2

Smrekar, S., Hensley, S., Helbert, J., Andrews-Hanna, J., Breuer, D., Buczkowski, D., Campbell, B., Davaille, A., DiAchille, G., Fassett, C., Gilmore, M., Herrick, R., Iess, L., Jozwiak, L., Konopliv, A., Mastrogiuseppe, M., Mazerico, E., Mueller, N., Nunes, D., … Zebker, H. (2020). VERITAS (VENUS EMISSIVITY , RADIO SCIENCE, INSAR, TOPOGRAPHY AND SPECTROSCOPY): A PROPOSED DISCOVERY MISSION. 51st Lunar and Planetary Science Conference. https://doi.org/10.1002/2015GC006210

Sparks, R. S. J., & Marshall, L. A. (1986). Thermal and mechanical constraints on mixing between mafic and silicic magmas. Journal of Volcanology and Geothermal Research, 29(1–4), 99–124. https://doi.org/10.1016/0377-0273(86)90041-7

Strom, R. G., Schaber, G. G., & Dawson, D. D. (1994). The global resurfacing of Venus. Journal of Geophysical Research: Planets, 99(E5), 10899–10926. https://doi.org/10.1029/94JE00388

Tera, F., & Wasserburg, G. J. (1972). U-Th-Pb systematics in three Apollo 14 basalts and the problem of initial Pb in lunar rocks. Earth and Planetary Science Letters, 14(3), 281–304. https://doi.org/10.1016/0012-821X(72)90128-8

Till, C. B., Kent, A. J. R., Abers, G. A., Janiszewski, H. A., Gaherty, J. B., & Pitcher, B. W. (2019). The causes of spatiotemporal variations in erupted fluxes and compositions along a volcanic arc. Nature Communications, 10(1). https://doi.org/10.1038/s41467-019-09113-0

Toksöz, M. N., Dainty, A. M., Solomon, S. C., & Anderson, K. R. (1974). Structure of the Moon. Reviews of Geophysics, 12(4), 539–567. https://doi.org/10.1029/RG012I004P00539

Wadhwa, M. (2008). Redox conditions on small bodies, the Moon, and Mars. Reviews in Mineralogy and Geochemistry, 68(1), 493-510. https://doi.org/10.2138/rmg.2008.68.17

Warren, P. H. (1985). The magma ocean concept and lunar evolution. Annual Review of Earth and Planetary Science, 13, 201–240.

Warren, P. H. (1986). Anorthosite assimilation and the origin of the Mg/Fe-related bimodality of pristine moon rocks: Support for the magmasphere hypothesis. Journal of Geophysical Research: Solid Earth, 91(B4), 331–343. https://doi.org/10.1029/jb091ib04p0d331

Warren, P. H., Jerde, E. A., & Kallemeyn, G. W. (1987). Pristine Moon rocks: A "large" felsite and a metal-rich ferroan anorthosite. Journal of Geophysical Research: Solid Earth, 92(B4), E303–E313. https://doi.org/10.1029/JB092IB04P0E303

Warren, P. H., Taylor, G. J., Keil, K., Shirley, D. N., & Wasson, J. T. (1983). Petrology and chemistry of two "large" granite clasts from the moon. Earth and Planetary Science Letters, 64(2), 175–185. https://doi.org/10.1016/0012-821X(83)90202-9

Wieczorek, Mark A.; Phillips, R. J. (2000). The Procellarum KREEP Terrane: Implications for mare volcanism and lunar evolution. Journal of Geophysical Research, 105(1999).

Wilson, L., & Head, J. W. (2003). Lunar Gruithuisen and Mairan domes: Rheology and mode of emplacement. Journal of Geophysical Research E: Planets, 108(2), 6–1. https://doi.org/10.1029/2002je001909

Wood, John A.; Dickey, John. S.; Marvin, Ursula, B.; and Powell, B. N. (1970). Lunar anorthosites and a geophysical model of the Moon. Proceedings of the Apollo 11 Lunar Science Conference, 1, 965–988.

Zhong, S., Parmentier, E. M., & Zuber, M. T. (2000). A dynamic origin for the global asymmetry of lunar mare basalts. Earth and Planetary Science Letters, 177(3–4), 131–140. https://doi.org/10.1016/S0012-821X(00)00041-8

CHAPTER 4

SPATIO-TEMPORAL ASSOCIATION OF MONS HANSTEEN AND HANSTEEN

CRATER: IMPLICATIONS FOR SILICIC MAGMA GENESIS

This is a manuscript in preparation with co-authors M. S. Robinson and J. D. Clark

4.1 Abstract

Lunar floor-fractured craters and silicic volcanic landforms typically occur along the boundary of the thermally anomalous Procellarum KREEP (potassium (K), rare earth elements (REE), and phosphorus (P)) Terrane. Though rare, lunar silicic volcanic landforms are closely spatially associated (within 50 km) with floor-fractured craters, leading to the question if they are also temporally associated and the implications for silicic magma genesis on the Moon.

Here we test the temporal association of the floor-fractured crater, Hansteen, the silicic volcanic landform, Mons Hansteen, and Billy crater. Based on Absolute Model Ages (AMAs) derived from Crater Size Frequency Distribution (CSFD) measurements, we find that Hansteen crater formed at 3.8 +0.04/-0.05 Ga, which was then followed by two contemporaneous events – the eruption of basalts on the floor of Hansteen crater (3.4 +0.1/- 0.3 Ga) and the formation of Mons Hansteen (3.4 +0.1/- 0.3 Ga), and finally the eruption of basalts at Billy crater (1.4 $\pm$ 0.1 Ga). Firstly, we show that Mons Hansteen is younger by ~0.3 Ga compared to previous estimates. Secondly, we interpret the temporal association of basalts at Hansteen crater and silicic lithologies at Mons Hansteen as a form of bimodal volcanism: that is the rising basaltic melt played a role in generating the silicic magmas. Lastly, we show that it is unlikely that the basaltic eruptions at Billy crater (1.4 $\pm$

0.08 Ga) contributed to the formation of ~2 Ga older Mons Hansteen, as proposed by previous studies.

4.2 Introduction

Lunar landforms such as floor-fractured craters and silicic volcanic constructs are surface expressions of thermal anomalies within the lithosphere (Fig. 4.1). The majority of floor-fractured craters ($>60\%$) and silicic volcanic landforms (five out of the six identified) are located along the boundary of the Procellarum KREEP (potassium (K), rare earth elements (REE), and phosphorus (P)) Terrane (PKT), a thermally and geochemically distinct province (Fig. 4.2; Jolliff et al., 2000; Wieczorek et al., 2000). The Compton-Belkovich Volcanic Complex (CBVC) is the only identified silicic volcanic landform that lies outside the PKT; CBVC formed within the Feldspathic Highlands Terrane (FHT) (Jolliff et al., 2011). All lunar silicic volcanic landforms, including the CBVC, are located within ~50 km of a floor-fractured crater (Fig. 4.2). Understanding the potential stratigraphic and geochemical association between floor-fractured craters and silicic volcanic landforms is essential to constraining models of the thermal and chemical evolution of the PKT.
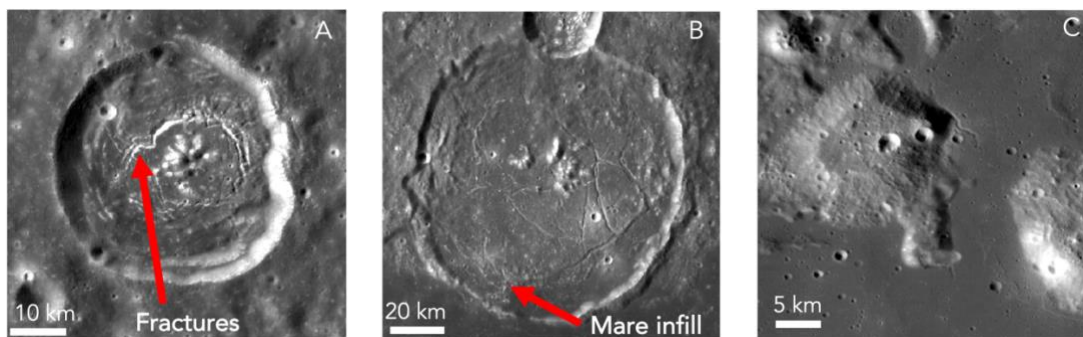
Figure 4.1 Examples of landforms relevant to this study. (A) Vitello crater (-30.4°, 322.5°) exhibits radial/concentric fractures, (B) Gassendi crater (-17.4°, 320°) exhibits

mare basalt infill, and (C) the Gruithuisen domes, silicic volcanic landforms in NW

Procellarum.

4.2.1 Floor-Fractured Craters and Silicic Volcanic Constructs
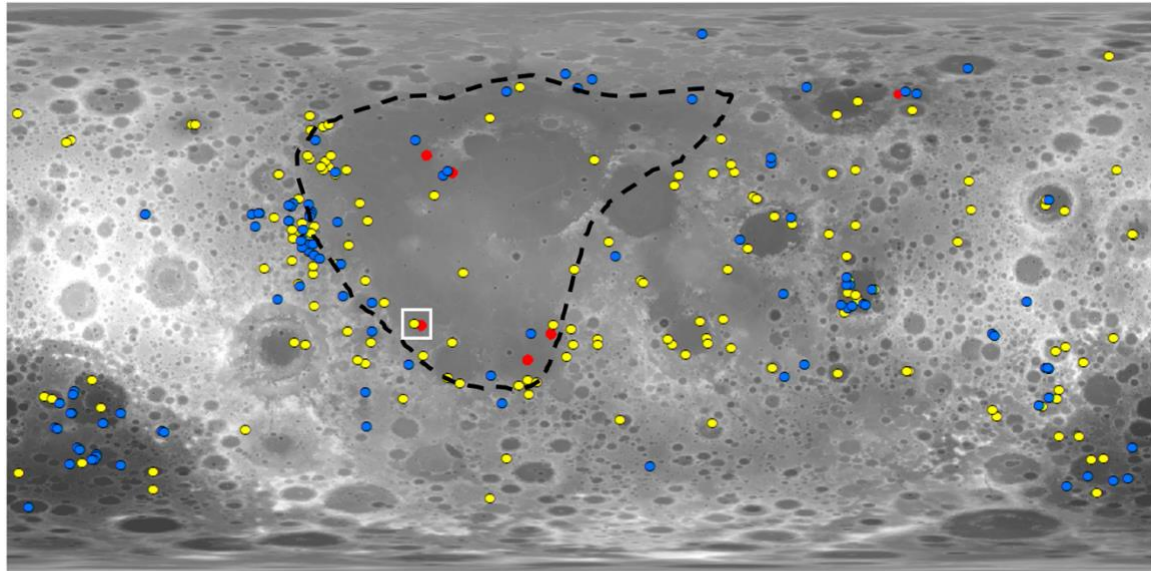
○ Floor-fractured craters (Jozwiak et al., 2012)
● Newly identified floor-fractured craters (Ravi & Robinson, 2019)
● Silicic volcanic landforms

Figure 4.2 Global spatial distribution of floor-fractured craters and silicic volcanic landforms. The PKT is outlined in black. The white box represents the location of the Hansteen region. <u>Base map</u>: LROC Wide Angle Camera (WAC) GLD100 Digital Terrain Model (DTM) (Scholten et al., 2012). Lat: $\pm$ 65°; Lon: $\pm$ 180°.

Floor-fractured craters are impact craters that underwent modification due to volcano-tectonic processes such as magmatic intrusion or viscous relaxation as evidenced by radial, concentric or polygonal fractures and they sometimes host volcanic landforms such as mare basalt or pyroclastic deposits (Schultz, 1976; Hall et al., 1981; Jozwiak et al., 2012; Ravi & Robinson, 2019; Fig. 4.1). In the magmatic intrusion hypothesis, crater floors

71

experience uplift caused by the intruding magma, thereby reducing the depth of the crater (Schultz, 1976). In the viscous relaxation hypothesis, short-wavelength morphologic features such as crater rims reduce in height as a response to thermal anomalies in the lunar lithosphere (Schultz, 1976; Hall et al., 1981). Based on morphometric measurements (i.e., d/D ratios and rim-crest heights) and heterogeneous gravity anomalies, previous studies concluded that magmatic intrusion was the sole mechanism contributing to floor-fracturing (Jozwiak et al., 2017). However, temporal heat flow models within the PKT show that the conditions were favorable for viscous relaxation during the period of floor-fracturing (4 Ga – 3.5 Ga). Thus we infer viscous relaxation is an equally viable mechanism (Ravi & Robinson, 2022). Regardless of the mechanism that contributed to the formation of floor-fractured craters, no constraints have been placed on the timing of modification of the crater floor relative to the host crater formation.

Volcanic landforms like Mons Hansteen were first proposed to be composed of silicic lithologies based on their high albedo and strong absorption in the UV (Malin, 1974), leading them to be called "red spots." The Lunar Prospector Gamma Ray Spectrometer (LP-GRS) detected thorium abundances associated with the "red spots" (Hagerty et al., 2006; Lawrence et al., 1999, 2000, 2005), which are comparable to evolved lithologies such as quartz monzogranites (QMGs) in the lunar sample suite ([Th] > 50ppm). Recent observations from the Lunar Reconnaissance Orbiter (LRO) Diviner radiometer confirmed the red spots contain > 65 wt% SiO_2 (Glotch et al., 2010). There are three proposed mechanisms for the formation of silicic magmas on the Moon:

1. Partial melting of the primary anorthositic crust by contact with basaltic magmas (Hagerty et al., 2006).

2. Fractional crystallization of KREEP enriched basalt magmas (Ryder, 1976).

3. Silicate Liquid Immiscibility (SLI), a variant of model 2, occurs when a basaltic magma undergoes > 90% fractional crystallization and splits into two immiscible yet coexisting melts – one that is SiO2 – rich and the other that is FeO-rich. However, thorium, a component of silicic magmas, partitions with the mafic melt, inconsistent with remote sensing observations of silicic domes and returned silicic fragments. As a result, this hypothesis has been discounted (Hagerty et al., 2006).

4.2.2 The Hansteen Region

Hansteen Region is located in SW PKT (Fig. 4.3) and consists of three features: (1) Hansteen crater, a floor-fractured crater (D = 45 km) with a basaltic infill within the northern portion of its floor; (2) Mons Hansteen, a silicic volcanic construct with an arrowhead-shaped mesa that topographically rises 900 m above the surrounding maria (Hawke et al., 2003; Wagner et al., 2010; Boyce et al., 2017; Qiu et al., 2022); (3) Billy crater (D = 45 km), an upper-Imbrian aged crater (3.88 ± 0.04 Ga; Wagner et al., 2010) inundated with mare basalts in its interior.
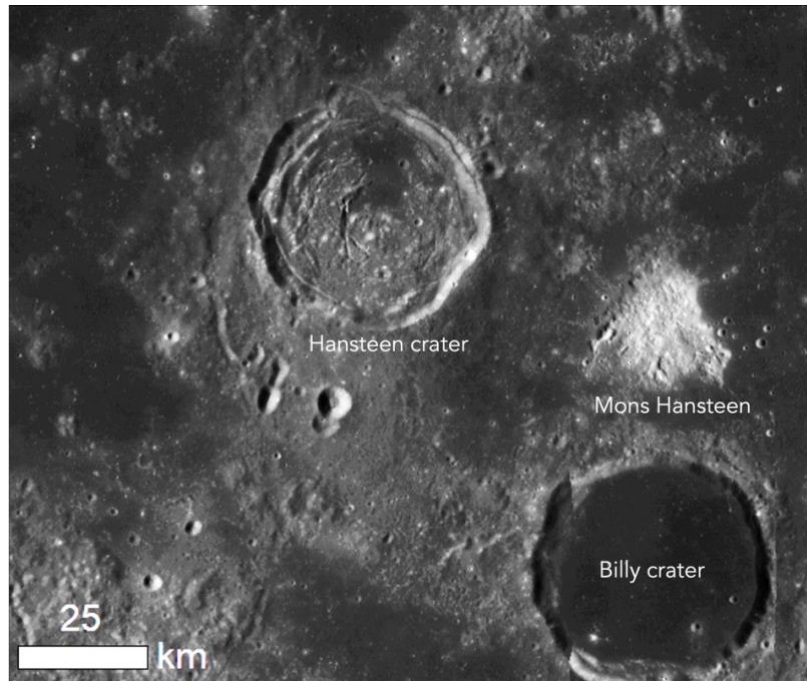
Figure 4.3 Regional context map showing the Hansteen Region in SW PKT. Base map:
LROC WAC monochrome mosaic (Robinson et al., 2010).

The relative ages of planetary surfaces can be derived from crater counting methods
(Hartmann, 1966; Neukum et al., 1975; Neukum et al., 1983; Hiesinger et al., 2010, 2012).
From Lunar Orbiter IV image based CSFDs Wagner et al. (2010) reported AMAs for Mons
Hansteen to be 3.74 ± 0.06 Ga, Billy crater ejecta to be 3.88 ± 0.04 Ga, and the mare filled
floor unit within Billy crater to be 1.65 ± 0.29 Ga.

Based on FeO wt% values derived from the Clementine UV-VIS images (Lucey et
al., 2000), Boyce et al. (2017) divided Mons Hansteen into three geologic units – Hilly and
Dissected unit, Pitted unit, and North Massif (Fig. 4.4). The AMAs derived for each of the
units of Mons Hansteen suggest volcanism began at the Hilly and Dissected unit at 3.74

+0.075/- 0.15 Ga followed by the Pitted unit at 3.50 +0.15/-1 Ga and the North Massif at 3.50 Ga (Boyce et al., 2017).
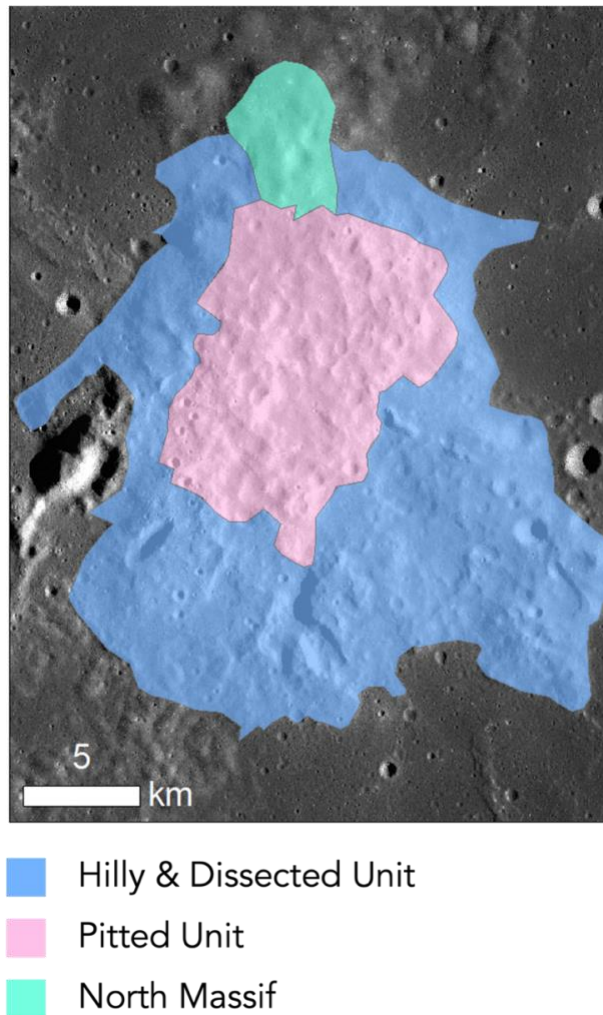
Figure 4.4 Geological units of Mons Hansteen identified by Boyce et al. (2017). Base map: Hansteen regional NAC mosaic.

Using Kaguya Terrain Camera (TC) images, TC DTM data, and LROC Narrow Angle Camera (NAC) DTMs, Qiu et al. (2022) derived AMAs of the three units of Mons Hansteen from Boyce et al. (2017). The new AMAs of the Hilly and Dissected unit 3.8 +0.02/-0.03 Ga, the Pitted Unit is 3.6 +0.06 /-0.09 Ga, and the North Massif is 3.6 +0.06 /-0.1 Ga (Qiu

et al., 2022). The study concludes that the Billy impact event caused uplift and partial melting of the mantle, thereby inundating Billy crater's floor with mare basalts and also causing partial melting of the pre-existing primary crust, giving rise to silicic lithologies found at Mons Hansteen (Qiu et al., 2022). However, the AMA of the mare basalts on the floor of Billy crater is 1.65 ± 0.29 Ga (Wagner et al., 2010), postdating the formation of Mons Hansteen by > 2 Ga. Therefore, it seems unlikely that the Billy crater impact event influenced the formation of Mons Hansteen.

In this study, we employed crater size-frequency measurements using image datasets from the Lunar Reconnaissance Orbiter Camera (LROC) (Robinson et al., 2010) to derive absolute model ages (AMAs) for the ejecta of and the basaltic floor unit of Hansteen crater, and Mons Hansteen to test the stratigraphic relationship between basaltic and silicic magmas on the Moon.

4.3 Data and Methods

We used both LROC NAC and WAC images (Table 1) to map relevant and homogenous areas for crater counting, as described in detail by e.g., Hartmann (1966), Crater Analysis techniques Working Group (1979), Neukum (1983), Hiesinger et al. (2000) and Michael and Neukum (2010). We counted craters ($D \geq 100$ m) in defined areas using the ArcGIS CraterTools program (Kneissl et al., 2011). The CSFD measurements when then plotted and fitted in Craterstats (Neukum, 1983; Michael and Neukum, 2010) using the production and chronology function of Neukum et al., 2001. The production function represents the number of new craters in a given size range within a square kilometer area (Neukum et al., 2001). The cratering chronology function is calibrated using the ages of Apollo samples to the crater counts for the locations from where the samples were collected

(Neukum & Ivanov, 1994; Stöffler & Ryder, 2001; Neukum et al., 2001). The production and chronology functions were used to derive AMAs using the Craterstats2 tool (Neukum et al., 2001; Michael & Neukum, 2010).

Quasi-circular features were included as impact craters in the studies of Boyce et al. (2017) and Qiu et al. (2022) but were excluded from our measurements because we do not interpret them as impact craters (Fig. 4.5). Qiu et al. (2022) argued that these quasi-circular features are degraded craters. However, these features exhibit raised rims, which are uncharacteristic of degraded craters. We interpret these quasi-circular features as degraded primary silicic flow fronts (Fig. 4.5). We observe a chain of secondary craters in SW Mons Hansteen, which were also excluded from our counts (Fig. 4.5). There is an apparent lack of impact craters in the Pitted unit identified by Boyce et al. (2017) and Qiu et al. (2022) (Fig. 4.6). We made CSFD measurements for the three units identified by Boyce et al. (2017) (Fig. 4.4) and find that the AMAs for both the Hilly and Dissected unit and the Pitted unit are 3.4 +0.1/-0.3 Ga (S1-S2). The AMA for the North Massif cannot be accurately derived since we have only identified $n = 4$ craters in this unit (S4). Moreover, we did not observe significant morphological differences among the units. Therefore, we treated the entire edifice as one unit (Figs. 4.4, 4.6, 4.7).
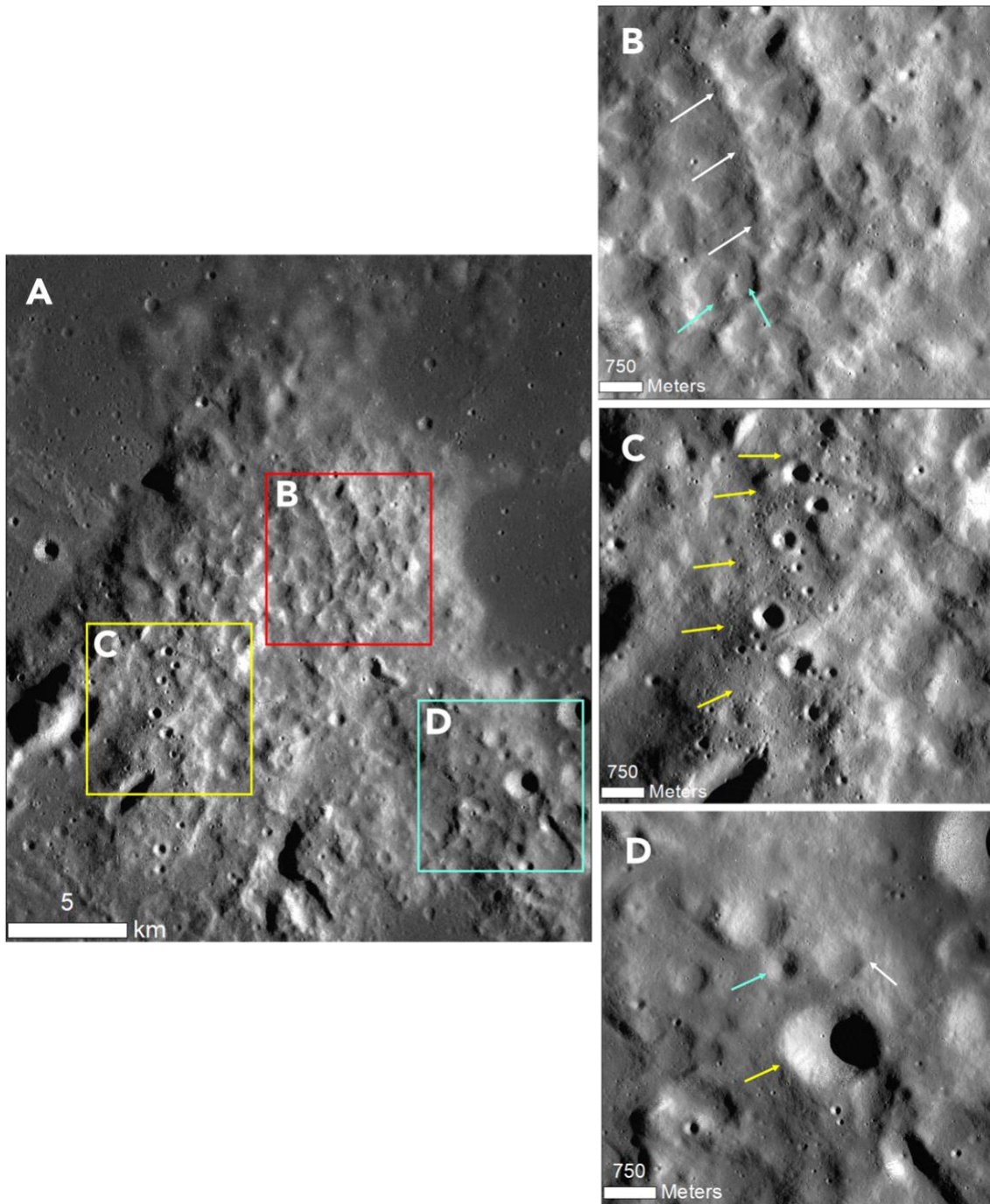
Figure 4.5 Illustrating the criteria for crater counting at (A) Mons Hansteen; (B) White arrows point to landforms here interpreted as flow fronts. Teal arrows point to quasi-circular features identified as degraded impact craters in Boyce et al. (2017) and Qiu et al. (2022). These quasi-circular features are here interpreted as degraded primary silicic flows

and are excluded from crater counts in this study; (C) yellow arrows point to a secondary crater chain in the SW of Mons Hansteen, excluded from crater counts in this study; (D) examples of impact craters included in this study – the yellow arrow points to a fresh impact crater with a raised rim; the teal arrow points to a degraded crater, and the white arrow points to a heavily degraded crater with subdued rims.

Table 4.1 Image datasets used for CSFD measurements.

Geologic Unit	Images	Incidence Angle	Pixel Scale (m/pixel)
Hansteen crater ejecta	M177981887 (WAC) M177975127 (WAC)	75°	65
Hansteen floor unit	M1320425430L/R (NAC)	67°	1.5
Mons Hansteen	NAC Regional Mosaic HANSTEENLOA made from the following NAC image pairs: M1154535012L/R M1154542131L/R M1154549249L/R	72°	1

| Billy crater | M1397916918L/R (NAC) M1397909887L/R (NAC) M1397902855L/R (NAC) | 66°-68° | 0.8 |
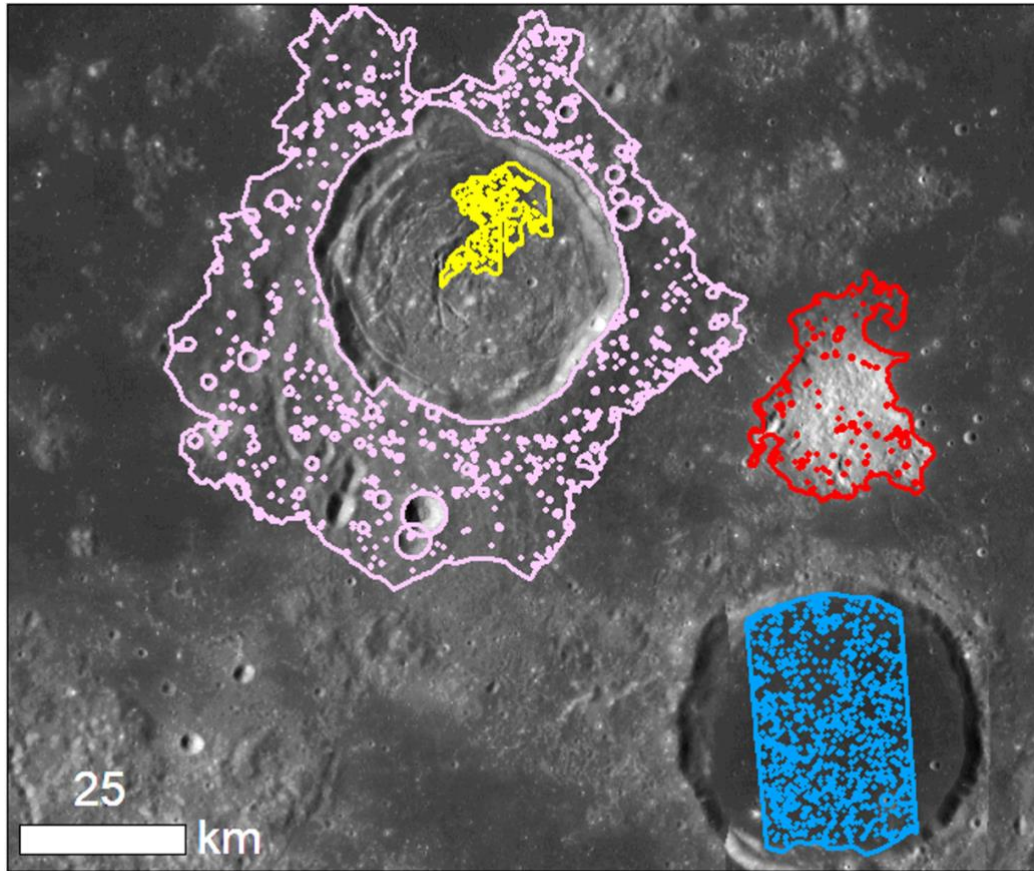
Figure 4.6 Study area with geologic units for CSFD measurements. Base map: LROC WAC monochrome mosaic (Robinson et al., 2010).

4.4 Results

The Hansteen crater ejecta unit covers an area of 5.65×10^3 km^2 and includes 601 craters. The AMA for this unit was derived by fitting craters 1.5 km to 4 km in diameter ($n = 15$), yielding an age of 3.8 +0.04/-0.05 Ga (Fig. 4.7). Craters in the smaller bins were excluded from the fit as they are in equilibrium (Trask, 1966).

Hansteen Crater Ejecta Unit
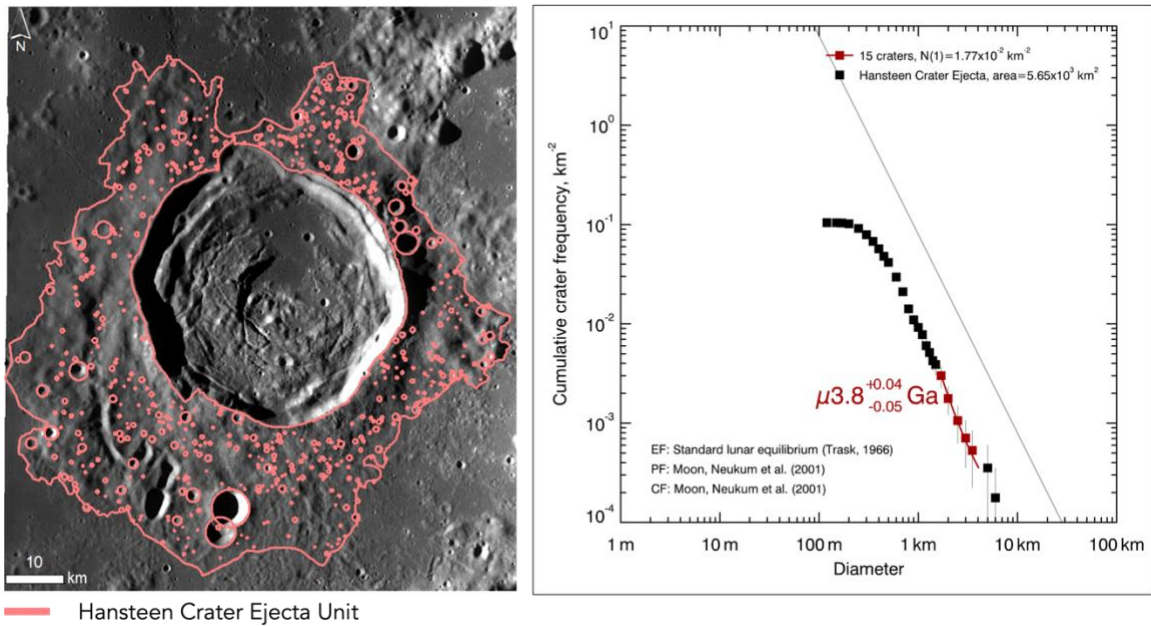
Figure 4.7 Crater counts for the Hansteen crater ejecta unit (left) and the corresponding AMA derived from CSFD measurments (right).

The basaltic deposit within Hansteen crater covers an area of 1.44 x 10^2 km^2 and includes 257 craters (Fig. 4.8; Table 4.2). The AMA for this unit was derived by fitting craters 300 m to 1 km in diameter (n = 16), yielding an age of 3.4 +0.1/ - 0.3 Ga (Fig. 4.8; Table 4.2).
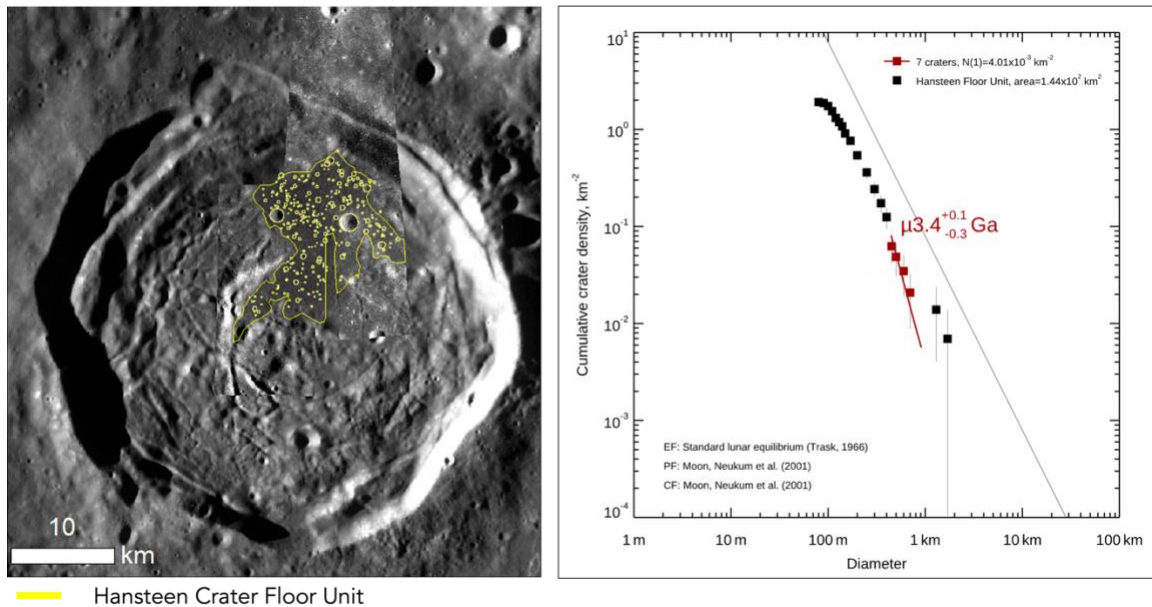
Figure 4.8 Crater counts for the Hansteen crater basalt unit (left) and the corresponding AMA derived from CSFD measurements (right).

Mons Hansteen covers an area of 5.04 x 10^2 km^2 and includes 101 craters (Fig. 4.9; Table 4.2). We treated Mons Hansteen as a one unit as opposed to three (Pitted Unit, Hilly & Dissected Unit, and North Massif) identified by Boyce et al., 2017, since we did not find significant morphological differences between the three units (S1-S3). The AMA for this unit was derived by fitting craters 500 m to 1 km in diameter ($n = 13$), yielding an age of 3.4 +0.1 /- 0.3 Ga (Fig. 4.9; Table 4.2). Areas with secondary crater population and steep slopes were excluded as they do not represent surfaces that are not in production and therefore were excluded from CSFD measurements (Fig. 4.9).
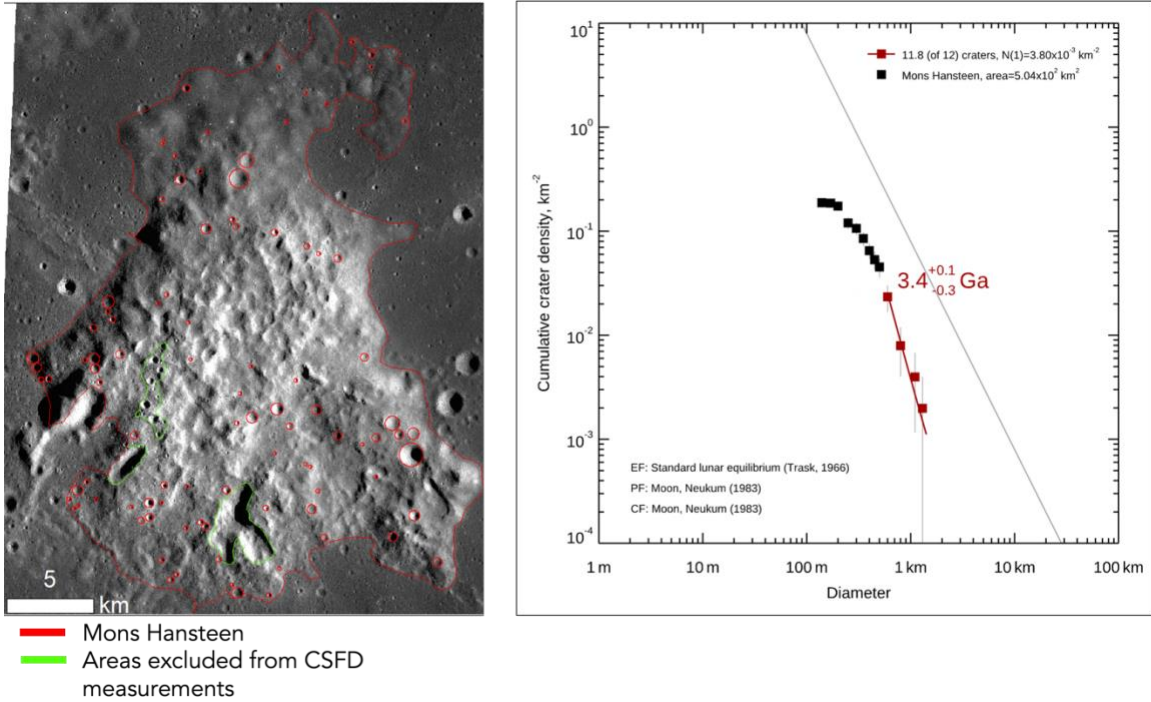
Figure 4.9 Crater counts for Mons Hansteen (left) and the corresponding AMA derived from CSFD measurements (right).

The Billy crater floor unit covers a count area of 8.26×10^2 km^2 and includes 1048 craters (Fig. 4.10; Table 4.2). The AMA for this unit was derived by fitting craters 200 m to 1 km in diameter (n = 161), yielding an age of 1.4 ± 0.08 Ga (Fig. 4.10; Table 4.2).

84

Figure 4.10 Crater counts for Mons Hansteen (left) and the corresponding AMA derived from CSFD measurements (right). Background WAC image of Billy crater with higher-resolution NAC images of the crater floor.
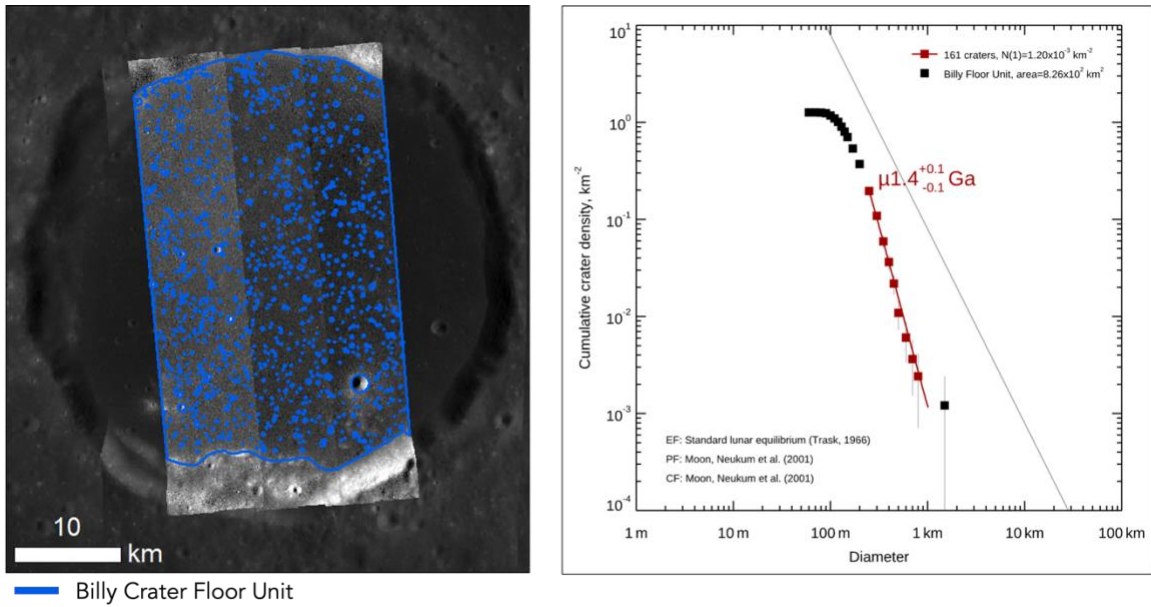
Table 4.1 Summary of geologic units, count areas and AMAs from this study.

Geologic unit	Area (km^2)	Craters	AMA (Ga)	Error bars (Ga)	Craters fit
Hansteen crater ejecta	5.65 x 10^3	601	3.8	+ 0.04/-0.05	15
Hansteen basaltic floor	1.44 x 10^2	127	3.4	+0.1/-0.3	7
Mons Hansteen	5.04 x 10^2	101	3.4	+0.1/-0.3	12
Billy crater floor unit	8.26 x 10^2	1048	1.4	$\pm$ 0.1	161

Table 4.3 Comparison of results between previous work and this study

Geologic Unit	AMA (Ga)	Study
Hansteen crater ejecta	3.80 +0.04/-0.05	This study
	3.87 +0.04/-0.06	Wagner et al. (2010)
Hansteen crater basaltic floor	3.4 +0.1/-0.3	This study
	3.5 $\pm$ 0.01	Wagner et al. (2010)
Mons Hansteen	3.67 +0.04/-0.06	Wagner et al. (2010)
	3.74 +0.075/- 0.15 to 3.5 +0.15/- 1	Boyce et al. (2017)
	3.8 +0.02/-0.03 to 3.6 +0.06/-0.1	Qiu et al. (2022)
	3.4 +0.1/-0.3	This study
Billy crater floor unit	1.65 $\pm$ 0.29	Hiesinger et al. (2003)
	1.67 +0.58/-0.59	Hiesinger et al. (2011)
	1.4 $\pm$ 0.1	This study

4.5 Discussion and Conclusion

In this study, we tested the stratigraphic relationship between floor-fractured crater, Hansteen, the nearby silicic volcanic landform, Mons Hansteen, and the Billy crater floor basalts by measuring the CSFDs of Hansteen crater ejecta, the basaltic unit within Hansteen crater floor and the Mons Hansteen edifice. AMAs derived from our CSFD measurements

87

show that the Hansteen crater impact event occurred at 3.8 +0.04/-0.05 Ga (Fig. 4.7). The floor of Hansteen crater was later modified by basaltic lavas at 3.4 +0.1/-0.3 Ga (Fig. 4.8), which was contemporaneous with the formation of Mons Hansteen at 3.4 +0.1/-0.3 Ga (Fig. 4.9). Previous CSFD measurements derived AMAs for Mons Hansteen to be 3.74 ± 0.06 Ga (Wagner et al., 2010), 3.74 +0.075/- 0.15 Ga to 3.5 +0.15/- 1 Ga (Boyce et al., 2017), and 3.8 +0.02/-0.03 Ga to 3.6 +0.06/-0.1 Ga (Qiu et al., 2022). The discrepancy between AMAs derived in this study and that of Wagner et al. (2010) can be attributed to the resolution limits (20 m/pixel) of the Lunar Orbiter IV images and the minimum crater diameter (200 m) used for CSFD measurements by Wagner et al. (2010). Furthermore, Boyce et al. (2017) and Qiu et al. (2022) did not exclude the chain of secondary craters we observed in SW Mons Hansteen and the quasi-circular features from their CSFD measurements, which could explain the large uncertainties in the AMAs derived by Boyce et al. (2017) and the relatively older age (3.7 – 3.8 Ga) calculated by both studies (Boyce et al., 2017; Qiu et al., 2022; Fig. 4.5). Silicic volcanic constructs on the Moon range in age from ~3.9 Ga to ~3.6 Ga (Wagner et al., 2010; Ashley et al., 2016; Shirley et al., 2016). Our estimate of ~3.4 Ga Mons Hansteen not only significantly reduced the uncertainties (Table 4.3) but also implies that silicic volcanism was active into the late Imbrian period.

Qiu et al. (2022) concluded that the Billy impact event caused an uplift and partial melting of the mantle thereby inundating Billy crater's floor with mare basalts. The rising basaltic magma resulted in partial melting of the pre-existing anorthositic crust, giving rise to silicic lithologies found at Mons Hansteen (Qiu et al., 2022). However, the AMA of the mare basalts on the floor of Billy crater is 1.4 ± 0. 1 Ga (Fig. 4.10, Tables 4.2, 4.3), postdating the formation of Mons Hansteen by ~2 Ga. Furthermore, previous studies based

on observations from the Gravity Recovery and Interior Laboratory (GRAIL) have shown the plausibility of mantle uplift following impact events of D > 100 km (Ding et al., 2021). Therefore, it seems unlikely that the Billy crater (D = 45 km) impact event caused mantle uplift and later influenced the formation of Mons Hansteen.

However, our CSFD measurements and corresponding AMAs show a temporal association of the basaltic floor unit of Hansteen crater (3.4 +0.1/-0.3 Ga; Fig 4.8) and Mons Hansteen (3.4 + 0.1/-0.3 Ga; Fig. 4.9). The spatiotemporal association of the basaltic lavas at Hansteen crater and the silicic lavas at Mons Hansteen is consistent with fractional crystallization of basaltic magmas giving rise to the silicic lithology found at Mons Hansteen. Similarly, the spatiotemporal association of basaltic and silicic lithologies is also observed at Compton crater (a floor-fractured crater) and the CBVC in the lunar FHT (Shirley et al., 2016). Shirley et al. (2016) computed AMAs for the basaltic floor unit at Compton crater to 3.6 ± 0.1 Ga contemporaneous with CBVC, analogous to the Hansteen crater basalts and Mons Hansteen.

We conclude that there is a plausibility that bimodal volcanism played a role in generating silicic magmas on the Moon based on the spatiotemporal association of floor-fractured craters and silicic volcanic landforms based on the similar AMAs determined for the two landforms. However, since this conclusion on only two cases (i.e., Hansteen crater and Mons Hansteen; Compton crater and CBVC), further work is needed to test temporal association of floor-fractured craters and silicic volcanic landforms.

Supplementary Material

Text S4.1.

The Hilly & Dissected unit covers an area of 2.9 x 10^2 km² and includes 23 craters. The AMA for this unit was derived by fitting craters 500 m to 900 m in diameter (n = 14), yielding an age of 3.4 Ga (+ 0.08 Ga, - 0.2 Ga).
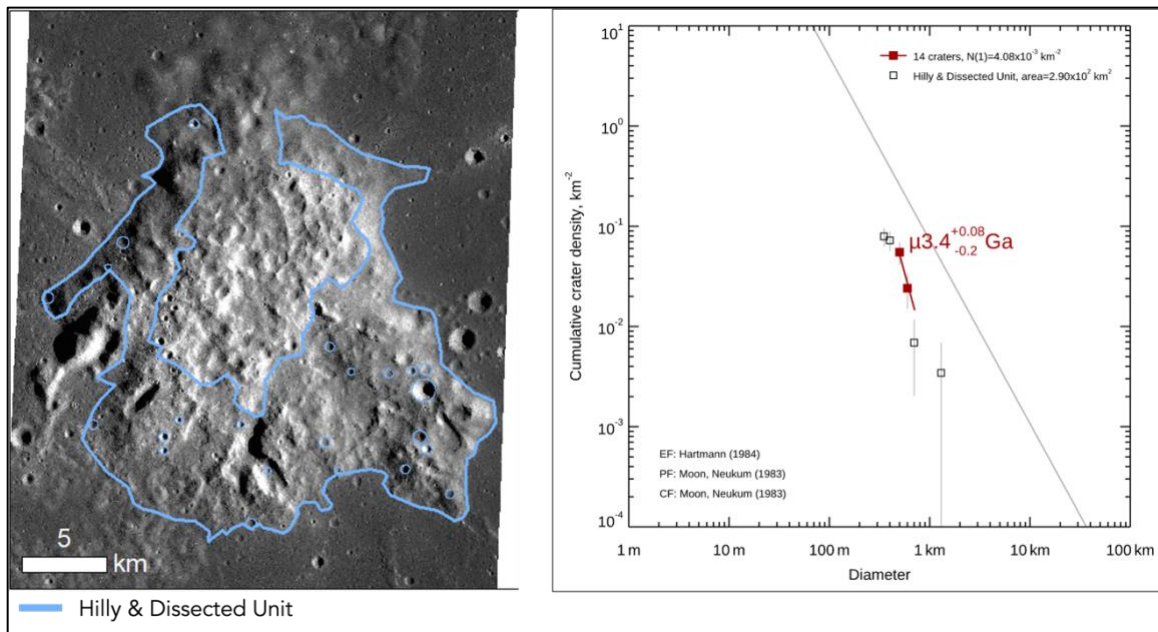
Figure S4.1. Crater counts for the Hilly & Dissected unit (left) and the corresponding AMA derived from CSFD measurement (right).

Text S4.2.

The Pitted unit covers an area of 1.19 x 10^2 km² and includes 14 craters. The AMA for this unit was derived by fitting craters 300 m to 600 m in diameter (n = 13), yielding an age of 3.4 Ga (+ 0.1 Ga, - 0.3 Ga).
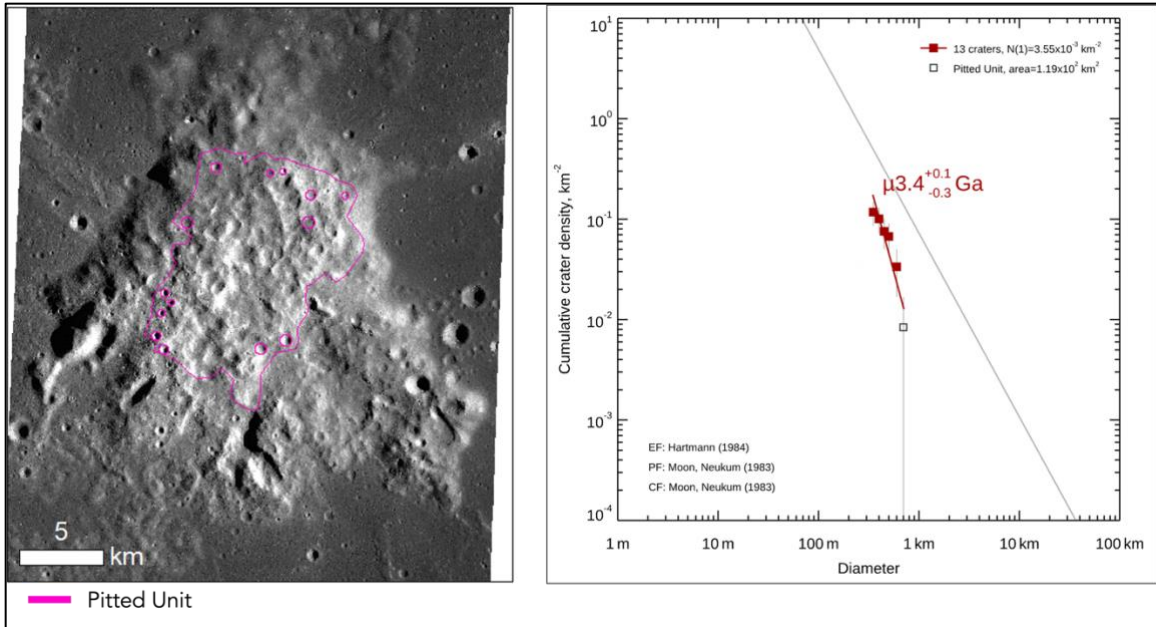
Figure S4.2. Crater counts for the Pitted unit (left) and the corresponding AMA derived from CSFD measurement (right).

Text S4.3.

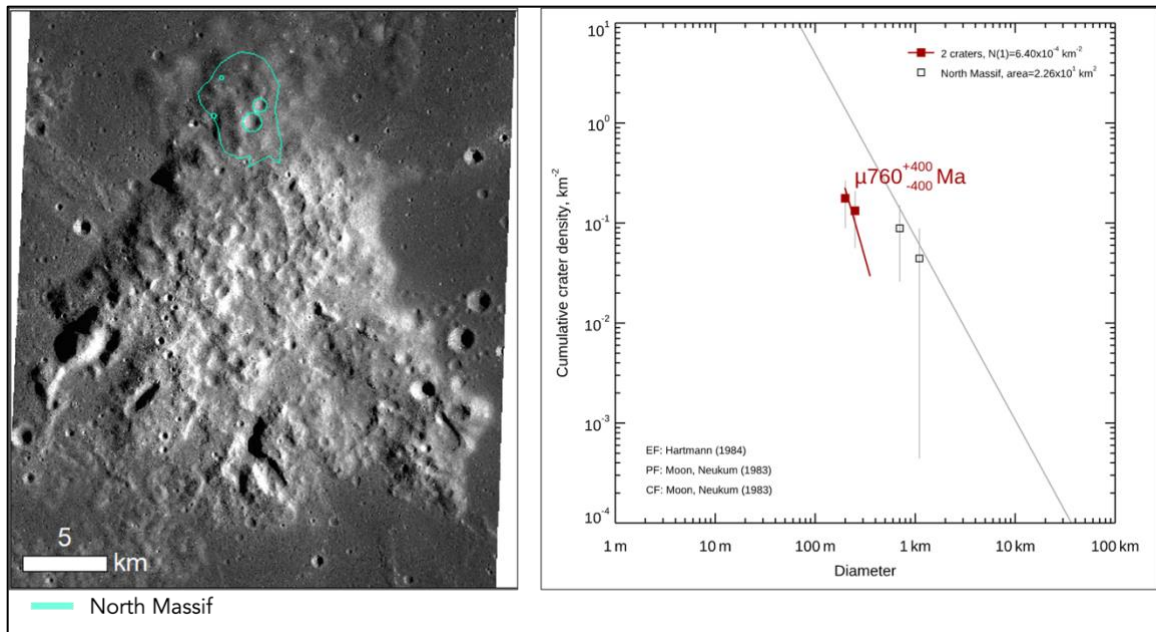The Pitted unit covers an area of 22.6 km² and includes 4 craters. The AMA for this unit was derived by fitting craters 200 m to 300 m in diameter ($n = 2$), yielding an age of 760 Ma $\pm$ 400 Ma.

Figure S4.3. Crater counts for the North Massif (left) and the corresponding AMA derived

from CSFD measurement (right).

References

Ashley, J. W., Robinson, M. S., Stopar, J. D., Glotch, T. D., Hawke, B. R., van der Bogert, C. H., Hiesinger, H., Lawrence, S. J., Jolliff, B. L., Greenhagen, B. T., Giguere, T. A., and Paige, D. A. (2016), The Lassell Massif – A Silicic Lunar Volcano. *Icarus, 273,* 248-261. doi: 10.1016/j.icarus.2015.12.036

Boyce, J. M., Giguere, T. A., Hawke, B. R., Mouginis-Mark, P. J., Robinson, M. S., Lawrence, S. J., Trang, D., and Clegg-Watkins, R. N. (2017), Hansteen Mons: An LROC Geological Perspective. *Icarus, 283,* 254-267. doi: 10.1016/j.icarus.2016.08.013

Boyce, J. M., Giguere, T., Mouginis-Mark, P., and Glotch, T. (2018), Geology of the Mairan Middle Dome: Its Implication to Silicic Volcanism on the Moon. *Planetary and Space Science, 162,* 62-72. doi: 10.1016/j.pss.2017.12.009

Crater Analysis Techniques Working Group (1979). Standard techniques for presentation and analysis of crater-size frequency data. *Icarus, 37,* 467-474. doi: 10.1016/0019-1035(79)90009-5

Ding, M., Soderblom, J. M, Bierson, C. J., and Zuber, M. T. (2021). Investigating the influences of crustal thickness and temperature on the uplift of mantle materials beneath

large impact craters on the Moon. *Journal of Geophysical Research: Planets, 126 (2),* e2020JE006533. doi: https://doi.org/10.1029/2020JE006533

Glotch, T. D., Lucey, P. G., Bandfield, J. L., Greenhagen, B. T., Thomas, I. R., Elphic, R. C., Bowles, N., Wyatt, M. B., Allen, C. C., Hanna, K. D., & Paige, D. A. (2010). Highly silicic compositions on the moon. *Science, 329(5998)*, 1510–1513. https://doi.org/10.1126/SCIENCE.1192148/SUPPL_FILE/GLOTCH.SOM.PDF

Hagerty, J. J., Lawrence, D. J., Hawke, B. R., Vaniman, D. T., Elphic, R. C., & Feldman, W. C. (2006). Refined thorium abundances for lunar red spots: Implications for evolved, nonmare volcanism on the Moon. *Journal of Geophysical Research E: Planets, 111(6),* 1–20. https://doi.org/10.1029/2005JE002592

Hall, J. L., Solomon, S. C., and Head, J. W. (1981), Lunar Floor-fractured craters: Evidence for Viscous Relaxation of Crater Topography. *Journal of Geophysical Research, 86*, 9537-9552. doi: 10.1029/JB086iB10p09537

Hartmann, W. K. (1966). Early lunar cratering. *Icarus, 5,* 406-418. doi: 10.1016/0019-1035(66)90054-6

Hawke, B. R., Lawrence, D. J., Blewett, D. T., Lucey, P. G., Smith, G. A., Spudis, P. D., and Taylor, G. J. (2003), Hansteen Alpha: A Volcanic Construct in the Lunar Highlands. *Journal of Geophysical Research: Planets, 108,* E7, 5069. doi: 10.1029/2002je002013

Hiesinger, H. Jaumann, R., Neukum, G., and Head, J. W. (2000). Ages of mare basalts on the lunar nearside. *Journal of Geophysical Research: Planets*, *105,* 29239-29275. doi: 10.1029/2000JE001244

Jolliff, B. L., Gillis, J. J., Haskin, L. A., Korotev, R. L., and Wieczorek, M. A. (2000). Major Lunar Crustal Terranes: Surface Expression and Crust-Mantle Origin. *Journal of Geophysical Research 105*, 4197-4216. doi: 10.1029/1999JE001103

Jolliff, B. L., Wiseman, S. A., Lawrence, S. J., Tran, T. N., Robinson, M. S., Sato, H., Hawke, B. R., Scholten, F., Oberst, J., Hiesinger, H., van der Bogert, C. H., Greenhagen, B. T., Glotch, T. D., Paige, D. A. (2011), Non-Mare Silicic Volcanism on the Lunar Farside at Compton Belkovich. *Nature Geoscience, 4,* 566-571. doi: 10.1038/ngeo1212

Jozwiak, L. M., Head, J. W., and Zuber, M. T. (2012), Lunar Floor-fractured craters: Classification, Distribution, Origin, and Implications for Magmatism and Shallow Crustal Structure. *Journal of Geophysical Research, 117*, E11005. doi: 10.1029/2012JE004134

Jozwiak, L. M., Head, J. W., Neumann, G. A., and Wilson, L. (2017), Observational Constraints on the Identification of Shallow Lunar Magmatism: Insights from Floor-fractured craters. *Icarus 283*, 224-231. doi: 10.1016/j.icarus.2016.04.020

Kneissl, T., van Gasselt S., and Neukum G. (2011), Map-projection-independent crater size-frequency determination in GIS environments — New software tool for ArcGIS. *Planetary and Space Science, 59,* 1243-1254. doi: 10.1016/j.pss.2010.03.015

Lawrence, D. J., Feldman, W. C., Barraclough, B. L., Binder, A. B., Elphic, R. C., Maurice, S., Miller, M. C., & Prettyman, T. H. (2000). Thorium abundances on the lunar surface. *Journal of Geophysical Research: Planets, 105(E8)*, 20307–20331. https://doi.org/10.1029/1999JE001177

Malin, M. C. (1974). Lunar Red Spots. Earth, 21, 331–341.

Michael, G.G., and Neukum G. (2010), Planetary surface dating from crater size-frequency distribution measurements: Partial resurfacing events and statistical age uncertainty. *Earth and Planetary Science Letters, 294 (3-4)*, 223-229. doi: 10.1016/j.epsl.2009.12.041

Neukum G. (1983). Meteoritenbombardement und Datierung planetarer Oberflachen. Habilitation Dissertation for Faculty Membership, University of Munich. 186 p.

Neukum, G., and Ivanov, B. A. (1994), Crater Size Frequency Distributions and Impact Probabilities on Earth from Lunar, Terrestrial-Planet, and Asteroid Cratering Data. *In: Hazard Due to Comets and Asteroids*, 359-416

Neukum, G., Ivanov, B. A., and Hartmann, W. K. (2001), Crater Records in the Inner-Solar System in relation to the Lunar Reference System. *Space Science Reviews 96*, 55-86. doi: 10.1023/A:1011989004263

Qiu, D., Ye, M., Yan, J., Zheng, C., Xiao, Z., Zhang, Q., Gao, Q., Liu, L., and Li., F. (2022), New Views of the Lunar Silicic Volcanism in the Mons Hansteen: Formation and Origins. *Journal of Geophysical Research: Planets, 127,* e2022JE007289. doi: 10.1029/2022JE007289

Ravi, S., and Robinson, M. S. (2019), Lunar Floor-Fractured Craters: A Case for Viscous Relaxation. *Lunar and Planetary Science Conference L,* Abstract #2677.

Ravi, S., and Robinson, M. S. (2022), Rheology of the Lunar Lithosphere and the Origin of Floor-Fractured Craters. *Lunar and Planetary Science Conference LII,* Abstract #1266.

Ravi, S., Robinson, M. S., and Clark, J. D. (2023), *Spatio-Temporal Association of Mons Hansteen and Hansteen Crater: Implications for Silicic Magma Genesis* (Dataset). Zenodo. doi: 10.5281/zenodo.7706699

Robinson, M. S., Brylow, S. M., Tschimmel, M., Humm, D., Lawrence, S.J., Thomas, P.C., Denevi, B.W., Bowman-Cisneros, E., Zerr, J., Ravine, M.A., Caplinger, M.A., Ghaemi, F.T., Schaffner, J.A., Malin, M.C., Mahanti, P., Bartels, A., Anderson, J., Tran, T.N., Eliason, E.M., McEwen, A.S., Turtle, E., Jolliff, B.L., Hiesinger, H. (2010), Lunar

Reconnaissance Orbiter Camera (LROC) Instrument Overview, *Space Science Reviews, 150*, 81-124. doi: 10.1007/S11214-010-9634-2

Ryder, G. (1976). Lunar sample 15405: Remnant of a KREEP basalt-granite differentiated pluton. *Earth and Planetary Science Letters,* 29(2), 255–268. https://doi.org/10.1016/0012-821X(76)90129-1

Scholten, F., Oberst, J., Matz, K.-D., Roatsch, T., Wählisch, M., Speyerer, E.J., and Robinson, M.S. (2012), GLD100: The Near-Global Lunar 100 m Raster DTM from LROC WAC Stereo Image Data. *Journal of Geophysical Research, 117*, E00H17. doi: 10.1029/2011JE003926

Schultz, P.H. (1976), Lunar Floor-fractured craters. *The Moon, 15*, 241-273. doi: 10.1007/BF00562240

Shirley, K. A., Zanetti, M., Jolliff, B., van der Bogert, C. H., and Hiesinger, H. (2016), Crater Size-Frequency Distribution Measurements and Age of the Compton-Belkovich Volcanic Complex. *Icarus, 273,* 214-223. doi: 10.1016/j.icarus.2016.03.015

Stöffler, D., and Ryder, G. (2001), Stratigraphy and Isotope Ages of Lunar Geologic Units: Chronological Standard for the Inner Solar System. *Space Science Reviews, 96,* 9-54. doi: 10.1023/A:1011937020193

Wagner, R., Head, J. W., Wolf, U., and Neukum, G. (2010), Lunar Red Spots: Stratigraphic Sequence and Ages of Domes and Plains in the Hansteen and Helmet Regions on the Lunar Nearside. *Journal of Geophysical Research, 115,* E06015. doi: 10.1029/2009JE003359

Wieczorek, M. A., and Phillips, R. J. (2000), The "Procellarum KREEP Terrane": Implications for Mare Volcanism and Lunar Evolution. *Journal of Geophysical Research, 105*, 20417-20430. doi: 10.1029/1999JE001092

CHAPTER 5
CONCLUSIONS

The work presented here investigated crustal deformation and silicic magma genesis within the lunar Procellarum KREEP Terrane (PKT). These investigations were made possible by the image and topography datasets from the Lunar Reconnaissance Orbiter Camera (LROC) (Robinson et al., 2010; Scholten et al., 2010) and the rhyolite-MELTS program (Gualda et al., 2012).

In Chapter 2: *Origin of Lunar Floor-Fractured Craters: Revisiting the Viscous Relaxation Hypothesis,* I presented a detailed study of floor-fractured crater morphology, variations in temporal heat flow, rheology, and global maps of floor-fractured craters with respect to impact basins. The overarching conclusion is that viscous relaxation cannot be ruled out as a viable mechanism for the formation of floor-fractured craters and that viscous relaxation and magmatic intrusion are not mutually exclusive, as has been argued in earlier studies. I conclude that floor-fractured craters likely underwent tectonic deformation followed by modification by magmatic intrusion.

In Chapter 3: *Lunar Silicic Magma Genesis: Insights from Petrological Modeling,* I demonstrate that fractional crystallization of KREEP basalt magmas is a plausible mechanism for the generation of silicic melts on the Moon. Specifically, the results of rhyolite-MELTS modeling suggest that following crystallization, the composition of the remaining ~30 wt.% liquids are consistent with returned lunar silicic fragments. Furthermore, fractional crystallization of anhydrous basalts, which produce lunar silicic melts, may be analogous to the terrestrial Proterozoic Anorthosite Mangerite Charnockite Granite (AMCG) suites. Since lunar silicic melts formed in anhydrous (low fO$_2$), high-

temperature magmas (900°C-950°C – from rhyolite-MELTS models) at shallow crustal depths, we conclude that the geothermal gradient within the PKT, where most of the silicic landforms are located, was relatively high at the time of silicic magma genesis (3.8-3.9 Ga).

In Chapter 4: *Spatio-Temporal Association of Hansteen Crater and Mons Hansteen: Implications for Silicic Magma Genesis,* I tested the stratigraphic relationship between floor-fractured crater, Hansteen, the silicic volcanic landform, Mons Hansteen, and the Billy crater floor basalts by measuring the Crater Size-Frequency Distribution (CSFD) of Hansteen crater ejecta, the basaltic unit within Hansteen crater floor and the Mons Hansteen edifice. AMAs derived from our CSFD measurements show that the Hansteen crater impact event occurred at 3.8 +0.04/-0.05 Ga. The floor of Hansteen crater was later modified by basaltic lavas at 3.4 +0.1/-0.3 Ga, which was contemporaneous with the formation of Mons Hansteen at 3.4 +0.1/-0.3 Ga. Our estimate of ~3.4 Ga Mons Hansteen not only significantly reduced the uncertainties but also implies that silicic volcanism was active into the late Imbrian period. The results of chapter 4 support that of chapter 3 in that it is plausible that bimodal volcanism played a role in generating silicic magmas on the Moon based on the spatiotemporal association of floor-fractured craters and silicic volcanic landforms based on the similar AMAs determined for the two landforms.

Future Work

The results of chapter 2 highlight the need for quantitative analysis of floor-fractured crater topography. Approximating the topographic profiles of floor-fractured craters Chebyshev polynomials (Mahanti et al., 2014) will improve the understanding of the extent of topographic deformation pre-existing craters undergo.

Chapter 3 shows the plausibility of silicic magmas forming from the fractional crystallization of KREEP basalts. Samples from the silicic targets are needed to validate the findings of the rhyolite-MELTS models.

Lastly, the pilot study presented in chapter 4 needs to be expanded to include all other cases of floor-fractured crater and silicic volcanic landform association.

References

Mahanti, P., Robinson, M. S., Humm, D. C., and Stopar, J. D., 2014. A Standardized Approach
for Quantitative Characterization of Impact Crater Topography. *Icarus 241*, 114-129.

Robinson, M. S., Brylow, S. M., Tschimmel, M., Humm, D., Lawrence, S.J., Thomas, P.C., Denevi, B.W., Bowman-Cisneros, E., Zerr, J., Ravine, M.A., Caplinger, M.A., Ghaemi, F.T., Schaffner, J.A., Malin, M.C., Mahanti, P., Bartels, A., Anderson, J., Tran, T.N., Eliason, E.M., McEwen, A.S., Turtle, E., Jolliff, B.L., Hiesinger, H. (2010), Lunar Reconnaissance Orbiter Camera (LROC) Instrument Overview. *Space Science Reviews, 150*, 81-124.

Scholten, F., Oberst, J., Matz, K.-D., Roatsch, T., Wählisch, M., Speyerer, E.J., and Robinson, M.S. (2012), GLD100: The Near-Global Lunar 100 m Raster DTM from LROC WAC Stereo Image Data. *Journal of Geophysical Research, 117*, E00H17.

REFERENCES

Anderson, J. L., & Bender, E. E. (1989). Nature and origin of Proterozoic A-type granitic magmatism in the southwestern United States of America. LITHOS. https://doi.org/10.1016/0024-4937(89)90021-2

Ashley, J. W., Robinson, M. S., Stopar, J. D., Glotch, T. D., Hawke, B. R., van der Bogert, C. H., Hiesinger, H., Lawrence, S. J., Jolliff, B. L., Greenhagen, B. T., Giguere, T. A., and Paige, D. A. (2016), The Lassell Massif – A Silicic Lunar Volcano. *Icarus, 273,* 248-261. doi: 10.1016/j.icarus.2015.12.036

Ashwal, L. D. (1993). Anorthosites. Springer-Verlag.

Barker, F., Wones, D. R., Sharp, W. N., & Desborough, G. A. (1975a). The Pikes Peak batholith, Colorado front range, and a model for the origin of the gabbro-anorthosite-syenite-potassic granite suite. Precambrian Research. https://doi.org/10.1016/0301-9268(75)90001-7

Barker, F., Wones, D. R., Sharp, W. N., & Desborough, G. A. (1975b). The Pikes Peak batholith, Colorado front range, and a model for the origin of the gabbro-anorthosite-syenite-potassic granite suite. Precambrian Research, 2(2). https://doi.org/10.1016/0301-9268(75)90001-7

Blanchard, D. P., Jacobs, J. W., & Brannon, J. C. (1977). Chemistry of the ANT-suite and felsite clasts from the consortium breccia 73255. Proceedings of the Eigth Lunar and Planetary Science Conference, 2507–2524.
Boyce, J. M., Giguere, T. A., Hawke, B. R., Mouginis-Mark, P. J., Robinson, M. S., Lawrence, S. J., Trang, D., and Clegg-Watkins, R. N. (2017), Hansteen Mons: An LROC Geological Perspective. *Icarus, 283,* 254-267. doi: 10.1016/j.icarus.2016.08.013

Boyce, J. M., Giguere, T., Mouginis-Mark, P., and Glotch, T. (2018), Geology of the Mairan Middle Dome: Its Implication to Silicic Volcanism on the Moon. *Planetary and Space Science, 162*, 62-72. doi: 10.1016/j.pss.2017.12.009

Boyce, J. M., Giguere, T., Mouginis-Mark, P., Glotch, T., & Taylor, G. J. (2018). Geology of Mairan middle dome: Its implication to silicic volcanism on the Moon. Planetary and Space Science, 162(January 2017), 62–72. https://doi.org/10.1016/j.pss.2017.12.009

Brunfelt, A. O., Heier, K. S., Nilssen, B., & Sundvoll, B. (1972). Distribution of elements between different phases of Apollo 14 rocks and soils. Proceedings of the Third Lunar Conference, 2, 1133–1147.

Cadogan, P. H. (1974), Oldest and Largest Lunar basin? *Nature, 250*, 315-316. doi: 10.1038/250315a0

Cadogan, P. H. (1975), The Gargantuan Basin: Some Implications. *Lunar and Planetary Institute.*

Chen, W., and Molnar, P. (1983), Focal depths of intracontinental and intraplate earthquakes and their implications for the thermal and mechanical properties of the lithosphere. *Journal of Geophysical Research, 88*, 4183–4214. doi: 10.1029/JB088IB05P04183

Cooper, K. M., and Kent, A. J. R. (2014). Rapid remobilization of magmatic crystals kept in cold storage. Nature, 506, 480-483.

Crater Analysis Techniques Working Group (1979). Standard techniques for presentation and analysis of crater-size frequency data. *Icarus, 37,* 467-474. doi: 10.1016/0019-1035(79)90009-5

de Vries, J., van den Berg, A., & van Westrenen, W. (2010). Formation and evolution of a lunar core from ilmenite-rich magma ocean cumulates. Earth and Planetary Science Letters, 292(1–2), 139–147. https://doi.org/10.1016/J.EPSL.2010.01.029

Ding, M. Zhu, M. H. (2022), Effects of regional thermal state on the crustal annulus relaxation of lunar large impact basins. *Journal of Geophysical Research Planets, 127* (3), e2021JE007132. doi: 10.1029/2021JE007132

Ding, M., Soderblom, J. M, Bierson, C. J., and Zuber, M. T. (2021). Investigating the influences of crustal thickness and temperature on the uplift of mantle materials beneath large impact craters on the Moon. *Journal of Geophysical Research: Planets, 126 (2),* e2020JE006533. doi: https://doi.org/10.1029/2020JE006533

Dombard, A.J., and Gillis, J.J. (2001), Testing the Viability of Topographic Relaxation as a Mechanism for the Formation of Lunar Floor-fractured craters. *Journal of Geophysical Research: Planets 106*, 27901-27909. doi: 10.1029/2000JE001388

Elkins-Tanton, L. T., Burgess, S., & Yin, Q. Z. (2011). The lunar magma ocean: Reconciling the solidification process with lunar petrology and geochronology. Earth and Planetary Science Letters, 304(3–4), 326–336. https://doi.org/10.1016/j.epsl.2011.02.004

Elkins-Tanton, L. T., Hager, B. H., & Grove, T. L. (2004). Magmatic effects of the lunar late heavy bombardment. Earth and Planetary Science Letters, 222(1), 17–27. https://doi.org/10.1016/j.epsl.2004.02.017

Emslie, R. F. (1978a). Anorthosite massifs, rapakivi granites, and late proterozoic rifting of north America. Precambrian Research. https://doi.org/10.1016/0301-9268(78)90005-0

Emslie, R. F. (1978b). Anorthosite massifs, rapakivi granites, and late proterozoic rifting of north America. Precambrian Research, 7(1), 61–98. https://doi.org/10.1016/0301-9268(78)90005-0

Emslie, R. F. (1985). Proterozoic anorthosite massifs. The Deep Proterozoic Crust in the North Atlantic Provinces, 39–60. https://doi.org/10.1007/978-94-009-5450-2_4

Emslie, R. F. (1991). Granitoids of rapakivi granite-anorthosite and related associations. Precambrian Research. https://doi.org/10.1016/0301-9268(91)90100-O

for Quantitative Characterization of Impact Crater Topography. Icarus 241, 114-129. Frost, C. D., & Frost, B. R. (1997). Reduced rapakivi-type granites: The tholeiite connection. Geology. https://doi.org/10.1130/0091-7613(1997)025<0647:RRTGTT>2.3.CO;2

Frost, C. D., Frost, B. R., Bell, J. M., & Chamberlain, K. R. (2002). The relationship between A-type granites and residual magmas from anorthosite: Evidence from the northern Sherman batholith, Laramie Mountains, Wyoming, USA. Precambrian Research. https://doi.org/10.1016/S0301-9268(02)00117-1

Gancarz, A. J., Albee, A. L., & Chodos, A. A. (1971). Petrologic and mineralogic investigation of some crystalline rocks returned by the Apollo 14 mission. Earth and Planetary Science Letters, 12(1), 1–18. https://doi.org/10.1016/0012-821X(71)90050-1

Gilmore, M. S., & Head, J. W. (2000). Sequential deformation of plains at the margins of Alpha Regio, Venus: Implications for tessera formation. Meteoritics and Planetary Science, 35(4), 667–687. https://doi.org/10.1111/J.1945-5100.2000.TB01451.X

Gilmore, M. S., Mueller, N., & Helbert, J. (2015). VIRTIS emissivity of Alpha Regio, Venus, with implications for tessera composition. Icarus, 254, 350–361. https://doi.org/10.1016/J.ICARUS.2015.04.008

Glotch, T. D., Hagerty, J. J., Lucey, P. G., Hawke, B. R., Giguere, T. A., Arnold, J. A., Williams, J. P., Jolliff, B. L., & Paige, D. A. (2011). The Mairan domes: Silicic volcanic constructs on the Moon. Geophysical Research Letters, 38(21), 1–5. https://doi.org/10.1029/2011GL049548

Glotch, T. D., Lucey, P. G., Bandfield, J. L., Greenhagen, B. T., Thomas, I. R., Elphic, R. C., Bowles, N., Wyatt, M. B., Allen, C. C., Hanna, K. D., & Paige, D. A. (2010). Highly silicic compositions on the moon. Science, 329(5998), 1510–1513. https://doi.org/10.1126/SCIENCE.1192148/SUPPL_FILE/GLOTCH.SOM.PDF

Glotch, T. D., Lucey, P. G., Bandfield, J. L., Greenhagen, B. T., Thomas, I. R., Elphic, R. C., Bowles, N., Wyatt, M. B., Allen, C. C., Hanna, K. D., & Paige, D. A. (2010). Highly silicic compositions on the moon. *Science, 329(5998)*, 1510–1513. https://doi.org/10.1126/SCIENCE.1192148/SUPPL_FILE/GLOTCH.SOM.PDF

Glotch, T.D.; Elder, C.M.; Hayne, P.O.; Greenhagen, B.T., Dhingra, D.; Kiefer, W. S. (2017). Overview of Silicic Magmatic Activity on the Moon. New Views of the Moon 2. https://doi.org/10.1017/CBO9781107415324.004

Greenhagen, Benjamin T.; Cahill, J.T.S.; Jolliff, B.L.; Lawrence, S.J.; Glotch, T. D. (2017). Investigating Evolved Compositions Around Wolf Crater. LPSC 2017. https://doi.org/10.1017/CBO9781107415324.004

Gualda, G. A. R., Ghiorso, M. S., Lemons, R. v., & Carley, T. L. (2012). Rhyolite-MELTS: A modified calibration of MELTS optimized for silica-rich, fluid-bearing magmatic systems. Journal of Petrology, 53(5), 875–890.

Gualda, G. A. R., Ghiorso, M. S., Lemons, R. v., & Carley, T. L. (2012). Rhyolite-MELTS: A modified calibration of MELTS optimized for silica-rich, fluid-bearing magmatic systems. Journal of Petrology, 53(5), 875–890. https://doi.org/10.1093/petrology/egr080
Gullikson, A. L., Hagerty, J. J., Reid, M. R., Rapp, J. F., & Draper, D. S. (2016). Silicic lunar volcanism : Testing the crustal melting model. 101(June), 2312–2321.

Haapala, I., & Rämö, O. T. (1999). Rapakivi granites and related rocks: An introduction. Precambrian Research. https://doi.org/10.1016/S0301-9268(98)00124-7

Hagerty, J. J., Lawrence, D. J., Hawke, B. R., Vaniman, D. T., Elphic, R. C., & Feldman, W. C. (2006). Refined thorium abundances for lunar red spots: Implications for evolved, nonmare volcanism on the Moon. Journal of Geophysical Research E: Planets, 111(6), 1–20.

Hagerty, J. J., Lawrence, D. J., Hawke, B. R., Vaniman, D. T., Elphic, R. C., & Feldman, W. C. (2006). Refined thorium abundances for lunar red spots: Implications for evolved, nonmare volcanism on the Moon. Journal of Geophysical Research E: Planets, 111(6), 1–20. https://doi.org/10.1029/2005JE002592

Hagerty, J. J., Lawrence, D. J., Hawke, B. R., Vaniman, D. T., Elphic, R. C., & Feldman, W. C. (2006). Refined thorium abundances for lunar red spots: Implications for evolved, nonmare volcanism on the Moon. *Journal of Geophysical Research E: Planets, 111(6),* 1–20. https://doi.org/10.1029/2005JE002592

Hall, J. L., Solomon, S. C., and Head, J. W. (1981), Lunar Floor-fractured craters: Evidence for Viscous Relaxation of Crater Topography. *Journal of Geophysical Research, 86*, 9537-9552. doi: 10.1029/JB086iB10p09537
Hall, J. L., Solomon, S. C., and Head, J. W. (1981), Lunar Floor-fractured craters: Evidence for Viscous Relaxation of Crater Topography. *Journal of Geophysical Research, 86*, 9537-9552. doi: 10.1029/JB086iB10p09537

Hartmann, W. K. (1966). Early lunar cratering. *Icarus, 5,* 406-418. doi: 10.1016/0019-1035(66)90054-6

Hauri, E. H., Wagner, T. P., & Grove, T. L. (1994). Experimental and natural partitioning of Th, U, Pb and other trace elements between garnet, clinopyroxene and basaltic melts. Chemical Geology, 117(1–4), 149–166. https://doi.org/10.1016/0009-2541(94)90126-0

Hawke, B. R., Lawrence, D. J., Blewett, D. T., Lucey, P. G., Smith, G. A., Spudis, P. D., and Taylor, G. J. (2003), Hansteen Alpha: A Volcanic Construct in the Lunar Highlands. *Journal of Geophysical Research: Planets, 108,* E7, 5069. doi: 10.1029/2002je002013

Hess, P. C., Rutherford, M. J., Guillemette, R. N., Ryerson, F. J., & Tuchfeld, H. A. (1975). Residual products of fractional crystallization of lunar magmas: an experimental study. Proceedings of the Sixth Lunar Science Conference, 895–909.

Hiesinger, H. Jaumann, R., Neukum, G., and Head, J. W. (2000). Ages of mare basalts on the lunar nearside. *Journal of Geophysical Research: Planets*, *105,* 29239-29275. doi: 10.1029/2000JE001244
Hildreth, W. (1981). Gradients in silicic magma chambers: Implications for lithospheric magmatism. Journal of Geophysical Research: Solid Earth, 86(B11), 10153–10192. https://doi.org/10.1029/JB086IB11P10153

Hubbard, F. H., & Whitley, J. E. (1978). Rapakivi granite, anorthosite and charnockitic plutonism. Nature. https://doi.org/10.1038/271439a0

Hubbard, N. J., Rhodes, J. M., Gast, P. W., Bansal, B. M., Shih, C.-Y., Weismann, H., & Nyquist, L. E. (1973). Lunar rock types: The role of plagioclase in non-mare and highland rock types. Proceedings of the Fourth Lunar Science Conference, 2, 1297–1312.

Jolliff, B. L., Floss. C, Mccallum, I. S., & Schwartz, J. M. (1999). Geochemistry, petrology, and cooling history of 14161,7373: A plutonic lunar sample with textural evidence of granitic-fraction separation by silicate-liquid immiscibility. American Mineralogist.

Jolliff, B. L., Gillis, J. J., Haskin, L. A., Korotev, R. L., & Wieczorek, M. A. (2000). Major lunar crustal terranes: Surface expressions and crust-mantle origins. Journal of Geophysical Research E: Planets, 105(E2), 4197–4216. https://doi.org/10.1029/1999JE001103

Jolliff, B. L., Gillis, J. J., Haskin, L. A., Korotev, R. L., and Wieczorek, M. A., 2000. Major Lunar Crustal Terranes: Surface Expression and Crust-Mantle Origin. Journal of Geophysical Research 105, 4197-4216.
Jolliff, B. L., Gillis, J. J., Haskin, L. A., Korotev, R. L., and Wieczorek, M. A. (2000). Major Lunar Crustal Terranes: Surface Expression and Crust-Mantle Origin. *Journal of Geophysical Research 105*, 4197-4216. doi: 10.1029/1999JE001103

Jolliff, B. L., Gillis, J. J., Haskin, L. A., Korotev, R. L., and Wieczorek, M. A. (2000). Major Lunar Crustal Terranes: Surface Expression and Crust-Mantle Origin. *Journal of Geophysical Research 105*, 4197-4216. doi: 10.1029/1999JE001103

Jolliff, B. L., Wiseman, S. A., Lawrence, S. J., Tran, T. N., Robinson, M. S., Sato, H., Hawke, B. R., Scholten, F., Oberst, J., Hiesinger, H., van der Bogert, C. H., Greenhagen, B. T., Glotch, T. D., Paige, D. A. (2011), Non-Mare Silicic Volcanism on the Lunar Farside at Compton Belkovich. *Nature Geoscience, 4,* 566-571. doi: 10.1038/ngeo1212

Jozwiak, L. M., Head, J. W., and Zuber, M. T. (2012), Lunar Floor-fractured craters: Classification, Distribution, Origin, and Implications for Magmatism and Shallow Crustal Structure. *Journal of Geophysical Research, 117*, E11005. doi: 10.1029/2012JE004134

Jozwiak, L. M., Head, J. W., and Zuber, M. T. (2012), Lunar Floor-fractured craters: Classification, Distribution, Origin, and Implications for Magmatism and Shallow Crustal Structure. *Journal of Geophysical Research, 117*, E11005. doi: 10.1029/2012JE004134

Jozwiak, L. M., Head, J. W., and Zuber, M. T., 2012. Lunar Floor-Fractured Craters: Classification, Distribution, Origin, and Implications for Magmatism and Shallow Crustal Structure. Journal of Geophysical Research 117, E11005.

Jozwiak, L. M., Head, J. W., Neumann, G. A., and Wilson, L. (2017), Observational Constraints on the Identification of Shallow Lunar Magmatism: Insights from Floor-fractured craters. *Icarus 283*, 224-231. doi: 10.1016/j.icarus.2016.04.020

Jozwiak, L. M., Head, J. W., Neumann, G. A., and Wilson, L. (2017), Observational Constraints on the Identification of Shallow Lunar Magmatism: Insights from Floor-fractured craters. *Icarus 283*, 224-231. doi: 10.1016/j.icarus.2016.04.020

Kamata, S., Sugita, S., Abe, Y. et al. (2013), Viscoelastic deformation of lunar impact basins: Implications for heterogeneity in the deep crustal paleo-thermal state and radioactive element concentration. *Journal of Geophysical Research Planets, 118* (3), 398-415. doi: 10.1002/JGRE.20056

Kaula, W. M. (1979). Thermal evolution of Earth and Moon growing by planetesimal impacts. Journal of Geophysical Research: Solid Earth, 84(B3), 999–1008. https://doi.org/10.1029/JB084IB03P00999

Klemme, S., Günther, D., Hametner, K., Prowatke, S., & Zack, T. (2006). The partitioning of trace elements between ilmenite, ulvospinel, armalcolite and silicate melts with implications for the early differentiation of the moon. Chemical Geology, 234(3–4), 251–263. https://doi.org/10.1016/J.CHEMGEO.2006.05.005

Kneissl, T., van Gasselt S., and Neukum G. (2011), Map-projection-independent crater size-frequency determination in GIS environments — New software tool for ArcGIS. *Planetary and Space Science, 59,* 1243-1254. doi: 10.1016/j.pss.2010.03.015

Korotev, R. L., Jolliff, B. L., Zeigler, R. A., Seddio, S. M., & Haskin, L. A. (2011). Apollo 12 revisited. Geochimica et Cosmochimica Acta, 75(6), 1540–1573. https://doi.org/10.1016/J.GCA.2010.12.018

Langseth, M. G., Keihm, S. J., and Peters, K. (1976), Revised lunar heat-flow values. *Lunar and Planetary Science Conference Proceedings, 7*, 3143–3171.
Lawrence, D. J., Feldman, W. C., Barraclough, B. L., Binder, A. B., Elphic, R. C., Maurice, S., Miller, M. C., & Prettyman, T. H. (1999). High resolution measurements of absolute thorium abundances on the lunar surface. Geophysical Research Letters, 26(17), 2681–2684.

Lawrence, D. J., Feldman, W. C., Barraclough, B. L., Binder, A. B., Elphic, R. C., Maurice, S., Miller, M. C., & Prettyman, T. H. (1999). High resolution measurements of absolute thorium abundances on the lunar surface. Geophysical Research Letters, 26(17), 2681–2684. https://doi.org/10.1029/1999GL008361
Lawrence, D. J., Feldman, W. C., Barraclough, B. L., Binder, A. B., Elphic, R. C., Maurice, S., Miller, M. C., & Prettyman, T. H. (2000). Thorium abundances on the lunar surface. Journal of Geophysical Research: Planets, 105(E8), 20307–20331. https://doi.org/10.1029/1999JE001177

Lawrence, D. J., Feldman, W. C., Barraclough, B. L., Binder, A. B., Elphic, R. C., Maurice, S., Miller, M. C., & Prettyman, T. H. (2000). Thorium abundances on the lunar surface. *Journal of Geophysical Research: Planets, 105(E8)*, 20307–20331. https://doi.org/10.1029/1999JE001177

Lawrence, D. J., Hawke, B. R., Hagerty, J. J., Elphic, R. C., Feldman, W. C., Prettyman, T. H., & Vaniman, D. T. (2005). Evidence for a high-Th, evolved lithology on the Moon at Hansteen Alpha. Geophysical Research Letters, 32(7), 1–4. https://doi.org/10.1029/2004GL022022

Mahanti, P., Robinson, M. S., Humm, D. C., and Stopar, J. D., 2014. A Standardized Approach

Malin, M. C. (1974). Lunar Red Spots. Earth, 21, 331–341.

McEwen, A., Davis, P., and Howington-Kraus, A. (1994). Evidence for a Pre-Nectarian Impact Basin in Northwestern Procellarum. *Lunar and Planetary Science Conference XXV*.

Melosh, H.J., Freed, A.M., Johnson, B.C., Blair, D.M., Andrews-Hanna, J.C., Neumann, G.A., Phillips, R.J., Smith, D.E., Solomon, S.C., Wieczorek, M.A., and Zuber, M.T.

(2013). The Origin of Lunar Mascon Basins. *Science 340* (6140), 1552-1555. doi: 10.1126/science.1235768

Michael, G.G., and Neukum G. (2010), Planetary surface dating from crater size-frequency distribution measurements: Partial resurfacing events and statistical age uncertainty. *Earth and Planetary Science Letters, 294 (3-4)*, 223-229. doi: 10.1016/j.epsl.2009.12.041

Mohit, P. S., and Phillips, R. J. (2006). Viscoelastic Evolution of Multi-Ring Basins. *Journal of Geophysical Research 111*, E12001. doi: 10.1029/2005JE002654

Moore, D. E., & Ponce, D. A. (2001). Petrography and Physical Properties of Selected Rock Types Associated with the Hayward Fault, California. United States Geological Survey Open-File Report 01-263, 1–33.
https://www.researchgate.net/publication/242169854

Muller, P.M., and Sjogren, W.L. (1968). Mascons: Lunar Mass Concentrations. *Science 161* (3482), 680-684. doi: 10.1126/SCIENCE.161.3842.680

Nakamura, R., Yamamoto, S., Matsunaga, T., Ishihara, Y., Morota, T., Hiroi, T., Takeda, H., Ogawa, Y., Yokota, Y., Hirata, N., Ohtake, M., and Saiki, K. (2012), Compositional evidence for an impact origin of the Moon's Procellarum region. *Nature Geoscience 5*, 775-778. doi: 10.1038/ngeo1614

Nash, W. P., & Crecraft, H. R. (1985). Partition coefficients for trace elements in silicic magmas. Geochimica et Cosmochimica Acta, 49(11), 2309–2322.
https://doi.org/10.1016/0016-7037(85)90231-5

National Rearch Council, 2011. Vision and Voyages for Planetary Science in the Decade 2013- 2022. Washington, DC: The National Academies Press.

Neukum G. (1983). Meteoritenbombardement und Datierung planetarer Oberflachen. Habilitation Dissertation for Faculty Membership, University of Munich. 186 p.

Neukum, G., and Ivanov, B. A. (1994), Crater Size Frequency Distributions and Impact Probabilities on Earth from Lunar, Terrestrial-Planet, and Asteroid Cratering Data. *In: Hazard Due to Comets and Asteroids*, 359-416

Neukum, G., Ivanov, B. A., and Hartmann, W. K. (2001), Crater Records in the Inner-Solar System in relation to the Lunar Reference System. *Space Science Reviews 96*, 55-86. doi: 10.1023/A:1011989004263

Neumann G. A., Zuber M. T., Smith D. E., Lemoine F. G. (1996), Global structure and signature of major basins. *Journal of Geophysical Research 101*, 16,841. doi: 10.1029/96JE01246

Nikolayeva, O. v. (1990). Geochemistry of the Venera 8 material demonstrates the presence of continental crust on Venus. Earth, Moon, and Planets 1990 50:1, 50(1), 329–341. https://doi.org/10.1007/BF00142398

O'Kelly, G. D., Eldridge, J. S., Northcutt, K. J., & Schonfeld, E. (1976). Radionuclide Concentrations in KREEP Basalt Samples 15382 and 15386. Lunar and Planetary Science Conference.

Qiu, D., Ye, M., Yan, J., Zheng, C., Xiao, Z., Zhang, Q., Gao, Q., Liu, L., and Li., F. (2022), New Views of the Lunar Silicic Volcanism in the Mons Hansteen: Formation and Origins. *Journal of Geophysical Research: Planets, 127,* e2022JE007289. doi: 10.1029/2022JE007289

Ravi, S., and Robinson, M. S. (2019), Lunar Floor-Fractured Craters: A Case for Viscous Relaxation. *Lunar and Planetary Science Conference L,* Abstract #2677.

Ravi, S., and Robinson, M. S. (2022), Rheology of the Lunar Lithosphere and the Origin of Floor-Fractured Craters. *Lunar and Planetary Science Conference LII,* Abstract #1266.

Ravi, S., and Robinson, M.S. (2019), So Creepy: Creep in the Procellarum KREEP Terrane, Abstract P53C-3460, presented at 2019 AGU Fall Meeting, San Francisco, CA

Ravi, S., Mahanti, P. M., Meyer, H. M., and Robinson, M. S. (2017), Impact Craters: Size-Dependent Degradation Rates, Abstract P41D-2864, presented at 2017 AGU Fall Meeting, New Orleans, LA, 11-15 Dec.

Ravi, S., Robinson, M. S., and Clark, J. D. (2023), *Spatio-Temporal Association of Mons Hansteen and Hansteen Crater: Implications for Silicic Magma Genesis* (Dataset). Zenodo. doi: 10.5281/zenodo.7706699

Ravi, S., Robinson, M.S., and Watters, T.R. (2022), *Origin of Lunar Floor-Fractured Craters: Revisiting the Viscous Relaxation Hypothesis* (Data set). Zenodo. doi: 10.5281/zenodo.7483821

Robinson, M. S., Brylow, S. M., Tschimmel, M., 2010. Lunar Reconnaissance Orbiter Camera (LROC) Instrument Overview, Space Science Reviews 150, 81-124.

Robinson, M. S., Brylow, S. M., Tschimmel, M., Humm, D., Lawrence, S.J., Thomas, P.C., Denevi, B.W., Bowman-Cisneros, E., Zerr, J., Ravine, M.A., Caplinger, M.A., Ghaemi, F.T., Schaffner, J.A., Malin, M.C., Mahanti, P., Bartels, A., Anderson, J., Tran, T.N., Eliason, E.M., McEwen, A.S., Turtle, E., Jolliff, B.L., Hiesinger, H. (2010), Lunar Reconnaissance Orbiter Camera (LROC) Instrument Overview, *Space Science Reviews, 150*, 81-124. doi: 10.1007/S11214-010-9634-2

Ryder, G. (1976). Lunar sample 15405: Remnant of a KREEP basalt-granite differentiated pluton. Earth and Planetary Science Letters, 29(2), 255–268. https://doi.org/10.1016/0012-821X(76)90129-1

Scholten, F., Oberst, J., Matz, K.-D., et al., 2012. GLD100: The Near-Global Lunar 100 m Raster DTM from LROC WAC Stereo Image Data. Journal of Geophysical Research 117, E00H17.

Schultz, P. H. and Spudis, P. D. (1985), Procellarum Basin: A Major Impact or the Effect of Imbrium? *Lunar and Planetary Science Conference XVI*

Schultz, P.H. (1976), Lunar Floor-fractured craters. *The Moon, 15*, 241-273. doi: 10.1007/BF00562240

Scoates, J. S., & Chamberlain, K. R. (2003). Geochronologic, geochemical and isotopic constraints on the origin of monzonitic and related rocks in the Laramie anorthosite complex, Wyoming, USA. Precambrian Research, 124(2–4), 269–304. https://doi.org/10.1016/S0301-9268(03)00089-5

Seddio, S. M., Jolliff, B. L., Korotev, R. L., & Carpenter, P. K. (2014). Thorite in an Apollo 12 granite fragment and age determination using the electron microprobe. Geochimica et Cosmochimica Acta, 135, 307–320. https://doi.org/10.1016/J.GCA.2014.03.020

Seddio, S. M., Jolliff, B. L., Korotev, R. L., & Zeigler, R. A. (2013). Petrology and geochemistry of lunar granite 12032,366-19 and implications for lunar granite petrogenesis. American Mineralogist, 98(10), 1697–1713. https://doi.org/10.2138/AM.2013.4330

Shirley, K. A., Zanetti, M., Jolliff, B., van der Bogert, C. H., and Hiesinger, H. (2016), Crater Size-Frequency Distribution Measurements and Age of the Compton-Belkovich Volcanic Complex. *Icarus, 273,* 214-223. doi: 10.1016/j.icarus.2016.03.015

Simmons, E. C., & Hanson, G. N. (1978). Geochemistry and origin of massif-type anorthosites. Contributions to Mineralogy and Petrology. https://doi.org/10.1007/BF00372151

Smith, D. R., Noblett, J., Wobus, R. A., Unruh, D., Douglass, J., Beane, R., Davis, C., Goldman, S., Kay, G., Gustavson, B., Saltoun, B., & Stewart, J. (1999). Petrology and geochemistry of late-stage intrusions of the A-type, mid-Proterozoic Pikes Peak batholith (Central Colorado, USA): Implications for petrogenetic models. Precambrian Research. https://doi.org/10.1016/S0301-9268(99)00049-2

Smrekar, S., Hensley, S., Helbert, J., Andrews-Hanna, J., Breuer, D., Buczkowski, D., Campbell, B., Davaille, A., DiAchille, G., Fassett, C., Gilmore, M., Herrick, R., Iess, L., Jozwiak, L., Konopliv, A., Mastrogiuseppe, M., Mazerico, E., Mueller, N., Nunes, D., … Zebker, H. (2020). VERITAS (VENUS EMISSIVITY , RADIO SCIENCE, INSAR, TOPOGRAPHY AND SPECTROSCOPY): A PROPOSED DISCOVERY MISSION. 51st Lunar and Planetary Science Conference. https://doi.org/10.1002/2015GC006210

Sparks, R. S. J., & Marshall, L. A. (1986). Thermal and mechanical constraints on mixing between mafic and silicic magmas. Journal of Volcanology and Geothermal Research, 29(1–4), 99–124. https://doi.org/10.1016/0377-0273(86)90041-7

Spudis, P. D., and Schultz, P. H. (1985), Geochemical Problems with Procellarum Basin. *Lunar and Planetary Science Conference XVI*

Spudis, P. H. (1993), The Geology of Multi-Ring Impact Basins. Cambridge Univ. Press, New York.

Stöffler, D., and Ryder, G. (2001), Stratigraphy and Isotope Ages of Lunar Geologic Units: Chronological Standard for the Inner Solar System. *Space Science Reviews, 96,* 9-54. doi: 10.1023/A:1011937020193

Strom, R. G., Schaber, G. G., & Dawson, D. D. (1994). The global resurfacing of Venus. Journal of Geophysical Research: Planets, 99(E5), 10899–10926. https://doi.org/10.1029/94JE00388

Tera, F., & Wasserburg, G. J. (1972). U-Th-Pb systematics in three Apollo 14 basalts and the problem of initial Pb in lunar rocks. Earth and Planetary Science Letters, 14(3), 281–304. https://doi.org/10.1016/0012-821X(72)90128-8

Till, C. B., Kent, A. J. R., Abers, G. A., Janiszewski, H. A., Gaherty, J. B., & Pitcher, B. W. (2019). The causes of spatiotemporal variations in erupted fluxes and compositions along a volcanic arc. Nature Communications, 10(1). https://doi.org/10.1038/s41467-019-09113-0

Toksöz, M. N., Dainty, A. M., Solomon, S. C., & Anderson, K. R. (1974). Structure of the Moon. Reviews of Geophysics, 12(4), 539–567. https://doi.org/10.1029/RG012I004P00539

Wadhwa, M. (2008). Redox conditions on small bodies, the Moon, and Mars. Reviews in Mineralogy and Geochemistry, 68(1), 493-510. https://doi.org/10.2138/rmg.2008.68.17

Wagner, R., Head, J. W., Wolf, U., and Neukum, G. (2010), Lunar Red Spots: Stratigraphic Sequence and Ages of Domes and Plains in the Hansteen and Helmet Regions on the Lunar Nearside. *Journal of Geophysical Research, 115,* E06015. doi: 10.1029/2009JE003359

Warren, P. H. (1985). The magma ocean concept and lunar evolution. Annual Review of Earth and Planetary Science, 13, 201–240.

Warren, P. H. (1986). Anorthosite assimilation and the origin of the Mg/Fe-related bimodality of pristine moon rocks: Support for the magmasphere hypothesis. Journal of Geophysical Research: Solid Earth, 91(B4), 331–343. https://doi.org/10.1029/jb091ib04p0d331

Warren, P. H., Jerde, E. A., & Kallemeyn, G. W. (1987). Pristine Moon rocks: A "large" felsite and a metal-rich ferroan anorthosite. Journal of Geophysical Research: Solid Earth, 92(B4), E303–E313. https://doi.org/10.1029/JB092IB04P0E303

Warren, P. H., Taylor, G. J., Keil, K., Shirley, D. N., & Wasson, J. T. (1983). Petrology and chemistry of two "large" granite clasts from the moon. Earth and Planetary Science Letters, 64(2), 175–185. https://doi.org/10.1016/0012-821X(83)90202-9

Watters, T.R. (2022), Lunar Wrinkle Ridges and the Evolution of the Nearside Lithosphere. *Journal of Geophysical Research Planets, 127*, e2021JE007058. doi: 10.1029/2021JE007058

Whitaker, E.A. (1981). The lunar Procellarum basin. *Multi-Ring Basins, Proceedings of the Lunar and Planetary Science Conference,* 12 A, 105-111.

Wieczorek, M. A., and Phillips, R. J. (1999), Lunar Multiring Basins and the Cratering Process. *Icarus 139* (2), 246-259. doi: 10.1006/ICAR.1999.6102

Wieczorek, M. A., and Phillips, R. J. (2000), The "Procellarum KREEP Terrane": Implications for Mare Volcanism and Lunar Evolution. *Journal of Geophysical Research, 105*, 20417-20430. doi: 10.1029/1999JE001092
Wieczorek, M. A., and Phillips, R. J., 2000. The "Procellarum KREEP Terrane": Implications for Mare Volcanism and Lunar Evolution. Journal of Geophysical Research 105, 20417-20430.

Wiens, D. A., and Stein, S. (1983), Age dependence of oceanic intraplate seismicity and implications for lithospheric evolution. *Journal of Geophysical Research, 88*, 6455–6468. doi: 10.1029/JB088IB08P06455
Wilhelms, D. E. (1983), Effects of the Procellarum Basin on Lunar Geology, Petrology, and Tectonism. *Lunar and Planetary Science Conference XIV*.

Wilhelms, D.E. (1987), The Geologic History of the Moon. *USGS Professional Paper 1348*. doi: 10.3133/PP1348

Wilson, L., & Head, J. W. (2003). Lunar Gruithuisen and Mairan domes: Rheology and mode of emplacement. Journal of Geophysical Research E: Planets, 108(2), 6–1. https://doi.org/10.1029/2002je001909

Wood, John A.; Dickey, John. S.; Marvin, Ursula, B.; and Powell, B. N. (1970). Lunar anorthosites and a geophysical model of the Moon. Proceedings of the Apollo 11 Lunar Science Conference, 1, 965–988.

Zhong, S., Parmentier, E. M., & Zuber, M. T. (2000). A dynamic origin for the global asymmetry of lunar mare basalts. Earth and Planetary Science Letters, 177(3–4), 131–140. https://doi.org/10.1016/S0012-821X(00)00041-8

APPENDIX A

STATEMENT OF CO-AUTHOR APPROVALS FOR MANUSCRIPTS IN

PREPARATION

Chapters 2-4 are manuscripts in preparation to be submitted for publication. I, Srinidhi Ravi, declare that I am the principal author of all three manuscripts and that all subsequent co-authors approve of the publication of these works.